GEOLOGICAL SURVEY OF CANADA

OPEN FILE 5594

Sedimentary petrology of the Lower Cretaceous in the Naskapi N-30 and Sambro I-29 wells, Scotian basin, offshore eastern Canada

G. Pe-Piper, D.J.W. Piper

2007

Natural Resources Canada Ressources naturelles Canada

Canada

GEOLOGICAL SURVEY OF CANADA

OPEN FILE 5594

Sedimentary petrology of the Lower Cretaceous in the Naskapi N-30 and Sambro I-29 wells, Scotian basin, offshore eastern Canada

G. Pe-Piper, D.J.W. Piper

2007

Available from
Geological Survey of Canada Atlantic
1 Challenger Drive
Dartmouth, Nova Scotia B2Y 4A2

Pe-Piper, G., Piper, D.J.W.
2007: Sedimentary petrology of the Lower Cretaceous in the Naskapi N-30 and Sambro I-29 wells, Scotian basin, offshore eastern Canada. Geological Survey of Canada, Open File 5594, 98 p.

Open files are products that have not gone through the GSC formal publication process.

Preface:

This Open File is one of a series on detrital and diagenetic mineralogy of the Lower Cretaceous rocks of the Scotian basin and their on-land equivalent, the Chaswood Formation, resulting from a collaborative program between Saint Mary's University and the Geological Survey of Canada. The work was funded by an NSERC Collaborative R&D project grant, the ExxonMobil Sable Project, and Petroleum Research-Atlantic Canada (PR-AC). This report provides the results of sedimentary petrography studies in the Naskapi N-30 and Sambro I-29 wells and complements previous Open Files on the Alma, Glenelg and North Triumph fields (GSC Open File 4836) and the Peskowesk A-99 well (GSC Open File 5383).

Acknowledgments:

We thank Patricia Stoffyn at the Regional Electron Microprobe Centre at Dalhousie University, Bob Mackay, and Lila Dolansky for help with the electron microprobe analyses, Gordon Brown for polished thin sections, Steve Ingram for logging the Naskapi core, and sampling of the core and cuttings, Thian Hundert and Owen Brown for grain size analysis, Ben Moulton for help with drafting, and the staff of the Canada-Nova Scotia Offshore Petroleum Board for access to cores and cutting samples. Reviews by Rob Fensome and Hans Wielans improved this report.

Authors' addresses:

Georgia Pe-Piper
Department of Geology, Saint Mary's University, Halifax, Nova Scotia, B3H 3C3, Canada
gpiper@smu.ca

David J.W. Piper
Geological Survey of Canada (Atlantic), Bedford Institute of Oceanography, P.O. Box 1006, Dartmouth, Nova Scotia, B2Y 4A2, Canada
dpiper@nrcan.gc.ca

Abstract

The Sambro I-29 and Naskapi N-30 wells are located about 25 km apart on the La Have Platform on the central Scotian Shelf. The Lower Cretaceous Logan Canyon and Missisauga formations are ~ 700 m thick in Naskapi N-30 and ~ 600 m thick in the more proximal Sambro I-29 well. Sedimentology and sedimentary petrography have been studied on a 9-m-long conventional core from the uppermost Missisauga Formation in Naskapi N-30 and petrographic studies were made of selected drill cuttings samples from Sambro I-29. The purpose of this work was to understand better the provenance and diagenesis of the Lower Cretaceous sandstones in the western part of the Scotian basin and to make comparisons of provenance with previously studied wells farther east (Alma and Glenelg fields, GSC Open File 4836; Peskowesk A-99, GSC Open File 5383). This Open File documents data collected in this study and provides preliminary interpretations.

The analysed sandstones differ from those farther east in the Scotian basin in their low abundance of feldspar, predominance of polycrystalline quartz in the lithic fraction, and lack of paragonite and chromite. They also differ in bulk geochemistry. On the other hand, they show strong mineralogical similarities to the Chaswood Formation of central Nova Scotia, notably in the composition of muscovite, ilmenite, monazite, and biotite.

Based on the correlation of sand supply to the Chaswood Formation in central Nova Scotia with sand supply to the Naskapi – Sambro deltas and published biostratigraphic data, a correlation of the major units within the Chaswood Formation with offshore stratigraphy is proposed. Major sandy intervals in the upper Mississauga Formation, Cree Member and Marmora Member probably correlated with thick sands in the upper part of seismic packet 1, seismic packet 3 and seismic packet 4 of the Chaswood Formation.

Introduction

This report continues a series of reports that present work on the sedimentary petrology of Lower Cretaceous of the Scotian Basin and correlative strata on land in the Chaswood Formation. The purpose of this work is to understand better the detrital petrology and diagenesis of the Lower Cretaceous rocks, which are important oil and gas reservoirs in the Scotian basin. This report includes studies of two wells: Naskapi N-30, and Sambro I-29, both at the margin of the Lahave Platform (Fig. 1). The samples studied are from conventional core for the Naskapi N-30 well, and cutting samples for the Sambro I-29 well (Appendix 1).

Included herein are:

a) a description of the Lower Cretaceous lithofacies interpreted from core in the Naskapi N-30 well and a comparison to the cutting samples from Sambro I-29 well.

b) a summary of the sedimentary petrography for the upper Missisauga Formation in Naskapi N-30 and for the Logan Canyon and Missisauga formations in Sambro I-29.

c) a detailed account of the detrital petrology and observations on diagenesis in both wells using electron microprobe chemical analyses of minerals and back scattered electron images.

d) whole rock geochemical analyses of five representative sandstones from Naskapi N-30 well and one silty mudstone from Sambro I-29 well.

A. Naskapi N-30 well

1. Lithostratigraphy

Lower Cretaceous rocks in the Naskapi N-30 well comprise sandstone and mudstone of the Missisauga and Logan Canyon formations (Fig. 2), which overlie mixed clastics and carbonates of the Upper Jurassic Mic Mac Formation. Assignment of formation boundaries (e.g. MacLean and Wade, 1993) is based partly on seismic correlation, refined by lithologic correlation and biostratigraphy. Biostratigraphy based on palynology (Williams, in Barss et al. 1979) is consistent with sparse picks based on calcareous microfossils (Ascoli, 1988). The Missisauga Formation is 230 m thick. No carbonate beds are recognised, so that the position of the O-marker is uncertain and any division into members is based solely on biostratigraphy. Going up section, the base of the Missisauga Formation is marked by the first predominance of sandstone. In general, the Missisauga Formation shows a coarsening-up succession from the Berriasian to the Hauterivian and then a slight fining through the Barremian.

The 150-m-thick Naskapi Member is recognised as a shale-prone interval of Aptian to early Albian age. The overlying Cree Member of Albian age is a 140-m-thick coarsening-up succession of sandstone and interbedded mudstone. The 100-m-thick Sable Member is shale prone and the overlying 70 m thick Cenomanian Marmora Member is again sand prone.

Seismic profiles near the well site (MacLean and Wade, 1993) show that faults that cut basement and define Triassic basins were reactivated as late as just before deposition of the Santonian to Maastrichtian Wyandot Formation.

2. Lower Cretaceous lithofacies interpreted from conventional core

The only conventional core from Naskapi N-30 is 7.5 m long (Fig. 3) from the middle of the Barremian upper member of the Missisauga Formation (Fig. 2). The predominant lithology is abundant to completely bioturbated fine-grained sandstone and lesser mudstone (Appendix 2b; photos 1-3, 9-12, 14, 16), interpreted as shoreface or inner shelf facies. Bioturbation terminology follows Bann et al. (2004).

Very coarse-grained sandstone lacking bioturbation (photos 6, 22, 23), in some cases with parallel lamination (photo 6), interbeds with thin beds of medium sandstone (photo 22), parallel laminated fine grained sandstone (photos 7, 8, 22, 23) and mudstone with thin siltstone

laminae (photo 8, 21). Phytodetritus, in some cases fragments several centimetres long and several millmetres thick (photos 20-22), occurs in some of these sediments. Phytodetritus is also common within many of the bioturbated fine sandstone beds (photos 1-3, 5, 9-12). The association of thin beds of very coarse grained sandstone, fine grained sandstone with phytodetritus, and mudstone with silty laminae is found in many other wells on the Scotian Shelf (e.g. Glenelg and Thebaud fields) and has been interpreted by Piper et al. (2007a) as evidence of hyperpycnal discharge from bedload-dominated rivers based on interpretations summarised by MacEachern et al. (2005) and Myrow et al. (2006). Some beds of this facies show syn-sedimentary deformation (photos 4, 5) similar to that interpreted from the Glenelg field as resulting from local liquefaction (Piper et al. 2004a).

There is also a fine-grained sandstone lacking prominent phytodetritus but with thin irregular mudstone drapes and uncommon to moderate bioturbation including mud-lined burrows (photos 15, 17, 18). Following MacRae and Jauer (2001) and Cummings et al. (2005, 2006a, 2006b), these sandstones are interpreted as tidally influenced sediments, likely within river estuaries.

One abundantly bioturbated interval (photo 19) overlies cross-laminated fine sandstone and includes scattered granules including a 6 mm lithic clast. This facies resembles transgressive surfaces seen elsewhere in conventional core from the Scotian Shelf, although the usually associated shelly bioclasts and siderite cementation are absent in this interval. It is overlain by tidally-influenced sandstone.

3. General sedimentary petrography

Polished thin sections have been prepared from the cored interval of the Missisauga Formation in Naskapi N-30 (Fig. 3). Standard descriptions of all sandstones have been prepared (Table 1), with features such as mean grain size, sorting, and percentage of minerals estimated using comparison charts.

All sandstones classify as quartz arenites (Fig. 4). Lithic rock fragments are present only in trace amounts, except for polycrystalline quartz, which makes up generally 1–20% and exceptionally as much as 80% of the grains (Table 1; Fig. 4). Mica is a very common component of sandstones of all grain sizes, comprising principally muscovite, which generally makes up 2–4% of the grains (Fig. 5). The sandstones, even those that lack bioturbation, have a variable

matrix component, ranging generally from 7– 44%, with one bioturbated sample with 65%, Most sandstones have a very low percentage of cement, <1 to 4%, of variable mineralogy as discussed below.

4. Grain size analyses

Grain size analyses were made by disaggregating loosely cemented sandstones and analysing them with a Coulter Laser analyser (Tables 2 and 3; Fig. 6). An additional 25 grain size analyses by sieving are also available from the Core Analysis Report (Shell 1970). Grain size distribution from three sandstones that are interpreted as from hyperpycnal-dominated facies are remarkably similar to size distribution of sands from the West Indian Road pit, in central Nova Scotia, of facies **Sh** and **Sr** analysed by Gobeil et al. (2006, their Fig. 12).

5. Detrital petrology

Methods

Because of the small amount of material, heavy mineral separation was inappropriate. Instead we prepared polished thin sections from the available core. In total, 12 polished thin sections were made and studied with both petrographic microscope and electron microprobe, which was used to obtain mineral chemical analyses (Table 4). These analyses were made at the Regional Microprobe centre of Dalhousie University. Minerals were analysed with a JEOL-733 electron microprobe having four wavelengths spectrometers and a Tracor Northern 145 eV energy-dispersion detector. The beam was operated at 15 kV and 20 nA, with a beam diameter of 1-10 μm. The objectives of the chemical mineralogy studies in these sandstones were:

a) to establish the detrital minerals present, in addition to quartz, and use these minerals as a guide to sandstone provenance.

b) to use the chemistry of suitable minerals to more precisely identify provenance.

c) To establish the types and order of the pore-filling diagenetic minerals.

Detrital minerals present

Table 1 lists the detrital and neomorphic minerals identified by petrographic microscope analysis at various depths in the well. The percentage of muscovite, polycrystalline quartz, matrix and cement for all studied samples is plotted on Fig. 5. The abundance of polycrystalline

quartz shows strong correlation with mean grain size.

Table 5 summarises the detrital and neomorphic mineral assemblages with depth in the short conventional core. No modal analyses of heavy mineral have been made, because of lack of heavy mineral separates and the percentage of heavy minerals in each sandstone polished thin section is < 5%. The highlights of the detrital petrology of the studied sandstones are:

a) By far the most common heavy minerals are the Fe-Ti oxides ilmenite and rutile.

b) Tourmaline and zircon are the most abundant translucent heavy detrital minerals, but monazite and apatite are also present.

c) Unstable minerals, notably plagioclase and biotite, are rare.

d) Muscovite is common in many sandstones

Chemical composition of detrital minerals

The chemical composition of detrital minerals in the Chaswood Formation has been shown to be diagnostic of source (e.g. Pe-Piper et al. 2004c; Piper et al. 2007b). These techniques can be applied to the minerals sampled at Naskapi N-30.

Muscovite can be interpreted in terms of its Ti, Mg and Na content (Fig. 7). Compared with wells farther east in the Scotian Basin, Naskapi N-30 has numerous high- Ti, low-Na muscovites and lacks high-Na muscovites. However, sandstones of the Chaswood Formation from the Shubenacadie Basin (Fig. 7) have a similar pattern of muscovite composition to Naskapi N-30.

Tourmaline compositions from Naskapi N-30 indicate a provenance predominantly from pelitic metasediment, based on the source fields identified by Henry and Guidotti (1985) and Kassoli-Fournaraki and Michailidis (1994). One analysis clearly falls in the field for Li-poor granite and a few other grains lie near the boundary between the metasediment and granite fields. In contrast, the Chaswood Formation at the West Indian Road pit and in the Shubenacadie Basin has a higher proportion of tourmaline derived from granite. Tourmaline from the Alma and Glenelg fields appears similar to that at Naskapi N-30, except that they have fewer grains near the boundary between the metasediment and granite fields.

Ilmenite is the most abundant heavy mineral. Most of the ilmenite is considerably altered into leucoxene, but nevertheless the abundance of trace elements such as Mn and Cr does not appear to be significantly affected by alteration, although Mg may be more mobile (Pe-Piper et

al. 2005a). All grains have < 3% MnO and < 0.4% Cr_2O_3 (Fig. 9). These abundances are comparable with potential sources in Avalon terrane rocks. The range of these elements in ilmenite from the Meguma terrane is much larger (Fig. 9), suggesting that the Meguma terrane was not a significant source of ilmenite. The elemental abundances in the ilmenite from Naskapi are similar to those in ilmenite from the Chaswood Formation from the Shubenacadie Basin and rather higher than those at Vinegar Hill in southern New Brunswick (Fig. 1).

Three ***monazite*** grains (19 analyses) were dated by electron microprobe chemical dating. The mean calculated age for these grains is 501±13.9 Ma (Fig. 10). These ages compare closely with the older mode for monazite ages from the Chaswood Formation in borehole RR-97-23 in the Elmsvale Basin reported by Pe-Piper and MacKay (2006).

5. Diagenetic minerals

While analysing the compositions of detrital minerals, observations and chemical analyses of neomorphic minerals were also made. The chemistry of the neomorphic minerals is reported in Table 4. The neomorphic mineral assemblages are summarised in Table 5. Abundance of kaolinite cement in sandstones was visually estimated (Fig. 3).

The most abundant diagenetic minerals are: kaolinite/halloysite, illite/hydromuscovite, and pyrite, although glauconite, limonite and silica also occur.

6. Whole rock geochemistry

Five representative sandstones were analysed for both major and trace elements (Table 6). The analyses were made by Activation Laboratories Ltd. using their lithium metaborate/ tetraborate fusion ICP whole rock package and a trace element ICP-MS package. For Cu, Ni, Pb, and Zn their 4B1 package was used.

The sandstones from the Naskapi N-30 well plot in the field for arkoses and in the area between arkose and quartz arenite fields (Fig. 11) and according to the plate boundary setting diagram of Bhatia (1983) three analyses plot in the field for a passive margin tectonic setting and two outside this field (Fig. 12).

B. Sambro I-29 well

1. Lithostratigraphy

Lower Cretaceous rocks in the Sambro I-29 well comprise sandstone and mudstone of the Missisauga and Logan Canyon formations (Fig. 13), that overlie mixed clastics and carbonates of the Upper Jurassic Mohawk Formation. Discrimination of formation boundaries (e.g. MacLean and Wade, 1993) is based partly on seismic correlation, refined by lithologic correlation and biostratigraphy. Biostratigraphy based on palynology and calcareous microfossils (Lentin, 1987) is not internally consistent. The Missisauga Formation as defined by MacLean and Wade (1993) is almost 200 m thick. No carbonate beds are recognised, so that the position of the O-marker is uncertain.

The 90-m-thick Naskapi Member is recognised as a shale-prone interval of Aptian age, with a central 15 m thick sandy unit. The overlying Cree Member is a 75-m-thick coarsening-up succession of sandstone and interbedded mudstone. The 95-m-thick Sable Member is shale prone, but the gamma log suggests a considerable amount of siltstone or sandstone is present. As at Naskapi N-30, the lower part of the overlying 110 m thick Albian to Cenomanian Marmora Member is also sand prone, but the proportion of shale increases upward through the member.

Seismic profiles near the well site (MacLean and Wade, 1993) show that faults which cut basement and define Triassic basins were reactivated as late as the Cenomanian (base Dawson Canyon Formation) marker.

2. Lower Cretaceous lithofacies interpreted from cutting samples

The Lower Cretaceous intervals of the Sambro I-29 well were logged from cuttings (Fig. 14). This technique tends to overemphasise the dominant lithologies, but confirms the division based on the wireline logs into the members of the Logan Canyon Formation.

3. Sedimentary petrography methods

Sample preparation

Representative sub-samples of archived unwashed cutting samples from the Canada Nova Scotia Offshore Petroleum Board (CNSOPB) Core Lab were taken from the Logan Canyon and Missisauga formations in this well. These cutting samples were washed with warm

tap water through a 63 μm sieve and were then sieved at 2 mm, allowing the separation of the grains into two groups: > 63 μm to < 2 mm and > 2 mm (Table 7). Heavy mineral separation was then performed on all sub-samples for the > 63 μm to < 2 mm fraction using the heavy liquid tetrabromoethane, which has a density of 2.95 kg/L (Table 8). The heavy separates of this fraction were then used to make polished thin sections.

Analysis of cuttings > 2 mm

Cuttings larger than 2 mm were analysed using a binocular microscope and were separated into groups based on lithology/mineralogy, grain size, colour or apparent cement. Each group of cuttings was placed into separate vials and labelled with the corresponding well, depth and lithology. Representative unidentified cuttings were used to make polished thin section mounts and analysed under a polarised/reflected-light microscope and an electron microprobe (Table 9). A numerical summary of the cuttings and clasts > 2 mm is given in Table 10. This table lists the quantity of rock cuttings and clasts for each identified lithology found at each sampled depth.

Identification of heavy fraction of cuttings < 2 mm

Polished-thin-section mounts of the heavy separates of the fraction > 63 μm to < 2 mm grains were made for all subsamples. The preliminary identification of mineralogy/ lithology of cuttings was done using a polarised/reflected light petrographic microscope and subsequently refined with the use of the electron microprobe (Table 11).

4. Detrital minerals and their chemical mineralogy

Samples from selected cuttings samples in the Logan Canyon and Missisauga formations were further studied by electron microprobe through both chemical analyses and back scattered electron (BSE) images, using polished thin sections from both the > 2 mm fraction and the heavy mineral separate of the > 63 micron to < 2 mm fraction. Representative chemical mineral analyses are given in Tables 13 and 14 and representative BSE images are given in Appendix 3. Table 15 summarises the minerals present in the well by stratigraphic level, based on data in Tables 10, 11, 12, 13 and 14. One sample (3170) is from the Cree Member; one (3740) is from the topmost Missisauga Formation at a horizon approximately correlative with the core in

Naskapi N-30; and three (3880, 4000, 4080) from deeper in the Missisauga Formation.

The detrital mineral assemblage is generally the same for both Logan Canyon and Missisauga formations in this well (Table 15). The highlights of the detrital petrology of the sandstones are as follows:

1. K-feldspar and muscovite are by far the most abundant translucent detrital minerals in addition to quartz. Other detrital minerals identified and analysed include biotite partly altered to chlorite (e.g. Fig. 14, Appendix 3), plagioclase, titanite, and detrital chlorite (e.g. Figures 7, 8, 10, 15, in Appendix 3), and epidote (e.g. Figs. 6 and 14 in Appendix 3) and occasionally staurolite (e.g. Fig. 12 in Appendix 3).

2. Several mineral assemblages are diagnostic of a particular type of rock source. The assemblage quartz + muscovite ± biotite + chlorite ± titanite + epidote ± ilmenite suggests a metamorphic rock source. One particular clast looks like a Goldenville Group metasandstone lithology (Table 10 and Fig. 6 in Appendix 3).

3. Most quartz grains do not contain any mineral inclusions. Some contain either muscovite or siderite, the latter probably resulting from the alteration of magnetite (e.g. Table 10). Quartz grains with muscovite inclusions suggests an origin from peraluminous felsic igneous rocks, whereas quartz grains without inclusions or with magnetite inclusions may suggest origin from metaluminous igneous rocks.

4. All detrital ilmenite grains have < 5% MnO and < 0.2% Cr_2O_3 (Fig. 9). These amounts are comparable with potential sources in the Avalon terrane, but the range of these elements in the Meguma terrane is much larger (Fig. 9). The elemental abundances in the ilmenite from Sambro I-29 are similar to those in ilmenite from the Chaswood Formation from the Shubenacadie Basin. The most common inclusions in the analysed ilmenite is quartz (Figs. 21 to 26 in Appendix 3). The morphology of such inclusions (e.g. Figs. 23, 25, 26 in Appendix 3) indicates that these are the result of melt crystallization, so that the host ilmenite crystals come from igneous felsic rocks. The other common inclusion in the ilmenite crystals is muscovite, which may indicate felsic igneous rocks of peraluminous character as the source of some of these ilmenite grains.

5. Feldspars analysed are principally K-feldspar with Or_{89-99} (Fig. 15). In contrast to feldspars from the Alma and Glenelg fields, plagioclase is extremely rare and no perthites in the range Or_{60-80} have been found.

6. Muscovite (Fig. 7) differs from that at Naskapi N-30 and more closely resembles that from the

Alma and Glenelg fields. In contrast to Naskapi, there are some Na-rich muscovites and Ti-rich muscovites are lacking. Secondary detrital muscovite with very low Ti is more abundant than at Naskapi. However, few muscovite grains were analysed and none were from sample 3740 that stratigraphically correlates with the samples from Naskapi.

7. Biotite (Fig. 16) shows the same range of composition as biotite from the Chaswood Formation at borehole RR-97-23. In contrast to the Alma and Glenelg fields, biotite with a calc-alkaline igneous source has not been found.

8. The sparse rutile grains from Naskapi N-30 and Sambro I-29 have MnO < 0.1 % and moderate levels of CaO (Fig. 17). They overlap in composition with some rutile from the Alma and Glenelg fields, but in general have higher CaO than rutile from the Chaswood Formation.

5. Diagenetic minerals

While analysing the compositions of detrital minerals, observations and chemical analyses of neomorphic minerals were also made. The chemistry of the neomorphic minerals is reported in Tables 13 and 15, and their morphologic textures as BSE images in Appendix 3. The neomorphic mineral assemblages are summarised in Table 15.

The most common diagenetic minerals are siderite and glauconite, but other minerals are also very common in individual samples such as calcite (e.g. Fig. 4 in Appendix 3), pyrite (in Figs. 13, 21, 22 in Appendix 3) and francolite (e.g. Figs. 4, 7, 8 in Appendix 3). Other diagenetic minerals seen include chlorite, galena, rutile from the alteration of ilmenite, hydromuscovite probably from alteration of detrital muscovite, and limonite. Siderite may be zoned (e.g. Fig. 2 in Appendix 3). Pyrite is often framboidal (e.g. Figs. 7, 11, 13 in Appendix 3).

Francolite has been found only in sample 3170 at 966 m in the Cree Member and it is in the form of cement in a poorly sorted fossiliferous muddy sandstone (Fig. 4 in Appendix 3) and in a phosphate-carbonate-cemented mudstone (e.g. Figs. 7, 8 in Appendix 3). The wireline logs suggest that this horizon immediately overlies a coarsening-up sandstone packet, at the base of a shaly unit, and it is probably at a transgressive or maximum flooding surface. Similar phosphorite cementation, together with coated grains, is found in proximal sediments in the Orpheus graben (Weir-Murphy, 2004).

Discussion

1. Stratigraphic correlation and depositional environments at Naskapi N-30 and Sambro I-29

The Naskapi N-30 and Sambro I-29 wells both overlie shallow Appalachian basement of the La Have platform, which shows evidence of movement on faults until after the accumulation of the Missisauga and Logan Canyon formations (see seismic sections in MacLean and Wade, 1993). The wells are only 25 km apart: two wells in such proximity should show close stratigraphic correlation. Varying thickness of stratigraphic units may reflect tectonically controlled creation of accommodation by subsidence. Sambro I-29 is paleogeographically more proximal than Naskapi N-30.

In both wells, the Missisauga Formation is sand prone and therefore likely consists predominantly of deltaic river mouth and shore face deposits. The total thickness is slightly greater in Naskapi N-30 (Fig. 19). The shale-prone Naskapi Member is 1.6 times thicker in Naskapi N-30 and the overlying Cree Member is almost twice as thick in Nasakapi N-30 as in Sambro I-29. Such major thickness variations in deltaic facies suggest that accommodation was created by greater tectonic subsidence at Naskapi N-30. In contrast, the Sable Member is of similar thickness in both wells and the Marmora Member is rather thicker in Sambro I-29. Similarly large variations in thickness of the Naskapi Member are known from the Orpheus graben (Weir-Murphy, 2004).

From the gamma logs, three types of sand body can be distinguished in the two wells. Based on lithostratigraphic correlation, these sand bodies appear to vary from proximal to distal settings. The most distinctive are 5–15 m thick clean sands with a blocky log response. One prominent example is in the middle of the Naskapi Member in Sambro I-29 (yellow bar in Fig. 19, from 1052–1078 m). This correlates with a 1–2 m thick sand unit in the more distal Naskapi N-30 (green bar in Fig. 19). Two similar sands in the upper Marmora Member at Sambro I-29 also correlate with thin sands at Naskapi N-30. Two similar blocky sand units in the Missisauga Formation at Sambro I-29 correlate with blocky sand units at Naskapi N-30 and a third correlates with a 1-2 m thick sand that has a similar log response to the coarse-grained sandstones of units 3 and 12 in the Naskapi N-30 conventional core (Fig. 3). In the Cree and basal Marmora members, thick, blocky, clean sands in Naskapi N-30 appear to correlate with coarsening-up mud to sand packets in the more proximal Sambro I-29 well (magenta bars in Fig. 19).

Identification of depositional environments is speculative. The conventional core at Naskapi N-30 includes distal fluvial distributary (likely distributary mouth) and estuarine sandstones and highly bioturbated shoreface sandstones with some interbedded mudstone. The coarse sandstones here have a different log response compared to the blocky thick clean sand bodies shown in yellow in Figure 19, which may resemble the delta-front turbidite massive sandstones in conventional core at Thebaud C-74. In the Logan Canyon Formation, several such units in Naskapi N-30 are equivalent in the more proximal Sambro I-29 well to cleaning-up sandstone beds and interbedded mudstones (the magenta units in Figure 19). These may be prograded shoreface sands laterally equivalent to the river mouth facies.

2. Source of sediment to Naskapi N-30 and Sambro I-29

It seems likely that the Naskapi and Sambro wells, only 25 km apart on a dip line seaward of the paleoshoreline trend, received most of their sediment from the same source. The cored section in Naskapi N-30 is at a stratigraphic level very close to cuttings sample 3740 from Sambro I-29. Other analysed samples from Sambro I-29 are 3170 from the Cree Member, in distal muddy sandstone, and a series of deeper samples from the Missisauga Formation, which are from mixed muddy sandstones, shales and in some cases blocky sandstones.

Sandstone from the Naskapi N-30 well is similar to that of the Chaswood Formation in bulk composition (Fig. 11). Lithic clasts are almost exclusively polycrystalline quartz (cf. Gobeil et al. 2006). There are also several similarities in mineral chemistry: particularly the similarity of muscovite to that from the Shubenacadie basin (Fig. 7). Ilmenite composition is also similar and demonstrates a lack of a significant Meguma terrane source (Fig. 9). The sparse monazite is also similar (Fig. 10). Biotite more closely resembles that of the Chaswood Formation than biotite from elsewhere in the Scotian basin (Fig. 16). However, other minerals show differences. Tourmaline more closely resembles the southwest Scotian basin than the Chaswood Formation (Fig. 8), as does rutile (Fig. 17).

The one analysed silty mudstone from the Sable Member in Sambro I-29 has similar bulk chemistry as sandstone of the Chaswood Formation, but is more arkosic than at Naskapi N-30 and most resembles sandstones of the Upper Member of the Chaswood Formation (Fig. 11).

As at Naskapi, most lithic clasts at Sambro I-29 are polycrystalline quartz. The feldspar compositions and abundances are similar to those of the Chaswood Formation (Fig. 15). The

greater abundance of feldspar at Sambro I-29 as compared with Naskapi N-30 is largely an artefact of sampling at different stratigraphic levels; in both wells, feldspar is very rare at the top of the Missisauga Formation and kaolinite cement is abundant, suggesting that there was some diagenetic effects of meteoric water and thus possibly an unconformity at this level. Interpretation of Sambro I-29 is limited by the need to work with cuttings samples and mineralogical data extends from the Cree Member to the Missisauga Formation. There may be important stratigraphic variation in the source of minerals. Overall, muscovite has a rather different compositional range from that at Naskapi N-30 (Fig. 7) and is more like that in southwest Scotian basin. It may be that much of the muscovite in Sambro is in more distal sands with the readily transported muscovite partly derived from the southwest Sable sub-basin.

In contrast to Naskapi N-30, the Lower Cretaceous of the southwestern Sable sub-basin in the Alma, Glenelg and North Triumph fields (Fig. 20) includes marker minerals such as chromite and paragonite not known from the Chaswood Formation, together with Proterozoic detrital monazite. These data point to a source farther east than the most easterly Chaswood Formation (Diogenes Brook in Cape Breton Island) (Fig. 1), likely from uplifted Grenville basement and ophiolites of western Newfoundland. This sediment might have been transported either by an ancestral St Lawrence river, with tributaries draining western Newfoundland, or from a smaller river draining only western Newfoundland.

Sandstones from the Peskowesk A-99 well (Pe-Piper et al. 2006a) are quite different from those of the southwestern Sable sub-basin (Pe-Piper et al. 2004b). At Peskowesk, the feldspar assemblage is dominated by K-feldspar (perthite) and lithic clasts are principally rhyolite - syenite - microgranite. Spessartine garnet is common in the southwestern Sable sub-basin, but was not detected at Peskowesk. Tourmaline is much less common at Peskowesk and the single analysed grain was derived from granite, compared with a metasedimentary source for tourmaline in the southwestern Sable sub-basin. Ilmenite, biotite and muscovite are more abundant at Peskowesk than in the southwest Sable sub-basin. Less comprehensive data from Dauntless D-35 in the east suggests that it received rather different sediment than did Peskowesk A-99.

Overall, the chemical and mineralogical data suggest that Naskapi N-30 and Sambro I-29 received similar sediment that substantially resembles that of the Chaswood Formation. There may have been some input from a river farther to the east, supplying more abundant tourmaline,

rutile and muscovite than the Chaswood Formation river system.

3. Stratigraphic correlation with the Chaswood Formation

The Chaswood Formation in Nova Scotia and New Brunswick has a local supply of lithic clasts from bedrock of the southern Appalachians (Pe-Piper et al. 2004a,c, 2005; Gobeil et al. 2006; Piper et al. 2007b), with some diagnostic minerals reworked from Carboniferous sediments. Assessment of primary detrital petrology in the Chaswood Formation is hindered by the pervasive alteration by meteoritic water, resulting in alteration of feldspars and ilmenite and even in some cases monazite and zircon. The source region developed a horst and graben topography in response to strike-slip motion along the Cobequid–Chedabucto fault zone and NE-trending splays (Pe-Piper and Piper, 2004a). U-Pb monazite dating shows that rocks supplying detritus to the Chaswood Formation were principally of Taconic age, likely from northern New Brunswick and three discrete rivers are recognised as having deposited the Chaswood Formation (Pe-Piper and MacKay, 2006). The central river drained through central Nova Scotia and is represented by thick gravelly sands at the West Indian Road pit (Gobeil et al., 2006) and in boreholes from the Shubenacadie Basin (Fig. 20).

In central Nova Scotia, the Chaswood Formation can be divided into four seismic packets (Fig. 20) (Piper et al., 2005) that are separated by intraformational unconformities (Hundert et al., 2006) as a result of syn-sedimentary deformation along faults related to dextral slip of the master Cobequid–Chedabucto fault zone (Pe-Piper and Piper, 2004a; Gobeil et al., 2006). Similar stratigraphic relationships to Early Cretaceous deformation are recognised at other Chaswood Formation localities such as Brierly Brook (Pe-Piper et al., 2005b) and Vinegar Hill (Piper et al., 2007b).

Sparse biostratigraphic data from the Chaswood Formation (Fig. 21) suggest that seismic packet 1, corresponding to the Lower Member of Stea and Pullan (2001), ranges in age from Valanginian to Aptian (Falcon-Lang et al., 2007). The Middle Member (seismic packet 2) is of Albian age, based on the presence of angiosperms reported by Eisnor (2002). The Upper Member (seismic packets 3 and 4) are not dated. At Vinegar Hill, lithostratigraphic correlation of the sand and gravel units is speculative, but these rocks are most likely part of the Upper Member (Piper et al., 2007b) and have been determined to most likely be of late Albian age by Falcon-Lang et al. (2003). The three intraformational unconformities in the Chaswood Formation

can be tentatively correlated with the top-Missisauga, top-Cree and early Cenomanian unconformities seen further along strike in Orpheus graben and the southwestern Grand Banks (Pe-Piper and Piper, 2004a). The biostratigraphic age of the Middle Member is similar to that of the Naskapi Member on the Scotian Shelf.

In the Shubenacadie basin, there are three horizons of thick, coarse-grained, gravelly sandstone beds: in the upper part of the Lower Member, in seismic packet 3 in the Upper Member and in seismic packet 4 in the Upper Member. The limited biostratigaphic control suggests that these correlate with the three major coarse sand packets in the Naskapi N-30 well (Fig. 2), namely the upper part of the Missisauga Formation, the Cree Member and the Marmora Member (Fig. 22).

Conclusions

1. Cored upper Missisauga Formation sandstone from the Naskapi N-30 well shows delta-front turbidites interbedded with more estuarine bioturbated fine sandstones.

2. The analysed sandstones from Naskapi N-30 and Sambro I-29 differ from those farther east in the Scotian basin in their low abundance of feldspar, predominance of polycrystalline quartz in the lithic fraction, and lack of paragonite and chromite. They show strong mineralogical similarities to the Chaswood Formation of central Nova Scotia, notably in the composition of muscovite, ilmenite, monazite, and biotite. They also resemble the Chaswood Formation in bulk geochemistry. Some detrital minerals, including rutile and tourmaline, are rather different from those in the Chaswood Formation.

3. Early diagenetic phosphorite is found in the Cree Member at Sambro I-29 and is comparable with phosphorite found in proximal sediments in Orpheus graben.

4. Major sandy intervals in the upper Mississauga Formation, Cree Member and Marmora Member probably correlate with thick sands in the upper part of seismic packet 1, seismic packet 3 and seismic packet 4 of the Chaswood Formation.

References

Ascoli, P. 1988. Mesozoic-Cenozoic foraminiferal, ostracod and calpionellid zonation of the North Atlantic margin of North America: Georges Bank-Scotian Basins and northeastern Grand Banks (Jeanne d'Arc, Carson and Flemish Pass Basins). Biostratigraphic correlation of 51 wells. GSC Open File 1791, 41 p.

Bann, K.L., Fielding, C.R., MacEachern, J.A. and Tye, S.C. 2004. Differentiation of estuarine and offshore marine deposits using integrated ichnology and sedimentology: Permian Pebbley Beach Formation, Sydney Basin, Australia. Geological Society of London Special Publication 228, 273-310.

Barss, M.S., Bujak, J.P., Williams, G.L., 1979. Palynological zonation and correlation of sixty-seven wells, eastern Canada. Geological Survey of Canada, Paper 78-24, 117 p

Bhatia, M. R., 1983. Plate tectonics and geochemical composition of sandstones. Journal of Geology, 91, 611-627.

CNSOPB (Canada - Nova Scotia Offshore Petroleum Board), 2000, Technical summaries of Scotian Shelf significant and commercial discoveries: Halifax, N.S., 257 p.

Cummings, D.I., Hart, B.S. and Arnott, R.W.C., 2006a. Sedimentology and stratigraphy of a thick, areally extensive fluvial-marine transition, Missisauga Formation, offshore Nova Scotia, and its correlation with shelf margin and slope strata. Bulletin of Canadian Petroleum Geology, 54, 152-174.

Cummings, D.I. and Arnott, R.W.C. 2005. Shelf margin deltas: a new (but old) play type offshore Nova Scotia. Bulletin of Canadian Petroleum Geology, 53, 211-236.

Cummings, D. I., Arnott, R.C.W. and Hart, B.S. 2006b. Tidal signatures in a shelf-margin delta. Geology, 34, 249-252.

Eisnor, K., 2002. Paleoenvironmental analysis of the Lower Cretaceous (Aptian-Albian) sediments of the Musquodoboit and Shubenacadie basins, Nova Scotia. Abstract, Atlantic Geoscience Society, 2002 Annual Colloquium, p. 15.

Falcon-Lang, H., Fensome, R.A. and Venugopal, D.V., 2003, The Cretaceous age of the Vinegar Hill silica deposit of southern New Brunswick: evidence from palynology and paleobotany: Atlantic Geology, 39, 39-46.

Falcon-Lang, H.J., Fensome, R.A., Gibling, M.R., Malcolm, J., Fletcher, K.R., and Holleman, M., 2007. Karst-related outliers of the Cretaceous Chaswood Formation of Maritime

Canada. Canadian Journal of Earth Sciences, 44, 619-642.

Gobeil, J.-P., Pe-Piper, G., and Piper, D.J.W. 2006. The Early Cretaceous Chaswood Formation in the West Indian Road pit, central Nova Scotia. Canadian Journal of Earth Sciences, 43, 391-403.

Henry, D. J., and Guidotti, C. V. 1985. Tourmaline as a petrogenetic indicator mineral: an example from the staurolite-grade metapelites of NW Maine. American Mineralogist, 70, 1-15.

Hundert, T., Piper, D.J.W. and Pe-Piper, G., 2006. Genetic model and exploration guidelines for kaolin beneath unconformities in the Lower Cretaceous fluvial Chaswood Formation, Nova Scotia. Exploration and Mining Geology, 15, 9-26.

Kassoli-Fournaraki, A. and Michailidis, K., 1994: Chemical composition of tourmaline in quartz veins from Nea Roda and Thasos areas in Macedonia, Northern Greece. Canadian Mineralogist, 32, 607-615.

Lentin International Biostrat. 1989. Biostratigraphic and maturation studies of the Scotian Shelf. Part 3. Union et al. Sambro I-29. GSC Open File 1854, 21 p

MacEachern, J.A., Bann, K.L., Bhattacharya, J.K. and Howell, C.D., 2005. Ichnology of deltas: organism responses to the dynamic interplay of rivers, waves, storms and tides. In: River deltas – concepts, models and examples, Bhattacharya, J.K. and Giosan, L. (eds.), SEPM Special Publication 83, 49-85.

MacLean, B.C. and Wade, J.A. 1993. Seismic markers and stratigraphic picks in Scotian Basin wells. Atlantic Geoscience Centre, Geological Survey of Canada.

MacRae, R.A. and Jauer, C. 2001. Sequence stratigraphy and palynology, Upper Missisauga Formation, Glenelg area, offshore Nova Scotia. [abstract of poster]. Atlantic Geology, 37, 117.

Myrow, P.M., Fischer, W. and Goodge, J.W., 2002. Wave-modified turbidites: combined-flow shoreline and shelf deposits, Cambrian, Antarctica. Journal of Sedimentary Research, 72, 641-656.

Pe-Piper, G. and Mackay, R.M. 2006. Electron microprobe geochronology and chemical variation of detrital monazite from the Lower Cretaceous sandstones of the Scotian basin and the Chaswood Formation, eastern Canada. Geological Survey of Canada Open File 5023.

Pe-Piper, G. and Mackay, R.M. 2006. Provenance of Lower Cretaceous sandstones onshore and offshore Nova Scotia from electron microprobe geochronology and chemical variation of detrital monazite. Bulletin of Canadian Petroleum Geology, 54, 366-379.

Pe-Piper, G. and Piper, D.J.W. 2004a. The effects of strike-slip motion along the Cobequid-Chedabucto-SW Grand Banks fault system on the Cretaceous - Tertiary evolution of Atlantic Canada. Canadian Journal of Earth Sciences, 41, 799-808.

Pe-Piper, G., and Piper, D.J.W., 2004b. The geology of the Chaswood Formation of Nova Scotia and New Brunswick. Final report for ExxonMobil Sable project.

Pe-Piper, G., Dolansky, L., and Piper, D.J.W. 2004a. Petrography of the mid-Cretaceous Chaswood Formation in borehole RR-97-23, Elmsvale Basin, Nova Scotia: sedimentary environment, detrital mineralogy and diagenesis. Geological Survey of Canada Open File 4837, 231 p.

Pe-Piper, G., Piper, D.J.W., and Dolansky, L.M., 2005a. Alteration of ilmenite in the Cretaceous sands of Nova Scotia, southeastern Canada. Clays and Clay Minerals, 53, 490-510.

Pe-Piper, G., Piper, D.J.W., Gould, K.M. and Shannon, J. 2006a. Depositional environment and provenance analysis of the Lower Cretaceous sedimentary rocks at the Peskowesk A-99 well, Scotian Basin. Geological Survey of Canada, Open File 5383, 171 p.

Pe-Piper, G., Piper, D.J.W., Hundert, T. and Stea, R.R. 2005b. Outliers of Lower Cretaceous Chaswood Formation in northern Nova Scotia: results of scientific drilling and studies of sedimentology and sedimentary petrography. Geological Survey of Canada Open File 4845, 305 p.

Pe-Piper, G., Okwese, A. and Piper, D.J.W., 2006b. Volcanic ash and lignite of the Lower Cretaceous Chaswood Formation, central Nova Scotia. Geological Survey of Canada Open File 4973.

Pe-Piper, G., Piper, D.J.W., Vaughan, A.D., Shannon, J. and Ingram S., 2004b. Sedimentary petrology of Lower Cretaceous rocks of the southwestern Sable sub-basin (North Triumph B-52, Alma K-85 and Glenelg N-49 wells), Scotian Basin. Geological Survey of Canada, Open File 4836.

Pe-Piper, G., Stea, R.R., Ingram, S., and Piper, D.J.W. 2004c. Heavy minerals and sedimentary petrology of the Cretaceous sands from the Shubenacadie outlier, Nova Scotia. Nova Scotia Department of Natural Resources, Open File Report ME 2004-5, 78 p.

Piper, D.J.W., Pe-Piper, G. and Ingram, S.I., 2004. Early Cretaceous sediment failure in the southwestern Sable sub-basin, offshore Nova Scotia. American Association of Petroleum Geologists Bulletin, 88, 991-1006.

Piper, D.J.W., Pe-Piper, G. and Douglas, E.V., 2005. Tectonic deformation and its sedimentary consequences during deposition of the Lower Cretaceous Chaswood Formation, Elmsvale basin, Nova Scotia. Bulletin of Canadian Petroleum Geology, 53, 189-199.

Piper, D.J.W., Noftall, R., McKee, H. and Pe-Piper, G., 2007a. How to get into deep water:sand transported seaward of early Cretaceous deltas in the Scotian basin. [abstract of poster]. Atlantic Geology, 43, 24.

Piper, D.J.W., Pe-Piper, G., Hundert, T. and Venugopal, D.K., 2007b. The Lower Cretaceous Chaswood Formation in southern New Brunswick: provenance and tectonics. Canadian Journal of Earth Sciences, 44, 665-677.

Shell, 1970. Well history report and logs, Naskapi N-30. On file with Canada Nova Scotia Offshore Petroleum Board.

Stea, R. and Pullan, S. 2001. Hidden Cretaceous basins in Nova Scotia. Canadian Journal of Earth Sciences, 38, 1335-1354.

Weir-Murphy, S.L., 2004. Cretaceous rocks of the Orpheus graben, offshore Nova Scotia. M.Sc. thesis, Saint Mary's University.

Williams, H. and Grant, A.C. 1998. Tectonic assemblages, Atlantic region, Canada. [1:3m map]. Geological Survey of Canada Open File 3657, 1 sheet.

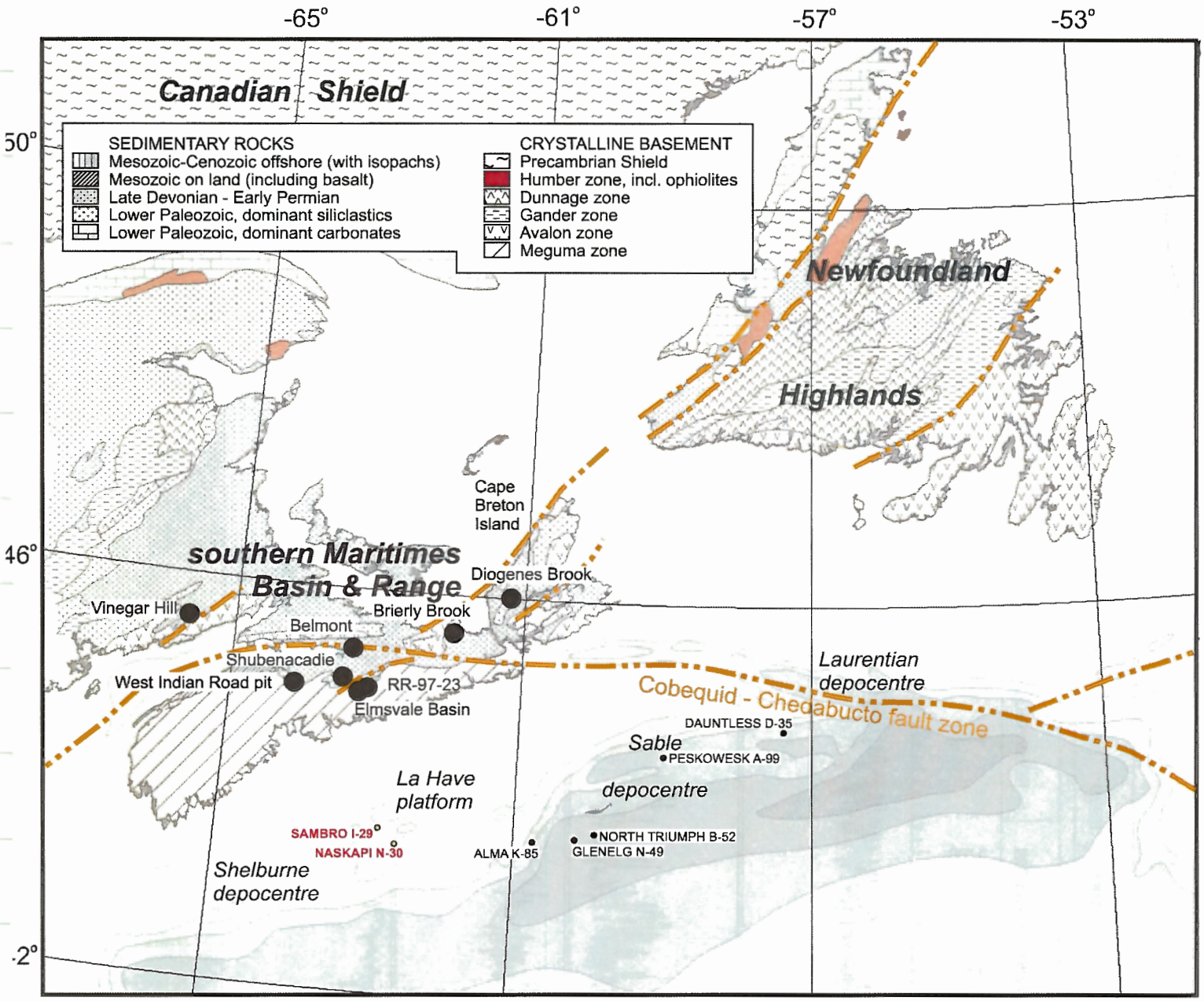

Fig. 1. Map showing location of Sambro I-29 and Naskapi N-30 wells. Also shows principal areas of Chaswood Formation on land (black dots), 2 km isopachs of offshore basins, principal rock types on land, and key paleogeographic elements of the early Cretaceous. Base map from Williams and Grant (1998).

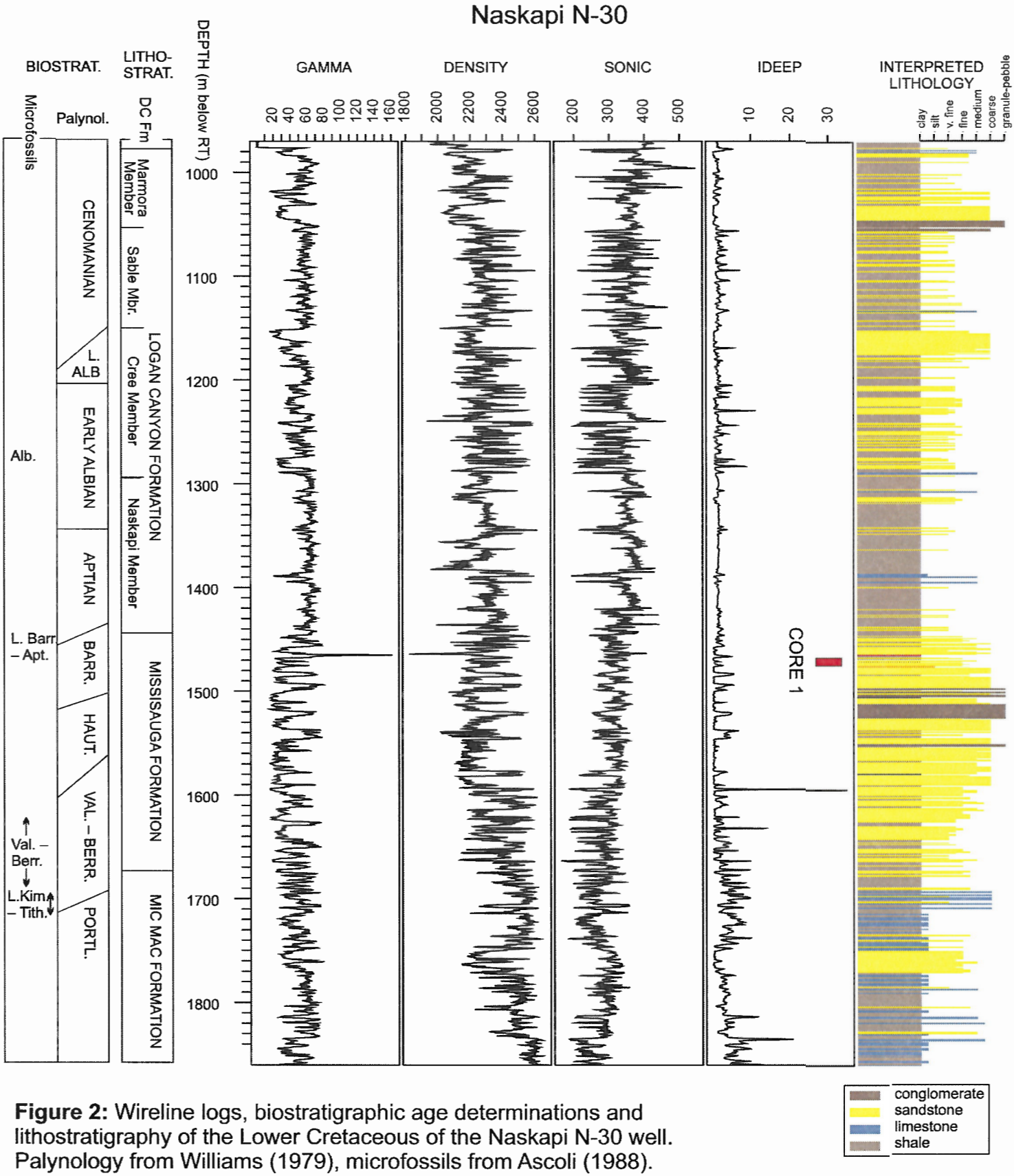

Figure 2: Wireline logs, biostratigraphic age determinations and lithostratigraphy of the Lower Cretaceous of the Naskapi N-30 well. Palynology from Williams (1979), microfossils from Ascoli (1988). Lithostratigraphy from MacLean and Wade (1993), subdivision of upper part of Logan Canyon Formation from this study. Schematic lithologic column interpreted from wireline logs using software developed by A. MacRae.

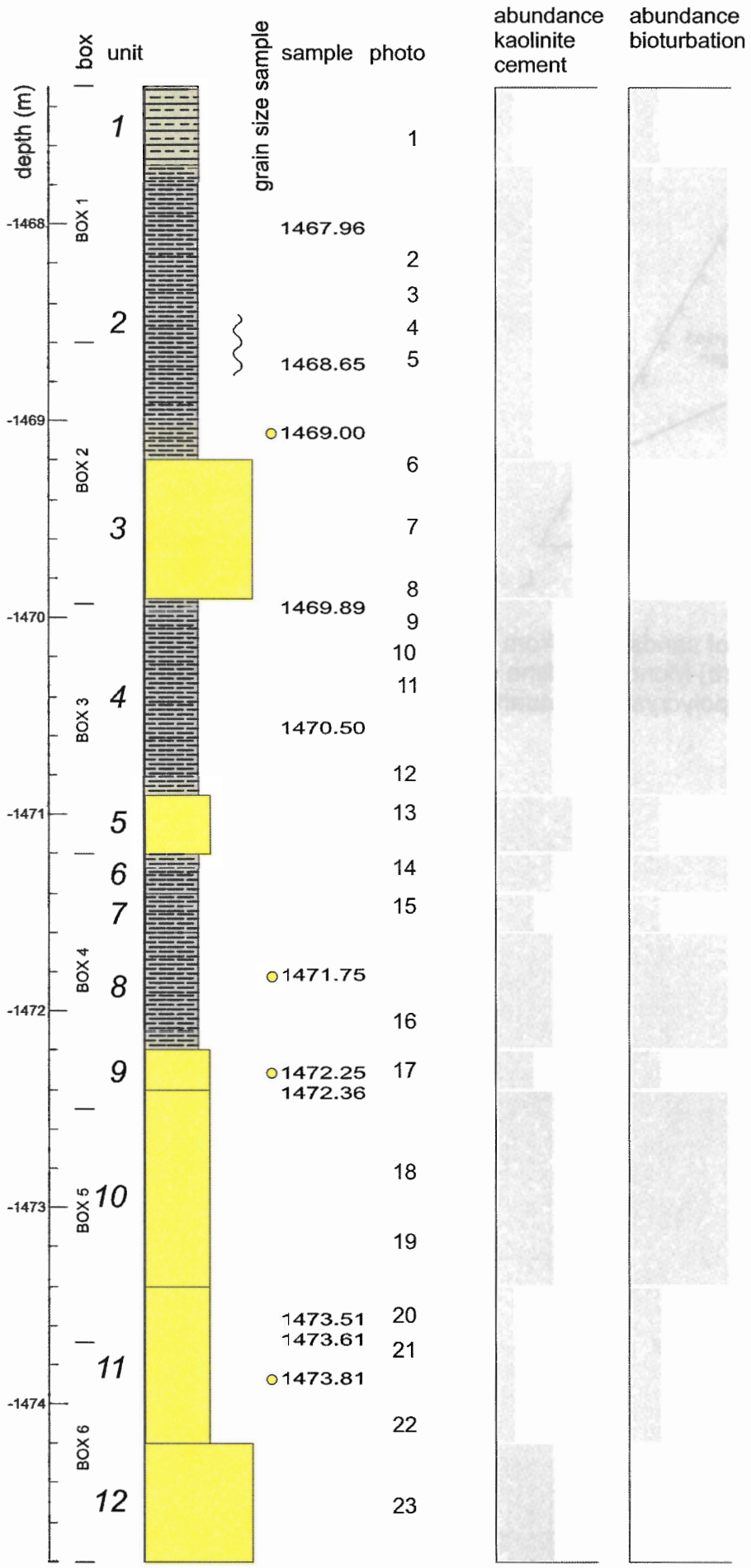

Figure 3: Log of conventional core from Naskapi N-30

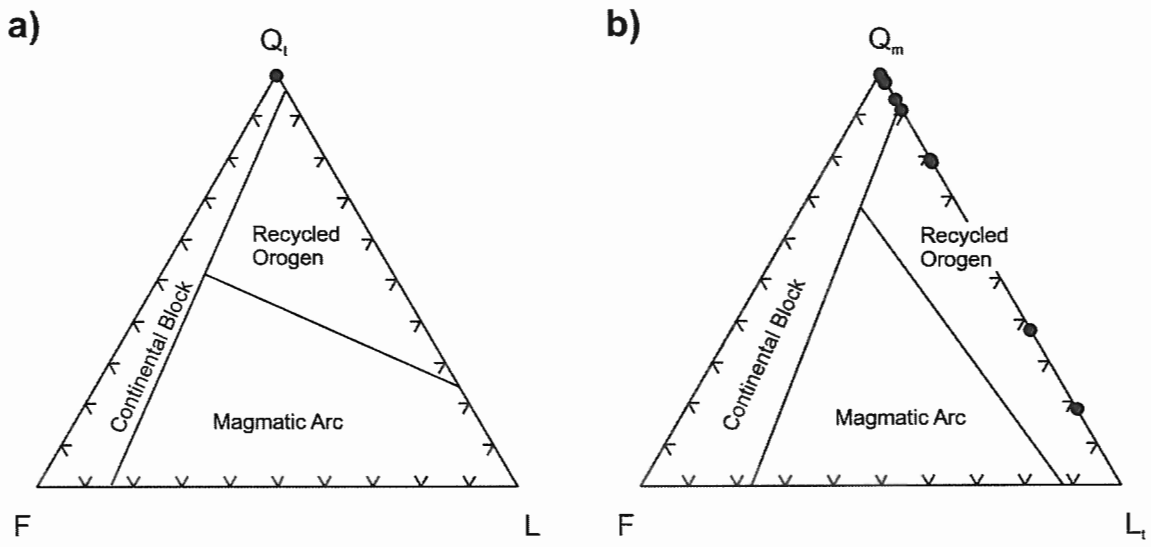

Figure 4: QFL plots of sandstones from Naskapi N-30. (a) Total quartz, feldspars and lithic fragments; (b) Monocrystalline quartz, feldspars and total lithic fragments (including polycrystalline quartz).

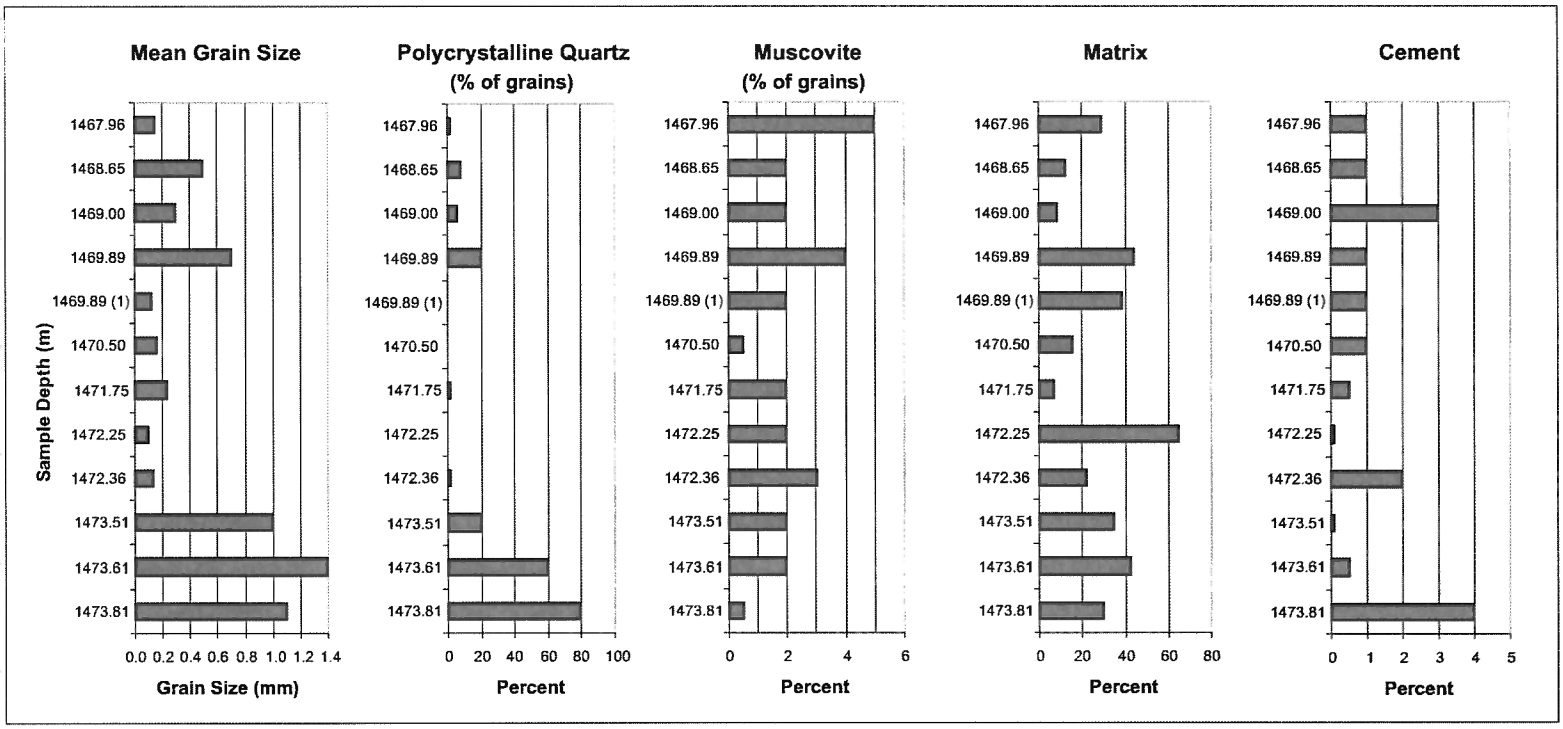

Figure 5: Modal distribution with depth of selected components of sandstones from conventional core in Naskapi N-30.

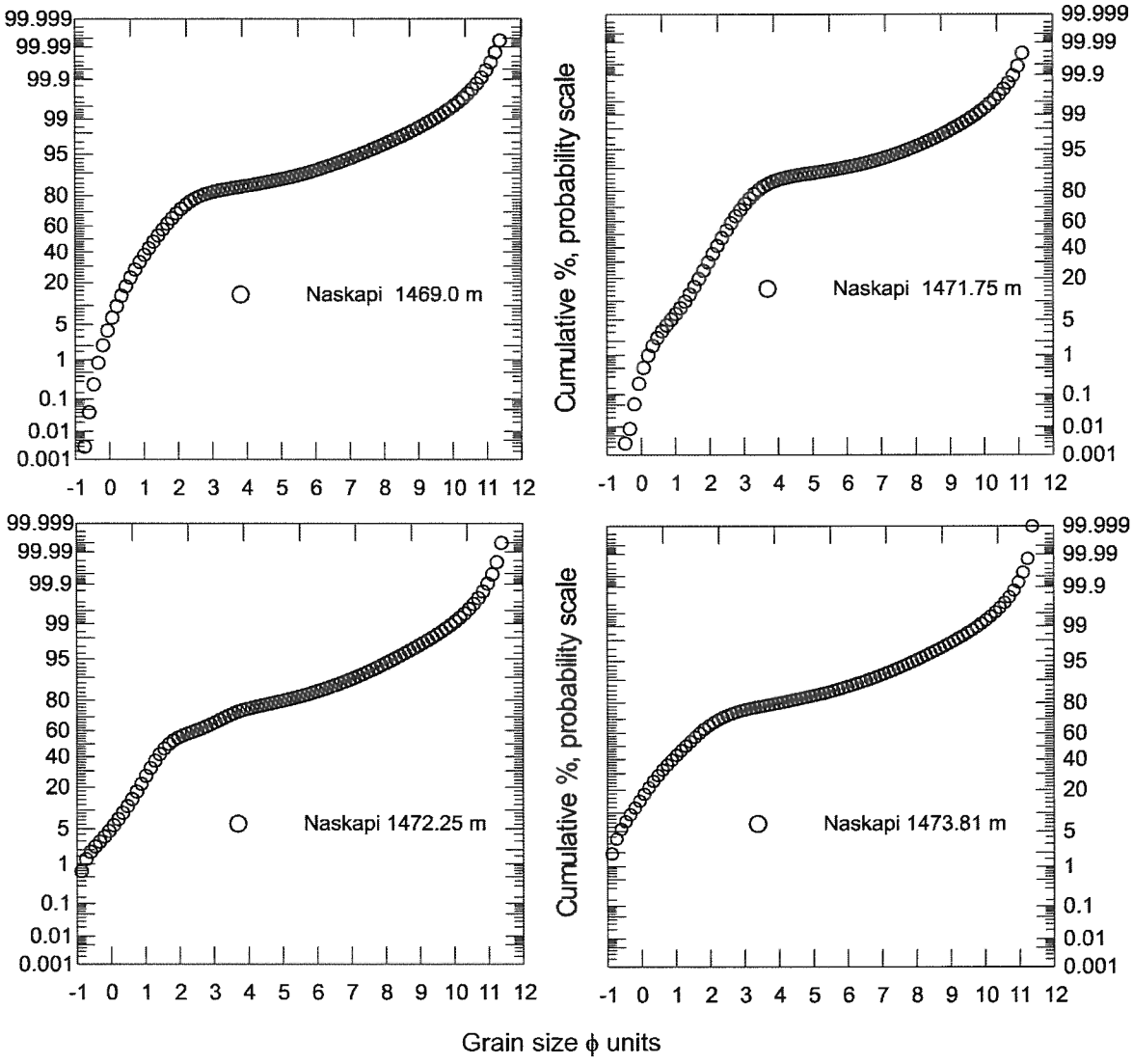

Figure 6: Grain size analyses of sands from Naskapi N-30. Plotted as cumulative frequency plots on a probability scale: analysis by Coulter laser analyser.

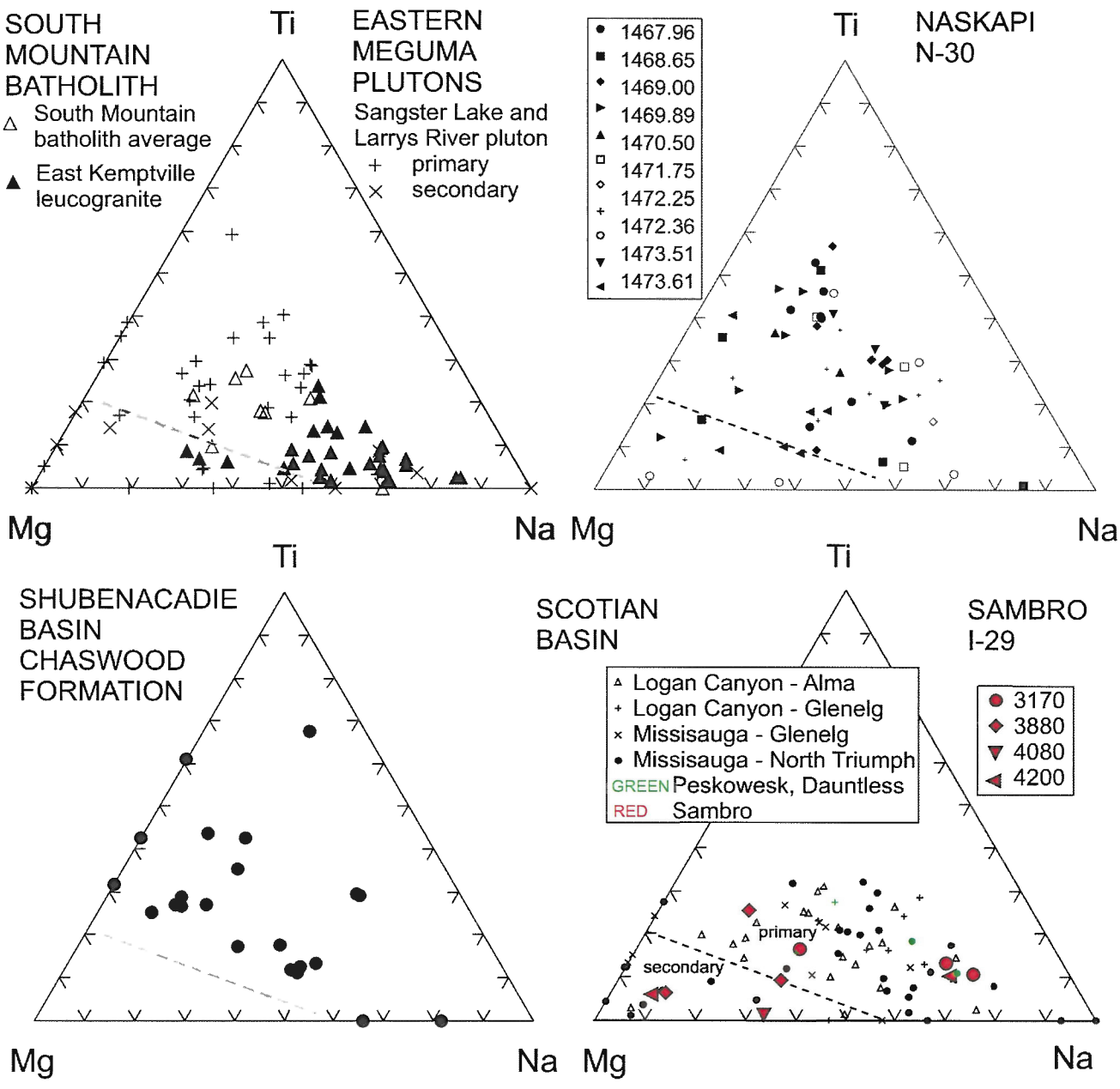

Figure 7: Composition of muscovite from Naskapi N-30 and Sambro I-29 compared with muscovite from elsewhere in the Scotian basin, the Chaswood Formation, and potential source plutons in the Meguma terrane.

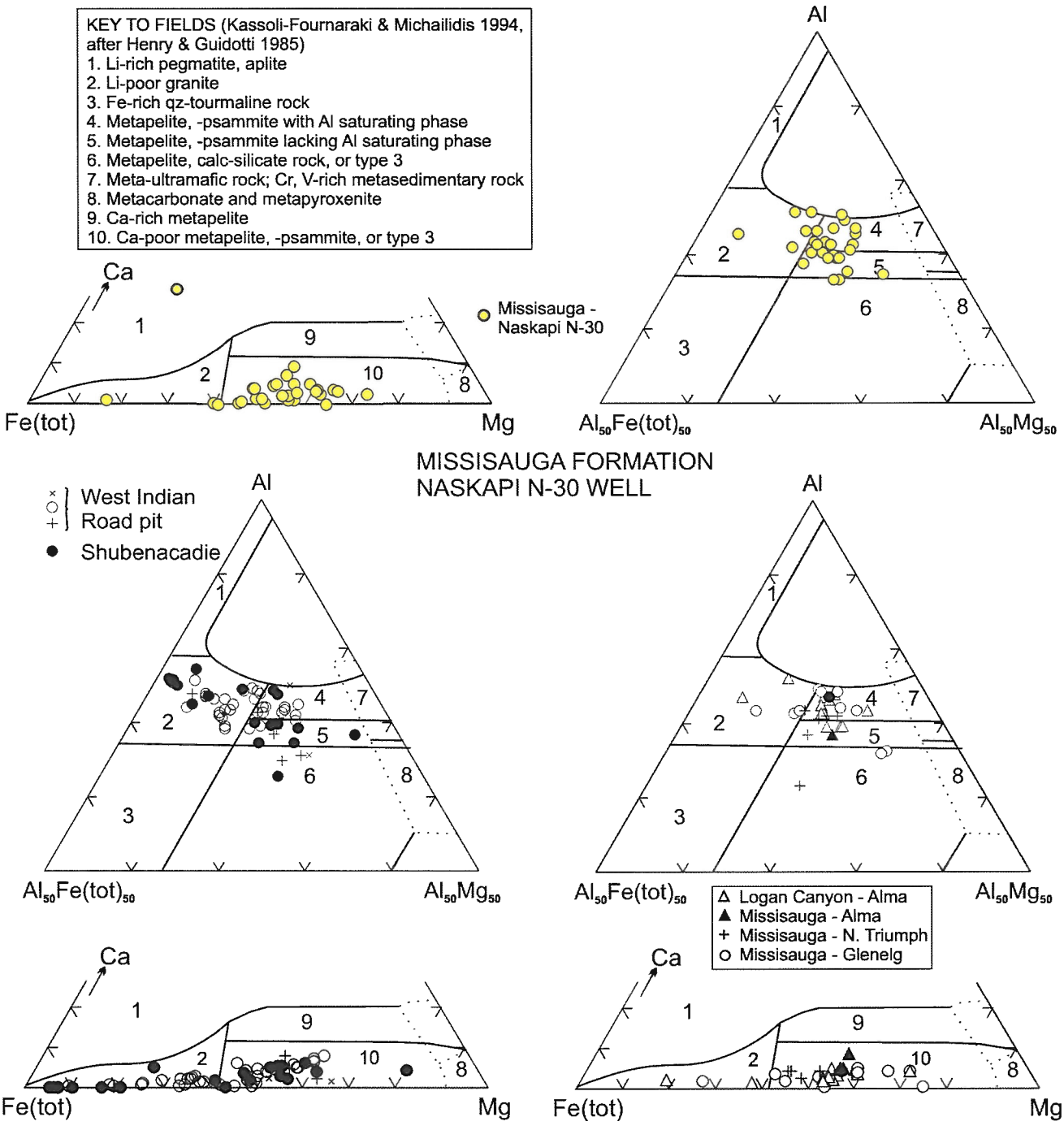

CHASWOOD FORMATION
CENTRAL NOVA SCOTIA

LOGAN CANYON AND MISSISAUGA FORMATIONS
SOUTH-EAST SABLE SUB-BASIN

Figure 8: Chemical composition of tourmaline from the Naskapi N-30 well compared with tourmaline from the southeast Sable sub-basin and the Chaswood Formation.

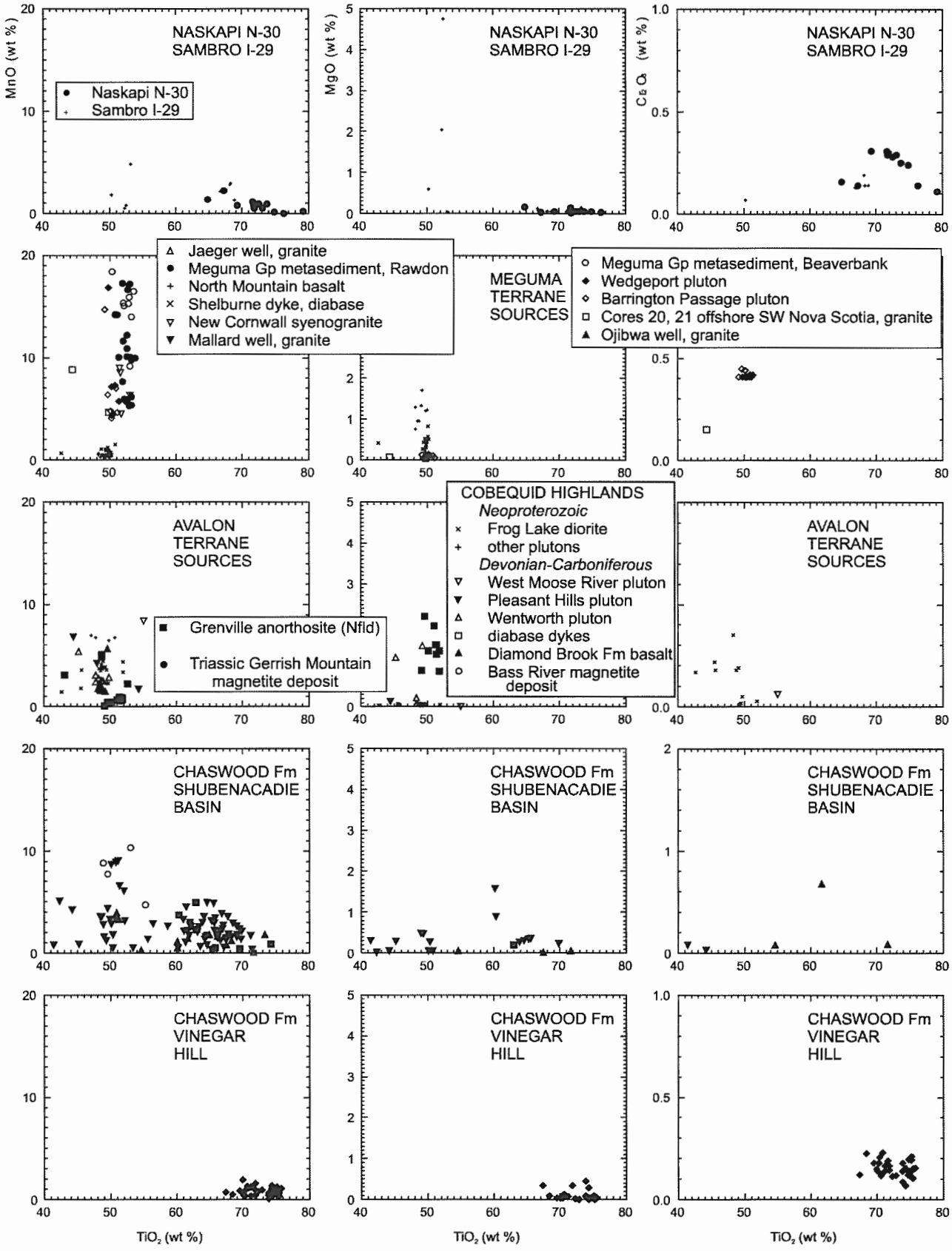

Figure 9: Chemical variation in ilmenite and altered ilmenite in Naskapi N-30 and Sambro I-29 compared with potential source rocks in the Meguma and Avalon terranes and Chaswood Formation at Shubenacadie and Vinegar Hill.

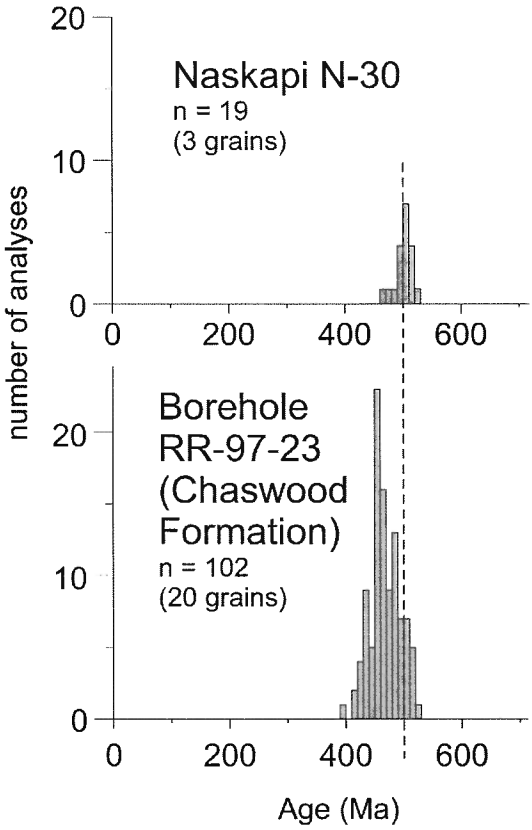

Figure 10: Electron microprobe chemical age determinations from monazite in the Naskapi N-30 well compared with determinations from the Chaswood Formation at borehole RR-97-23 in the Elmsvale basin.

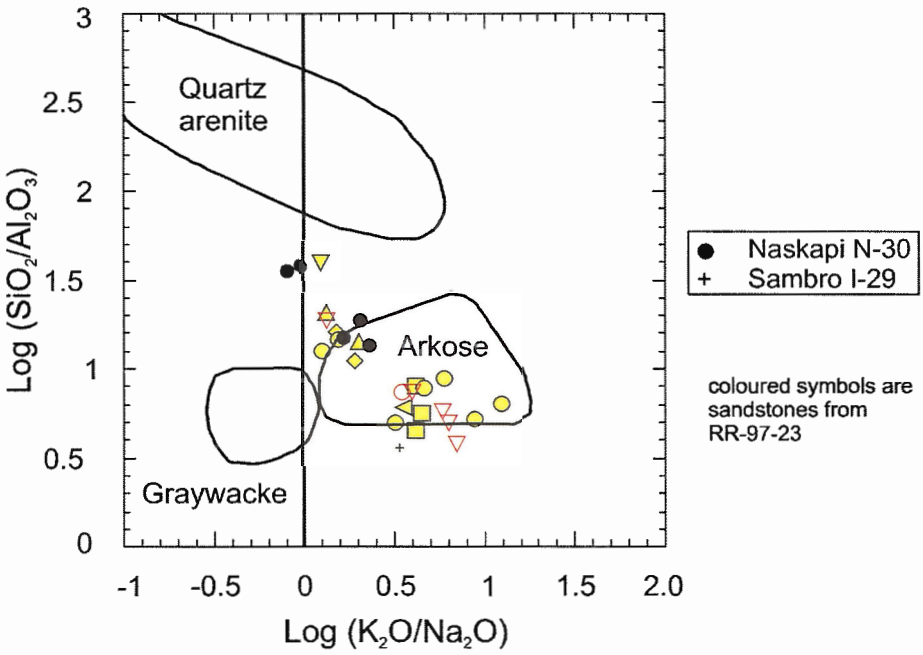

Figure 11: Geochemical classification of sandstone in the Naskapi N-30 and Sambro I-29 wells.

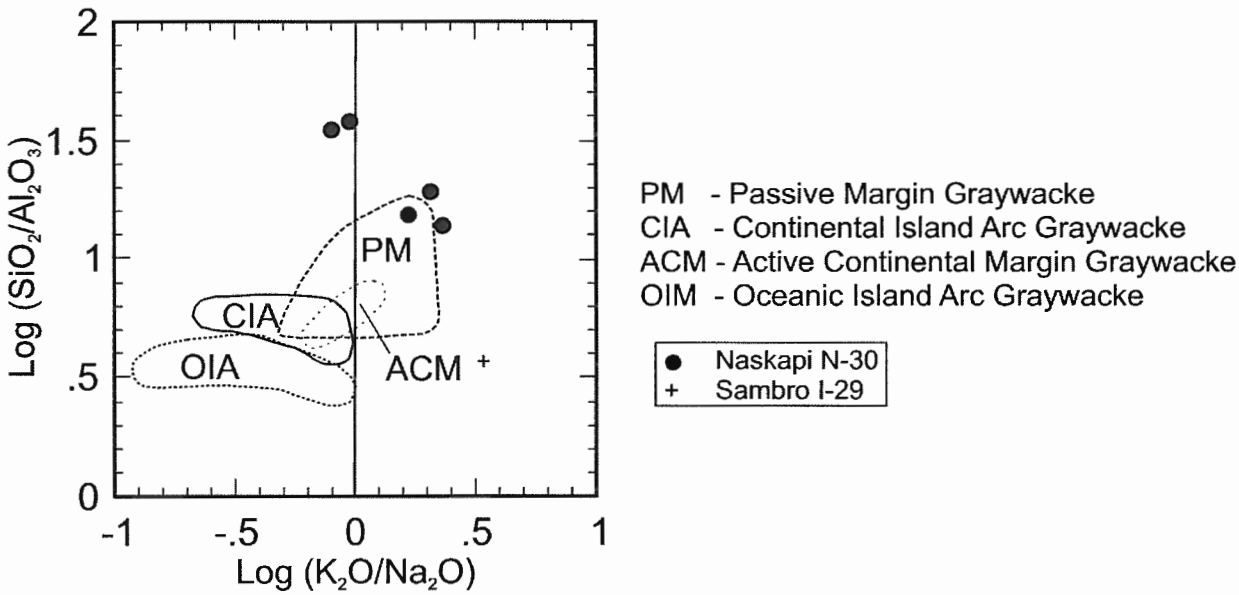

Figure 12: Geochemical classification of tectonic affinity of source area for sandstone in the Naskapi N-30 and Sambro I-29 wells.

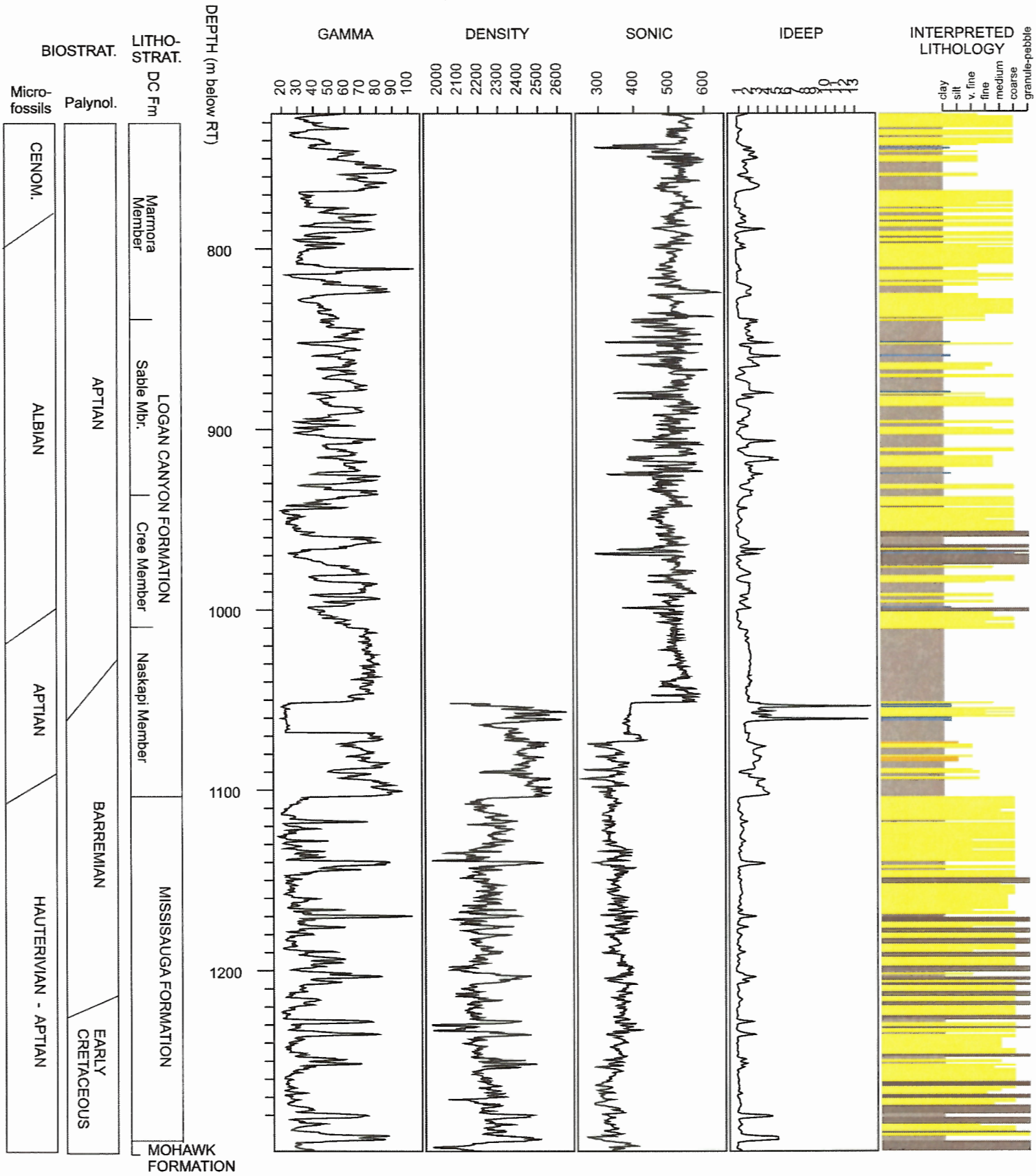

Figure 13: Wireline logs, biostratigraphy and lithostratigraphy of the Lower Cretaceous of the Sambro I-29 well. Palynology and microfossils from Lentin (1987). Lithostratigraphy from MacLean and Wade (1993), subdivision of upper part of Logan Canyon Formation from this study. Schematic lithologic column interpreted from wireline logs using software developed by A. MacRae. Legend as in Fig. 2.

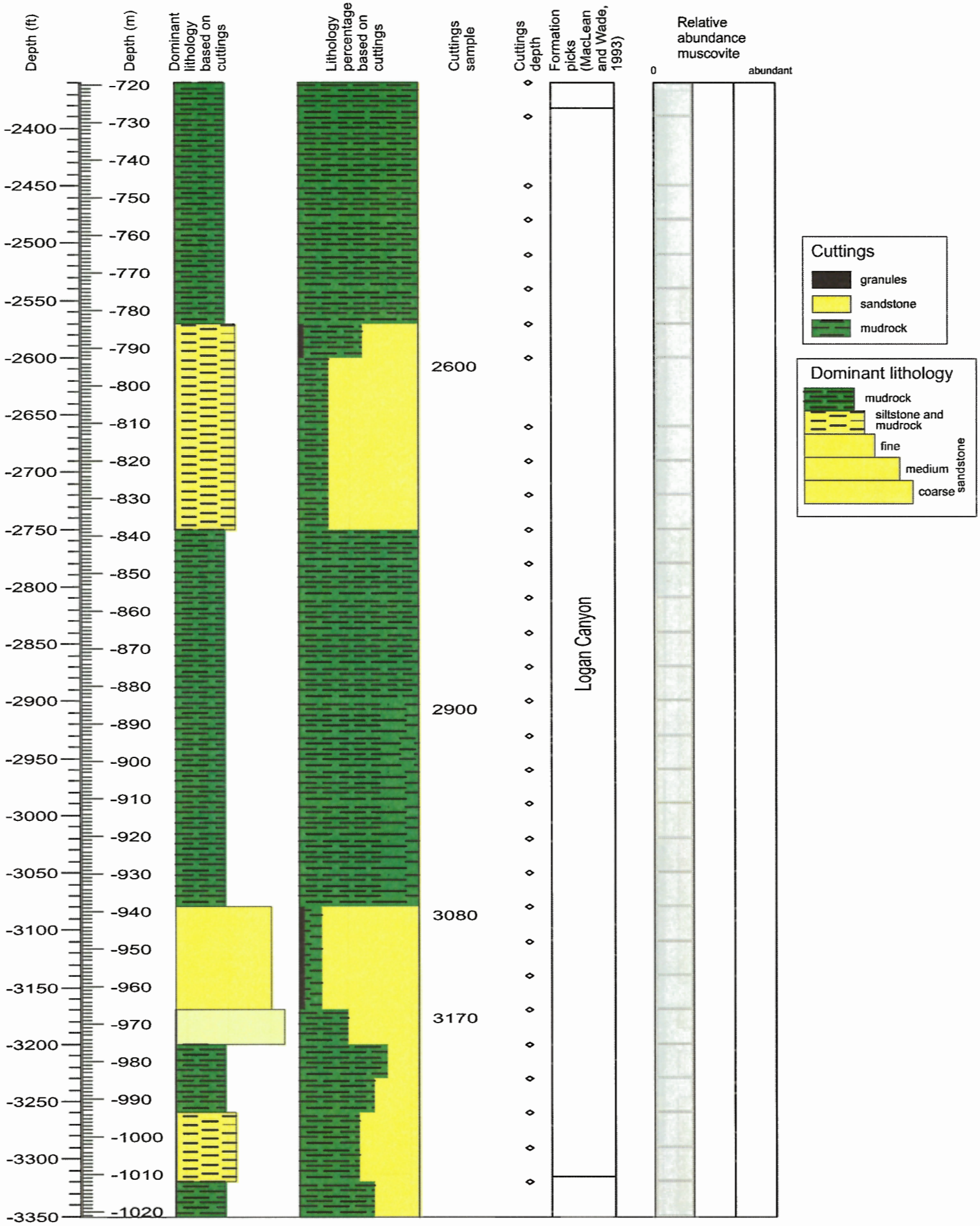

Figure 14a: Log based on cuttings samples of the Logan Canyon Formation (Cree to Marmora members) of Sambro I-29.

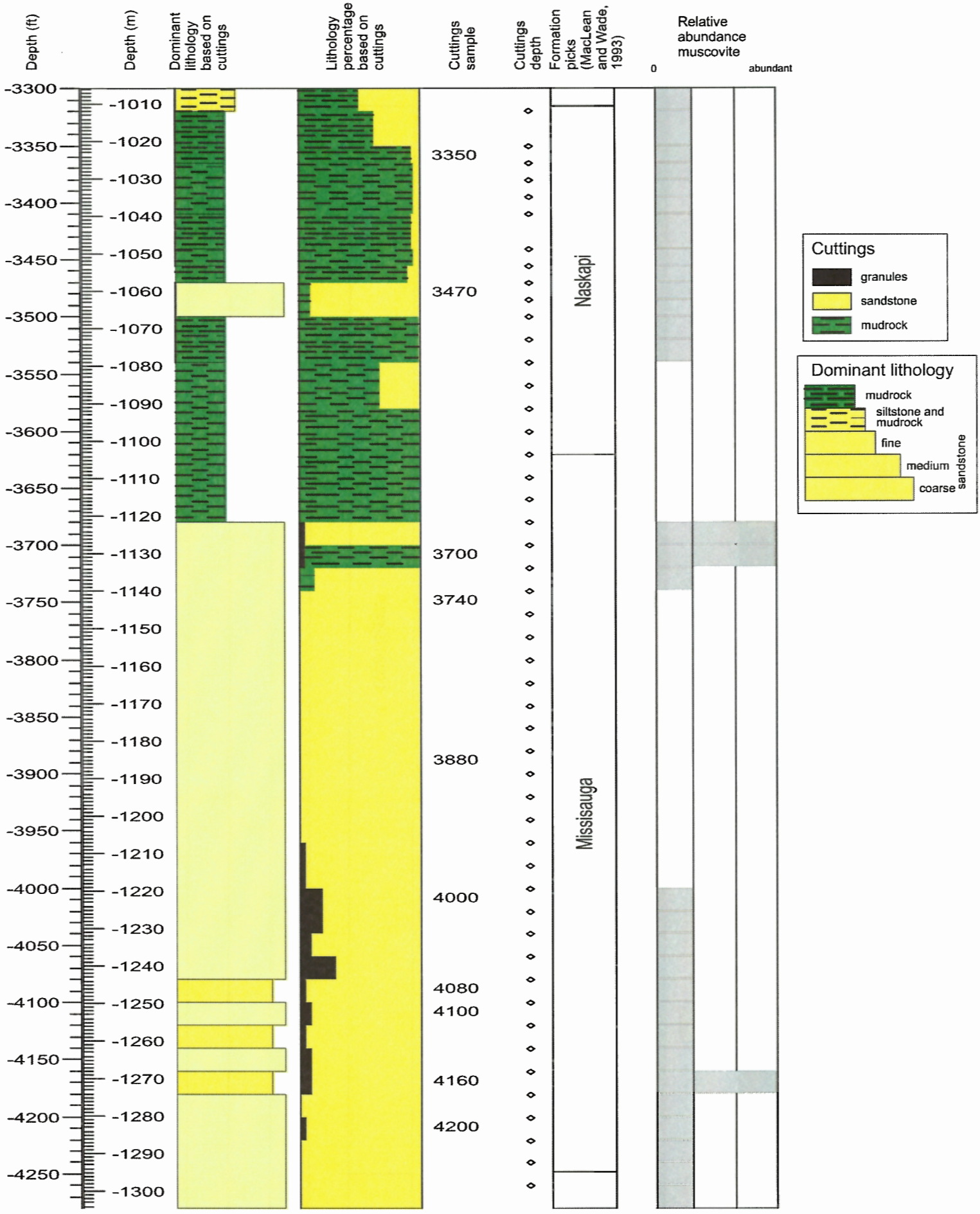

Figure 14b: Log based on cuttings samples of the Logan Canyon Formation (Naskapi member) and Missisauga Formation of Sambro I-29.

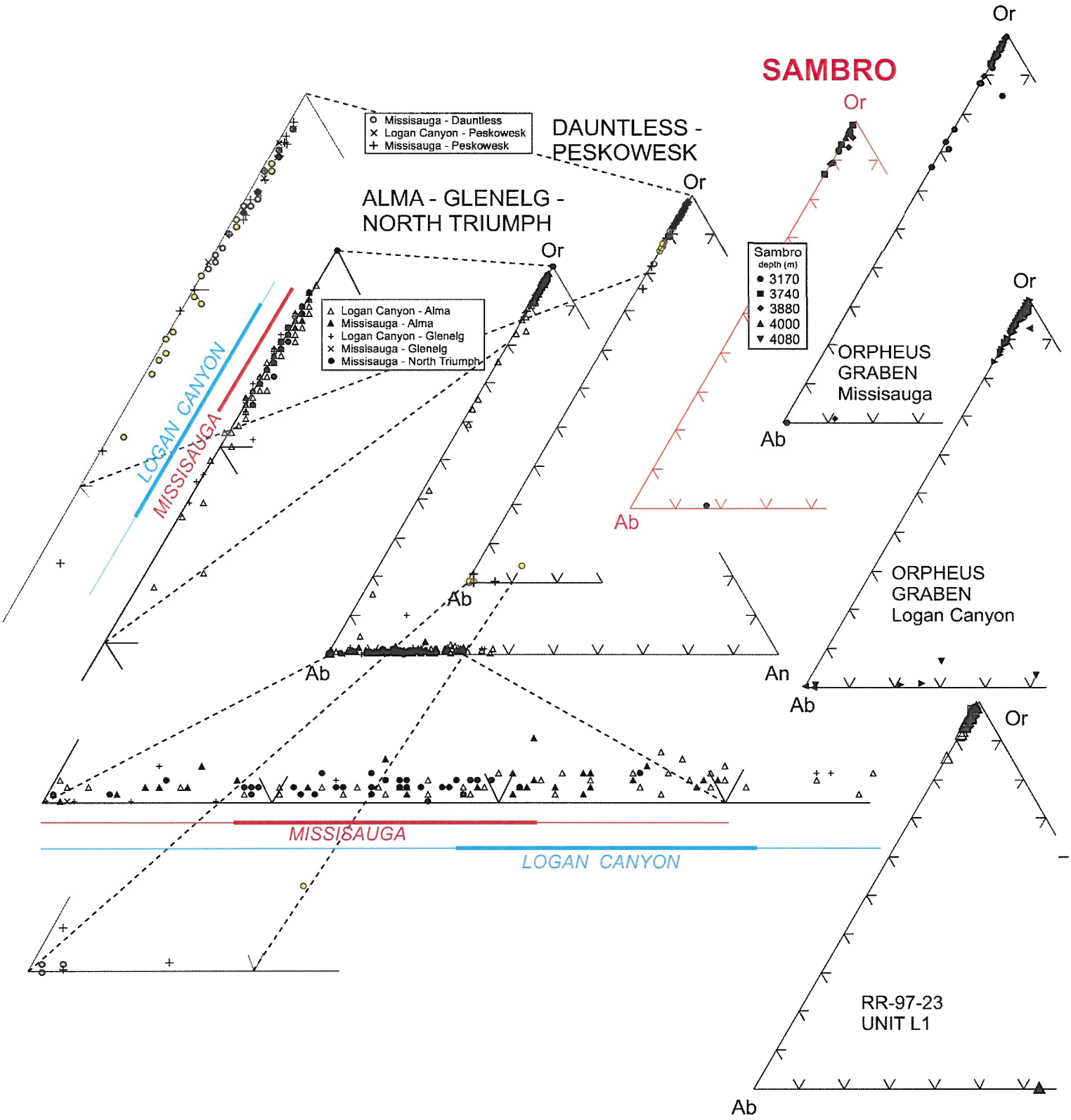

Figure 15: Composition of feldspars from Sambro I-29 compared with other offshore wells and the Chaswood Formation in borehole RR-97-23.

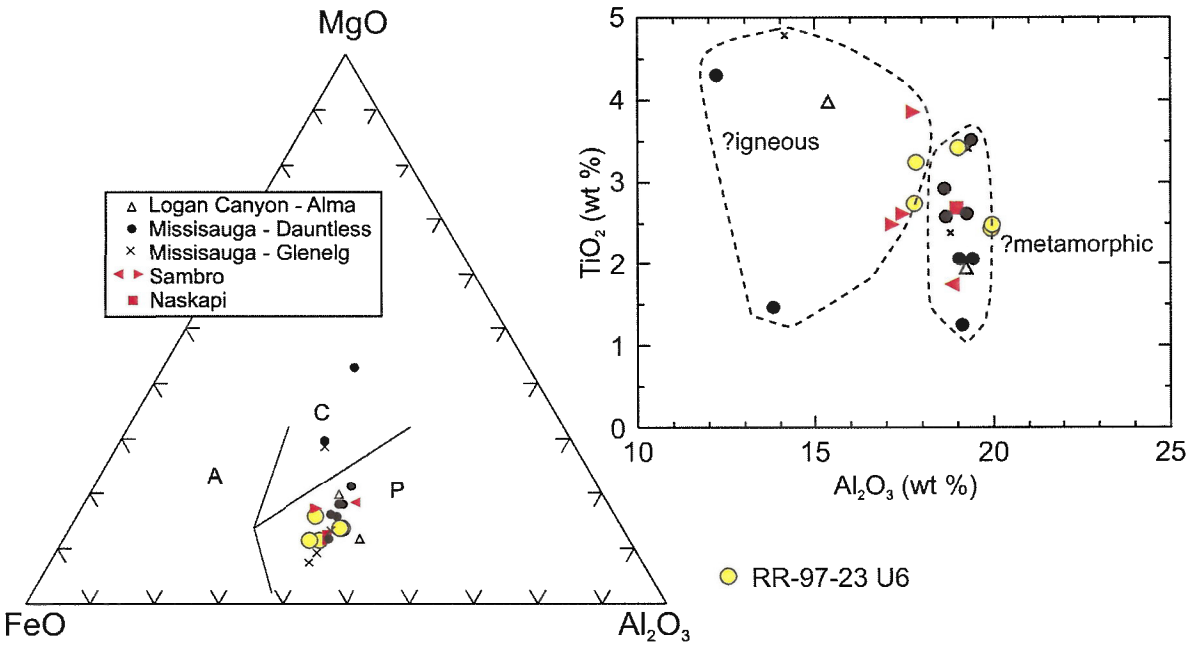

Figure 16: Composition of biotite from Sambro I-29 and Naskapi N-30 compared with other Scotian basin wells and with the Chaswood Formation at borehole RR-97-23.

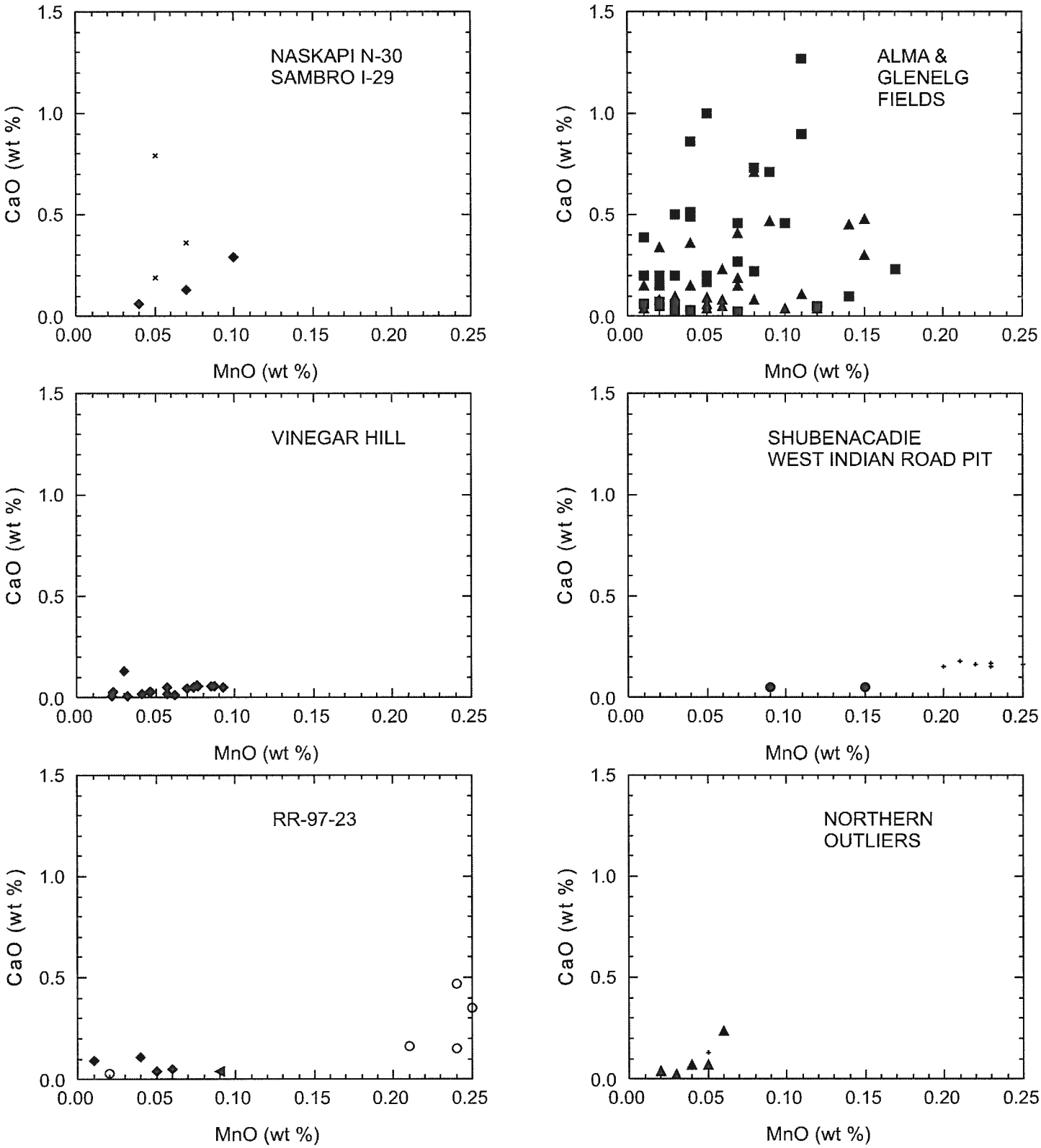

Figure 17: Analyses of rutile grains from Naskapi N-30 and Sambro I-29 compared with those from the Alma and Glenelg fields and with those from the Chaswood Formation.

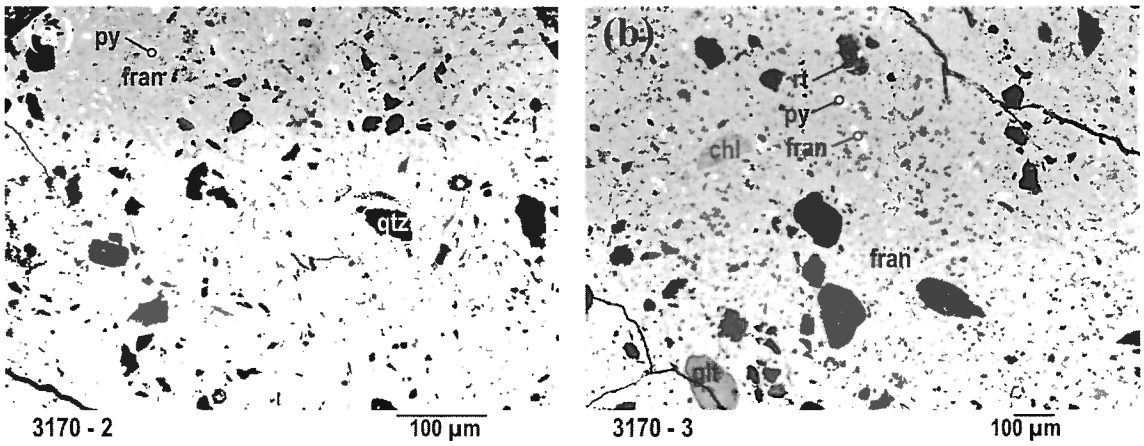

Figure 18: Backscattered electron images of phosphatic mudstone, 965 m, upper Cree Member, Sambro I-29.

chl = chlorite; glt = glauconite; fran = francolite; kfs = K-feldspar; py = pyrite; qz = quartz; rt = rutile.

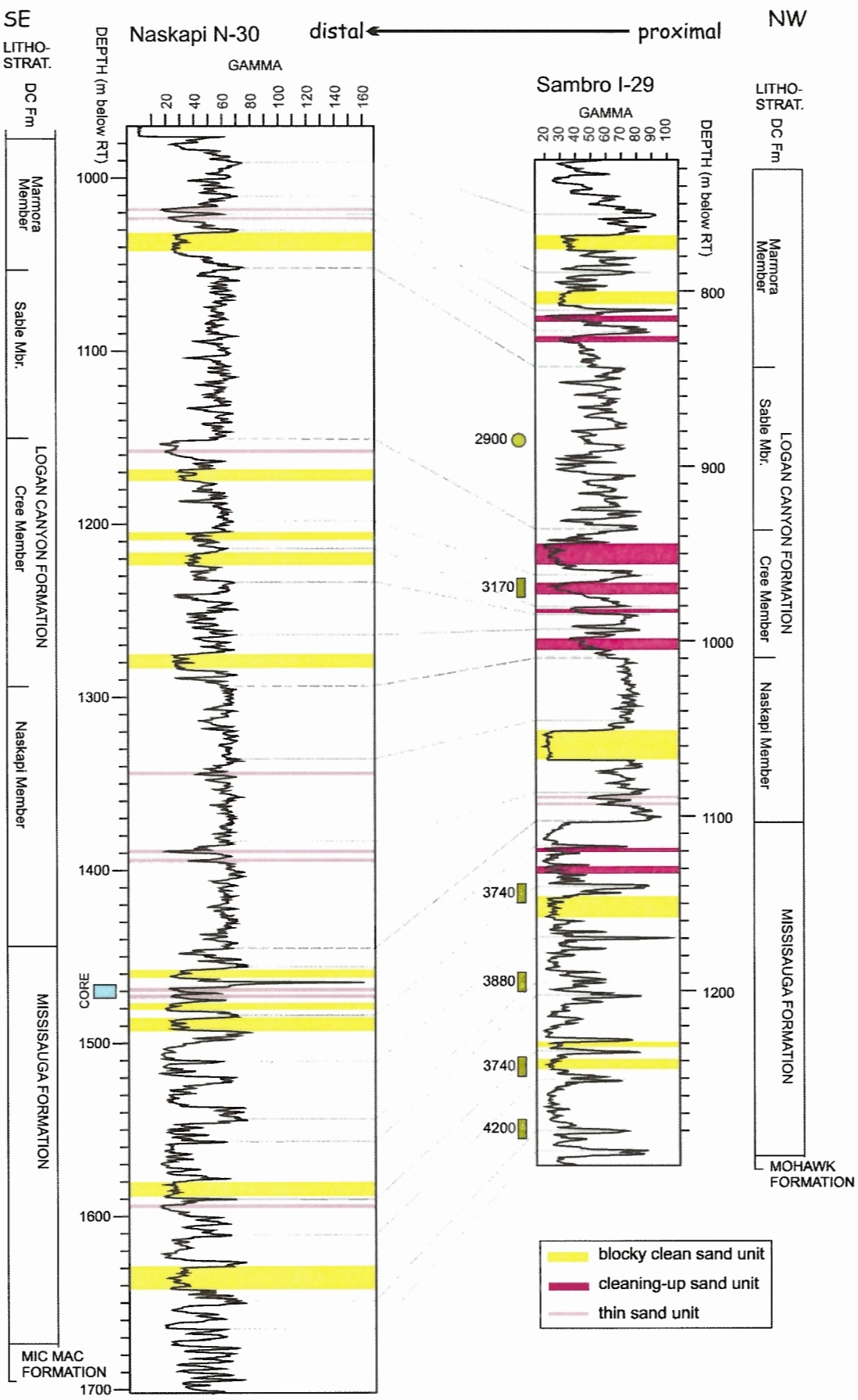

Figure 19: Correlation of the Lower Cretaceous of Sambro I-29 and Naskapi N-30. For further explanation, see text.

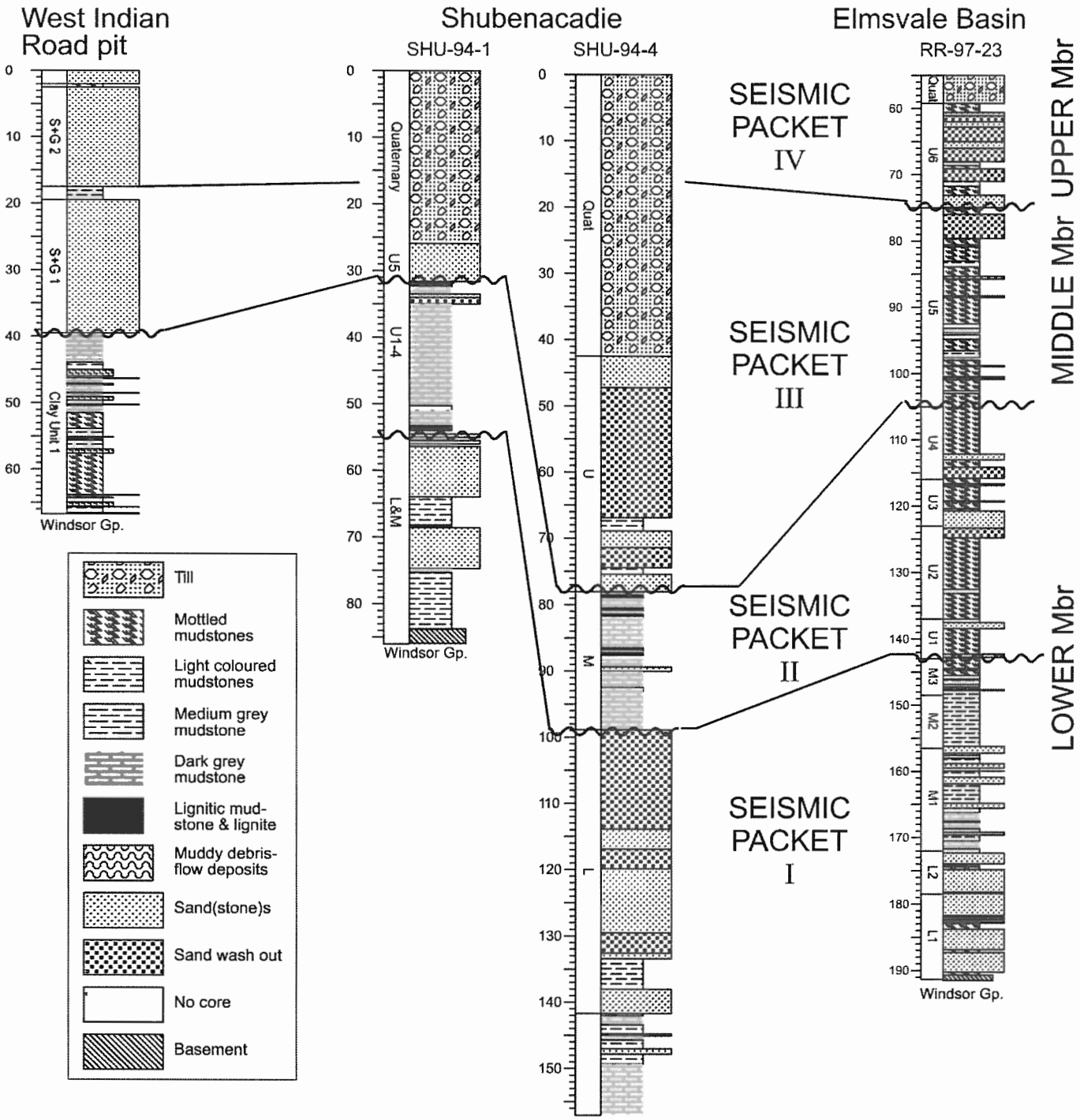

Figure 20: Stratigraphic logs of the Chaswood Formation in central Nova Scotia (from Pe-Piper et al. 2005a) showing regional correlation and the distribution of coarse sandstones.

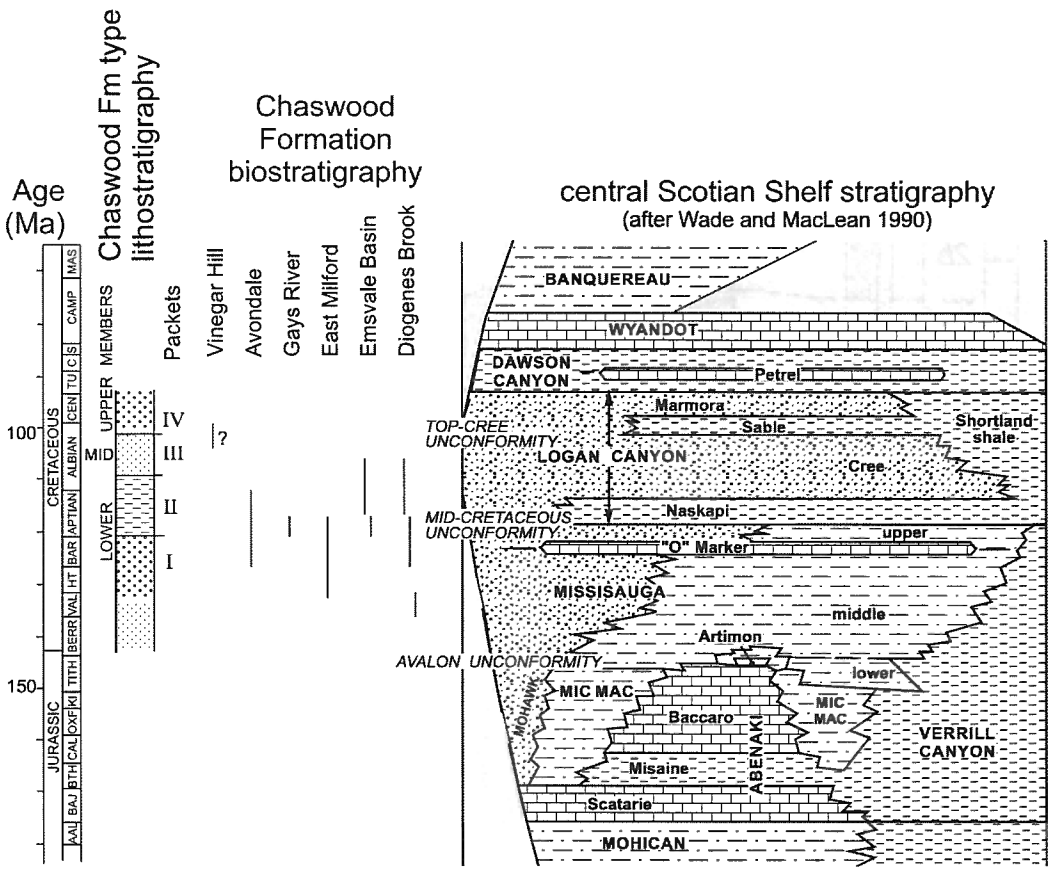

Figure 21: Biostratigraphic ages for the Chaswood Formation compared with the regional stratigraphy of the Scotian basin. (Biostratigraphy from various sources, summarized by Falcon-Lang et al. (2007) and by Pe-Piper and Piper, 2004b).

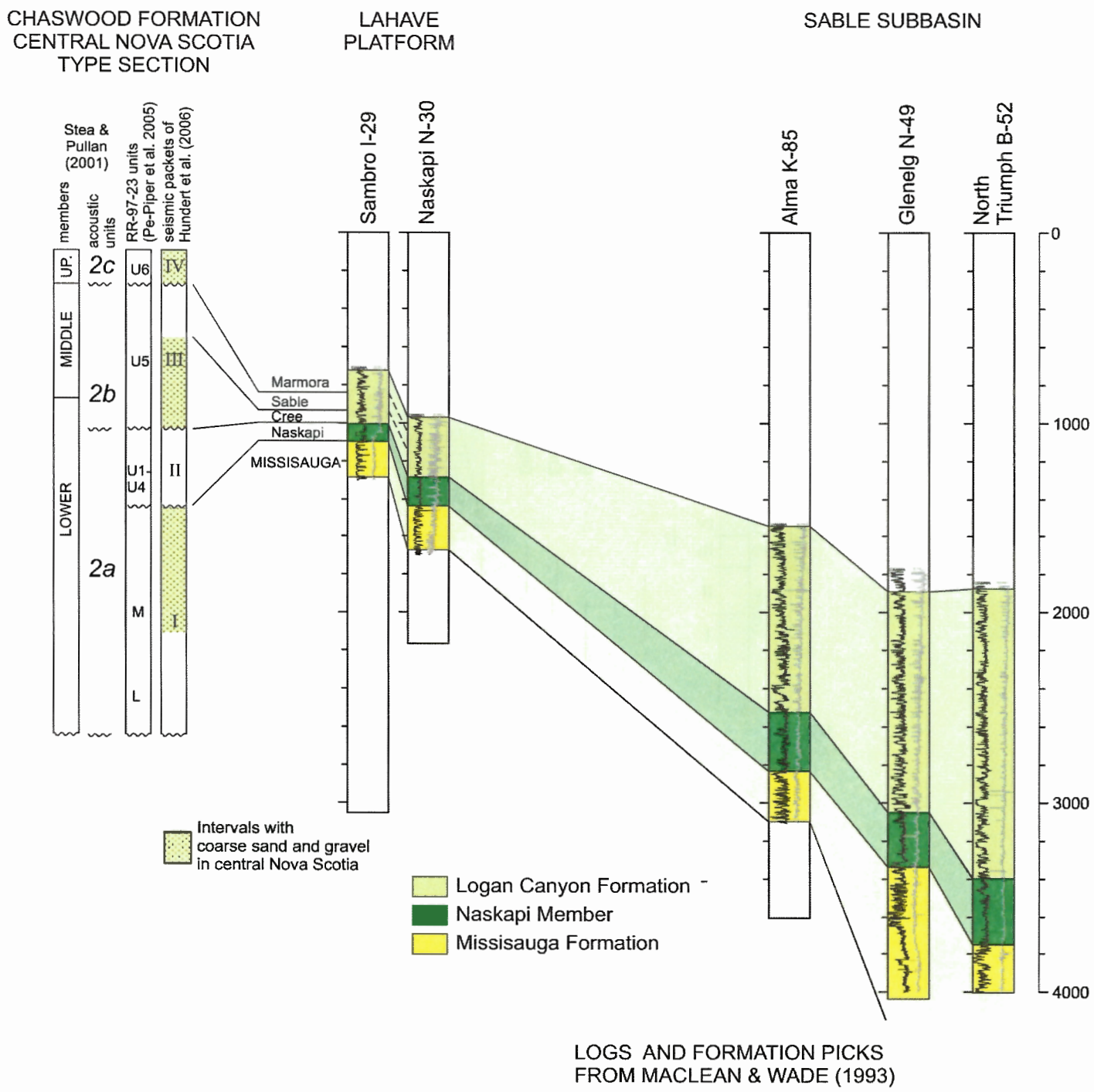

Figure 22: Correlation of the La Have platform wells with the southwestern Sable sub-basin and the Chaswood Formation.

Table 1: Petrography of sandstones from conventional core in the Naskapi N-30 well (upper Missisauga Formation).

Sample No.	Unit	Rock Name	Grains				*for each mineral or rock-type, number of grains as a percentage of total grains*																Matrix		Cement					Porosity
depth (m)	see Fig. 3		% of total rock	mean size (μm)	sorting	roundness of quartz grains	moncrystalline (mxt) quartz	polycrystalline quartz	foliated mxt quartz crystals	feldspar	muscovite	biotite	glauconite	Fe-Ti oxides	light-coloured heavy minerals	igneous rock fragments	metamorphic rock fragments	sedimentary rock fragments	carbonate rock fragments	intraformational clasts	fossils (plant matter)	% of total rock	description of material	% of total rock	cement 1: mineral	cement 2: mineral	cement 3: mineral	cement 4: mineral	remaining porosity as % of total rock
1467.96	2	FN SST	**70**	150	P	SUB-A	87	2	2	0	5	0	<1	3	<1	0	0	0	0	tr	<1	**29**	muddy matrix + detrital clays	**1**	illite	pyrite	kaolinite	halloysite	**<1**
1468.65	2	GRADED SST	**80**	500	M	SUB-R	82	8	4	0	2	<1	tr	3	<1	0	0	0	0	<1	0	**13**	muddy matrix + detrital clays	**1**	kaolinite	illite	halloysite		**6**
1469.00	2	MED SST	**80**	300	M	SUB-A	89	6	2	0	2	<1	0	<1	<1	0	tr	0	0	0	0	**9**	muddy matrix + detrital clays	**3**	kaolinite	illite	halloysite	limonite; silica	**8**
1469.89	3	CRS SST	**45**	700	VP	SUB-R	65	20	10	0	4	0	0	1	<1	0	0	0	0	0	0	**44**	muddy silt to fine sand	**1**	pyrite	kaolinite	illite	limonite	**10**
1469.89 (1)	3	V FN SST	**60**	120	M	SUB-A	91	1	<1	0	2	0	0	3	<1	0	0	0	0	0	2	**39**	muddy matrix + detrital clays	**1**	pyrite				**<1**
1470.50	4	FN SST	**80**	160	VP	SUB-R	96	<1	1	0	<1	0	tr	1	<1	0	0	0	0	tr	<1	**16**	muddy matrix + detrital clays	**1**	kaolinite (tr)	pyrite			**3**
1471.75	8	FN SST	**90**	240	P	SUB-A	95	2	<1	0	2	0	0	<1	<1	0	0	0	0	0	0	**7**	muddy matrix + detrital clays	**<1**	pyrite	illite (tr)			**3**
1472.25	9	V FN SST	**35**	100	M	SUB-A	91	<1	0	tr	2	0	<1	6	<1	0	0	tr	0	0	0	**65**	muddy matrix + detrital clays	**tr**	pyrite				**0**
1472.36	9	FN SST	**75**	140	VP	SUB-R	88	2	3	tr	3	0	0	4	<1	0	0	0	0	0	0	**22**	muddy matrix + detrital clays	**2**	pyrite	illite (tr)	kaolinite (tr)		**1**
1473.51	11	CRS-V CRS SST	**65**	1000	VP	SUB-R	72	20	3	0	2	0	tr	1	<1	0	<1	0	0	0	2	**35**	muddy silt to fine sand	**tr**	illite				**<1**
1473.61	11	V CRS SST	**55**	1400	VP	SUB-R	28	60	8	0	2	0	0	2	<1	0	0	0	0	0	0	**43**	muddy silt to medium sand	**<1**	pyrite	halloysite			**2**
1473.81	11	V CRS SST	**60**	1100	P	SUB-R	16	80	2	0	<1	0	0	2	tr	0	0	0	0	0	0	**30**	muddy fine to medium sand	**4**	kaolinite	illite	pyrite	silica (tr)	**6**

Abbreviations:

Rock Name: CRS, coarse; FN, fine; MED, medium; SST, sandstone; V, very. Sorting: M, moderate; P, poor; VP, very poor. Roundness: SUB-A, subangular; SUB-R, subrounded. Other abbreviations: tr, trace.

Additional notes:

1. "foliated monocrystalline (mxt) quartz crystals" have very pronounced wavy or undulose extinction, commonly observed as nearly parallel bands in the extinction pattern.
2. "muddy matrix" refers to Fe-rich particulate matter interspered with detrital clays in the matrix; it is distinguished by a reddish-brown appearance in plane polarized light and lack of crystalline structure.

1467.96 intraformational clasts are claystones
1468.65 some muscovite is altered to kaolinite; intraformational clasts are siltstones
1469.00 some muscovite is altered to kaolinite; metamorphic rock fragments are quartzites; limonite cement may be from alteration of siderite nodules
1469.89 limonite cement may be from alteration of siderite nodules
1470.50 intraformational clasts are siltstones
1472.25 feldspar grain is altered to kaolinite; sedimentary rock fragment is quartz arenite
1472.36 some muscovite is altered to kaolinite
1473.51 some muscovite is altered to kaolinite; metamorphic rock fragments are quartzites

Table 2: Results from Coulter laser grain size analysis

Well	Naskapi		Naskapi 1471.75 m		Naskapi 1472.25 m		Naskapi 1473.81 m	
Depth	1469.0 m		1471.75 m		1472.25 m		1473.81 m	
Sample ID	N-30 D4-1-4		N-30 D4-1-8		N-30 D4-1-9		N-30 D4-1-13	
	Volume	Cumulative	Volume	Cumulative	Volume	Cumulative	Volume	Cumulative
µm	%	volume %	%	volume %	%	volume %	%	volume %
2000	0.000	0.00	0.000	0.00	0.000	0.00	0.000	0.00
1822	0.000	0.00	0.000	0.00	0.690	0.69	1.900	1.90
1660	0.003	0.00	0.000	0.00	0.599	1.29	1.790	3.69
1512	0.038	0.04	0.000	0.00	0.540	1.83	1.780	5.47
1377	0.211	0.25	0.003	0.00	0.518	2.35	1.850	7.32
1255	0.599	0.85	0.006	0.01	0.570	2.92	2.050	9.37
1143	1.190	2.04	0.044	0.05	0.715	3.63	2.390	11.76
1041	1.870	3.91	0.148	0.20	0.931	4.56	2.810	14.57
948.2	2.600	6.51	0.310	0.51	1.200	5.76	3.220	17.79
863.9	3.310	9.82	0.481	0.99	1.490	7.25	3.520	21.31
786.9	3.920	13.74	0.619	1.61	1.840	9.09	3.690	25.00
716.9	4.410	18.15	0.724	2.33	2.280	11.37	3.730	28.73
653	4.740	22.89	0.809	3.14	2.840	14.21	3.700	32.43
594.9	4.940	27.83	0.902	4.05	3.510	17.72	3.630	36.06
541.9	5.050	32.88	1.040	5.09	4.200	21.92	3.580	39.64
493.6	5.080	37.96	1.250	6.34	4.800	26.72	3.560	43.20
449.7	5.050	43.01	1.560	7.90	5.180	31.90	3.550	46.75
409.6	4.980	47.99	2.000	9.90	5.230	37.13	3.530	50.28
373.1	4.830	52.82	2.570	12.47	4.920	42.05	3.470	53.75
339.8	4.610	57.43	3.240	15.71	4.310	46.36	3.350	57.10
309.6	4.310	61.74	3.970	19.68	3.540	49.90	3.150	60.25
282.1	3.920	65.66	4.680	24.36	2.760	52.66	2.860	63.11
256.8	3.480	69.14	5.290	29.65	2.110	54.77	2.530	65.64
234.1	3.000	72.14	5.740	35.39	1.640	56.41	2.180	67.82
213.2	2.520	74.66	6.000	41.39	1.380	57.79	1.850	69.67
194.2	2.060	76.72	6.040	47.43	1.270	59.06	1.560	71.23
176.8	1.650	78.37	5.870	53.30	1.270	60.33	1.320	72.55
161.2	1.290	79.66	5.540	58.84	1.330	61.66	1.130	73.68
146.8	1.000	80.66	5.080	63.92	1.410	63.07	0.962	74.64
133.7	0.775	81.44	4.530	68.45	1.500	64.57	0.826	75.47
121.8	0.615	82.05	3.930	72.38	1.570	66.14	0.715	76.18
111	0.510	82.56	3.330	75.71	1.610	67.75	0.629	76.81
101.1	0.445	83.01	2.740	78.45	1.600	69.35	0.568	77.38
92.09	0.406	83.41	2.200	80.65	1.510	70.86	0.525	77.91
83.9	0.382	83.79	1.720	82.37	1.350	72.21	0.497	78.40
76.43	0.365	84.16	1.320	83.69	1.150	73.36	0.480	78.88
69.62	0.353	84.51	1.000	84.69	0.955	74.32	0.472	79.35
63.41	0.349	84.86	0.766	85.45	0.792	75.11	0.474	79.83
57.77	0.351	85.21	0.599	86.05	0.681	75.79	0.485	80.31
52.63	0.359	85.57	0.486	86.54	0.621	76.41	0.500	80.81
47.93	0.370	85.94	0.411	86.95	0.601	77.01	0.513	81.33
43.66	0.379	86.32	0.361	87.31	0.602	77.62	0.520	81.85
39.77	0.383	86.70	0.324	87.63	0.605	78.22	0.518	82.36
36.24	0.383	87.09	0.296	87.93	0.600	78.82	0.508	82.87
33	0.380	87.47	0.274	88.20	0.589	79.41	0.496	83.37
30.07	0.381	87.85	0.260	88.46	0.579	79.99	0.488	83.86
27.38	0.386	88.23	0.253	88.72	0.578	80.57	0.490	84.35
24.95	0.398	88.63	0.253	88.97	0.591	81.16	0.502	84.85
22.73	0.415	89.05	0.258	89.23	0.616	81.77	0.522	85.37
20.7	0.432	89.48	0.266	89.49	0.644	82.42	0.542	85.91

Well	Naskapi		Naskapi 1471.75 m		Naskapi 1472.25 m		Naskapi 1473.81 m	
Depth	1469.0 m		1471.75 m		1472.25 m		1473.81 m	
Sample ID	N-30 D4-1-4		N-30 D4-1-8		N-30 D4-1-9		N-30 D4-1-13	
	Volume	Cumulative	Volume	Cumulative	Volume	Cumulative	Volume	Cumulative
µm	%	volume %	%	volume %	%	volume %	%	volume %
18.86	0.447	89.93	0.275	89.77	0.667	83.08	0.557	86.47
17.18	0.456	90.38	0.284	90.05	0.679	83.76	0.563	87.03
15.65	0.460	90.84	0.294	90.35	0.680	84.44	0.563	87.60
14.26	0.460	91.30	0.305	90.65	0.676	85.12	0.558	88.15
12.99	0.457	91.76	0.316	90.97	0.671	85.79	0.553	88.71
11.83	0.452	92.21	0.327	91.29	0.669	86.46	0.550	89.26
10.78	0.445	92.66	0.338	91.63	0.669	87.13	0.547	89.80
9.819	0.436	93.09	0.347	91.98	0.670	87.80	0.544	90.35
8.944	0.426	93.52	0.356	92.33	0.671	88.47	0.540	90.89
8.147	0.414	93.93	0.362	92.70	0.669	89.14	0.535	91.42
7.421	0.402	94.33	0.367	93.06	0.666	89.80	0.528	91.95
6.761	0.388	94.72	0.370	93.43	0.659	90.46	0.520	92.47
6.158	0.374	95.10	0.371	93.80	0.649	91.11	0.509	92.98
5.611	0.359	95.45	0.370	94.17	0.636	91.75	0.496	93.48
5.111	0.344	95.80	0.368	94.54	0.618	92.37	0.481	93.96
4.656	0.328	96.13	0.363	94.91	0.597	92.96	0.463	94.42
4.241	0.313	96.44	0.357	95.26	0.573	93.54	0.444	94.86
3.862	0.297	96.74	0.349	95.61	0.547	94.08	0.424	95.29
3.519	0.282	97.02	0.340	95.95	0.518	94.60	0.402	95.69
3.206	0.266	97.28	0.329	96.28	0.489	95.09	0.381	96.07
2.92	0.251	97.54	0.318	96.60	0.460	95.55	0.359	96.43
2.66	0.237	97.77	0.305	96.90	0.431	95.98	0.338	96.77
2.423	0.222	97.99	0.291	97.19	0.402	96.38	0.317	97.08
2.207	0.208	98.20	0.277	97.47	0.375	96.76	0.297	97.38
2.01	0.195	98.40	0.263	97.73	0.349	97.11	0.278	97.66
1.832	0.182	98.58	0.249	97.98	0.324	97.43	0.259	97.92
1.669	0.169	98.75	0.234	98.22	0.301	97.73	0.241	98.16
1.52	0.156	98.90	0.219	98.44	0.278	98.01	0.224	98.38
1.385	0.144	99.05	0.204	98.64	0.257	98.27	0.208	98.59
1.261	0.133	99.18	0.190	98.83	0.238	98.51	0.193	98.78
1.149	0.122	99.30	0.175	99.01	0.218	98.72	0.178	98.96
1.047	0.111	99.41	0.160	99.17	0.200	98.92	0.163	99.13
0.953	0.100	99.51	0.146	99.31	0.182	99.11	0.148	99.27
0.869	0.090	99.60	0.132	99.44	0.165	99.27	0.135	99.41
0.791	0.081	99.69	0.118	99.56	0.148	99.42	0.121	99.53
0.721	0.071	99.76	0.104	99.67	0.131	99.55	0.107	99.64
0.657	0.061	99.82	0.090	99.76	0.114	99.66	0.093	99.73
0.598	0.052	99.87	0.076	99.83	0.097	99.76	0.079	99.81
0.545	0.043	99.91	0.063	99.89	0.081	99.84	0.066	99.87
0.496	0.034	99.95	0.049	99.94	0.063	99.90	0.052	99.93
0.452	0.023	99.97	0.034	99.98	0.044	99.95	0.036	99.96
0.412	0.016	99.99	0.023	100.00	0.030	99.98	0.024	99.99
0.375	0.009	99.99	0.013	100.01	0.017	100.00	0.013	100.00

Table 3: Descriptive statistics from Coulter laser grain size analysis

Well	Naskapi	Naskapi	Naskapi	Naskapi
Depth	1469.0 m	1471.75 m	1472.25 m	1473.81 m
Sample ID	N-30 D4-1-4	N-30 D4-1-8	N-30 D4-1-9	N-30 D4-1-13
Mean:	431.9	216.4	353.4	527.5
Median:	394.4	186.5	308.8	412.7
D(3,2):	30.09	23.33	17.45	21.78
Mean/Median Ratio:	1.095	1.16	1.144	1.278
Mode:	517.2	203.5	429.2	751.1
95% Conf. Limits:	0	0	0	0
95% Conf. Limits:	1032	549.3	1042	1461
S.D.:	306.2	169.8	351.2	476.2
Variance:	93766	28846	1.23E+05	2.27E+05
C.V.:	70.89	78.49	99.37	90.27
Skewness:	0.584	1.737	1.648	1.025
Kurtosis:	-0.101	4.631	3.759	0.463
Specific Surf. Area	1994	2572	3438	2754
% <				
10	18.6	17.39	7.231	10.43
25	210.1	113.3	64.34	141.1
50	394.4	186.5	308.8	412.7
75	628.1	278.9	511.1	786.6
90	860.2	408	759.2	1225
Volume	Particle	Particle	Particle	Particle
%	Diameter	Diameter	Diameter	Diameter
	µm <	µm <	µm <	µm <
10	18.6	17.39	7.231	10.43
25	210.1	113.3	64.34	141.1
50	394.4	186.5	308.8	412.7
75	628.1	278.9	511.1	786.6
90	860.2	408	759.2	1225

Table 4: Chemical analyses by electron microprobe of minerals in representative sandstone samples of Naskapi N-30 well

Well	Depth	Analysis (Min22)	Mineral	SiO_2	TiO_2	Al_2O_3	Cr_2O_3	FeO_t	MnO	MgO	CaO	Na_2O	K_2O	Total
Naskapi N-30	1469.00	545	Biotite	34.09	2.68	18.97	0.02	21.75	0.36	5.76	0.02	0.10	10.36	94.11
Naskapi N-30	1469.89	610	Glauconite	47.94	0.16	13.08	0.04	17.09	0.00	2.34	0.37	0.08	7.23	88.33
Naskapi N-30	1472.25	609	Glauconite	48.67	0.13	9.66	0.04	16.17	0.09	2.36	0.02	0.39	4.52	82.05
Naskapi N-30	1467.96	616	Ilmenite*	1.13	71.77	0.83	0.29	11.59	0.78	0.15	0.18	0.71	0.02	87.45
Naskapi N-30	1471.75	626	Ilmenite*	0.77	74.90	0.77	0.24	3.82	0.17	0.05	0.11	0.18	0.00	81.01
Naskapi N-30	1471.75	627	Ilmenite*	0.31	76.36	0.48	0.14	7.29	0.05	0.04	0.07	0.11	0.02	84.87
Naskapi N-30	1472.36	617	Ilmenite*	0.66	67.29	0.50	0.14	10.12	2.22	0.04	0.07	0.34	0.00	81.38
Naskapi N-30	1472.36	618	Ilmenite*	1.19	71.84	0.73	0.30	9.70	0.51	0.02	0.11	0.29	0.07	84.76
Naskapi N-30	1472.36	619	Ilmenite*	0.87	69.27	0.78	0.31	11.89	0.81	0.05	0.10	0.57	0.09	84.74
Naskapi N-30	1472.36	620	Ilmenite*	0.81	71.58	0.89	0.31	10.10	1.15	0.07	0.13	0.81	0.07	85.92
Naskapi N-30	1472.36	621	Ilmenite*	0.51	73.03	0.75	0.29	6.36	0.51	0.06	0.12	0.16	0.04	81.83
Naskapi N-30	1472.36	622	Ilmenite*	0.00	79.19	0.14	0.11	7.57	0.20	0.00	0.11	0.10	0.03	87.45
Naskapi N-30	1472.36	623	Ilmenite*	0.29	64.79	0.50	0.16	15.10	1.40	0.16	0.12	0.85	0.05	83.42
Naskapi N-30	1472.36	624	Ilmenite*	0.71	72.48	0.74	0.28	8.42	0.96	0.06	0.12	0.69	0.04	84.50
Naskapi N-30	1472.36	625	Ilmenite*	0.88	73.80	0.81	0.25	9.73	0.92	0.06	0.25	0.12	0.05	86.87
Naskapi N-30	1469.89	544	Kaolinite	45.39	0.02	38.27	0.00	0.20	0.00	0.11	0.12	0.02	0.01	84.14
Naskapi N-30	1469.89	606	Kaolinite	46.67	0.00	36.34	0.01	1.97	0.00	0.14	0.08	0.05	0.05	85.31
Naskapi N-30	1469.89	607	Kaolinite	45.99	0.01	37.21	0.00	1.34	0.00	0.10	0.02	0.08	0.11	84.86
Naskapi N-30	1472.36	600	Kaolinite	35.40	0.58	34.12	0.03	9.15	0.08	2.03	0.19	1.91	0.04	83.53
Naskapi N-30	1472.36	601	Kaolinite	46.88	0.00	37.91	0.00	0.23	0.03	0.04	0.01	0.04	0.01	85.15
Naskapi N-30	1472.36	602	Kaolinite	46.94	0.01	38.66	0.00	0.16	0.00	0.00	0.05	0.03	0.02	85.87
Naskapi N-30	1472.36	603	Kaolinite	44.88	0.00	35.49	0.00	0.42	0.00	0.23	0.00	0.10	1.81	82.93
Naskapi N-30	1472.36	604	Kaolinite	47.18	0.00	37.35	0.00	0.68	0.00	0.14	0.02	0.06	0.39	85.82
Naskapi N-30	1472.36	605	Kaolinite	46.33	0.00	37.47	0.02	0.92	0.00	0.08	0.05	0.05	0.00	84.92
Naskapi N-30	1467.96	497	Muscovite	45.71	0.77	34.28	0.03	2.19	0.00	0.67	0.00	0.49	10.49	94.63
Naskapi N-30	1467.96	498	Muscovite	45.49	0.79	34.59	0.03	2.39	0.04	0.68	0.00	0.49	10.48	94.98
Naskapi N-30	1467.96	499	Muscovite	46.50	1.53	34.29	0.06	1.15	0.00	0.85	0.00	0.51	10.32	95.21
Naskapi N-30	1467.96	500	Muscovite	45.71	0.17	36.34	0.07	1.07	0.00	0.46	0.00	0.86	9.58	94.26
Naskapi N-30	1467.96	501	Muscovite	45.58	1.04	33.24	0.01	3.78	0.00	0.70	0.00	0.51	10.12	94.98
Naskapi N-30	1467.96	502	Muscovite	58.23	0.15	29.92	0.06	0.60	0.00	0.28	0.04	0.30	7.84	97.42
Naskapi N-30	1467.96	504	Muscovite	45.95	0.21	35.98	0.03	1.58	0.00	0.71	0.00	0.51	10.81	95.78
Naskapi N-30	1467.96	505	Muscovite	45.62	0.62	35.47	0.03	1.27	0.00	0.59	0.00	0.27	9.81	93.68

Table 4: (continued)

Well	Depth	Analysis (Min22)	Mineral	SiO_2	TiO_2	Al_2O_3	Cr_2O_3	FeO_t	MnO	MgO	CaO	Na_2O	K_2O	Total
Naskapi N-30	1468.65	507	Muscovite	44.44	1.12	33.06	0.01	2.87	0.04	0.64	0.03	0.43	9.93	92.57
Naskapi N-30	1468.65	508	Muscovite	47.06	0.90	32.11	0.06	2.00	0.04	1.44	0.01	0.20	9.98	93.80
Naskapi N-30	1468.65	509	Muscovite	46.85	0.32	32.87	0.07	2.18	0.03	1.38	0.00	0.26	10.50	94.46
Naskapi N-30	1468.65	530	Muscovite	45.23	0.02	36.52	0.04	0.28	0.07	0.27	0.20	1.66	6.21	90.50
Naskapi N-30	1469.00	510	Muscovite	46.29	0.13	34.74	0.02	2.00	0.01	0.72	0.00	0.56	10.16	94.63
Naskapi N-30	1469.00	511	Muscovite	45.89	0.69	34.49	0.03	3.17	0.04	0.68	0.00	0.92	9.55	95.46
Naskapi N-30	1469.00	512	Muscovite	44.79	1.75	34.60	0.00	1.62	0.00	0.74	0.00	0.59	10.97	95.06
Naskapi N-30	1469.00	513	Muscovite	45.64	0.64	34.14	0.03	3.14	0.00	0.62	0.00	0.85	9.81	94.87
Naskapi N-30	1469.00	514	Muscovite	45.90	0.62	35.88	0.00	0.78	0.00	0.54	0.00	0.89	9.12	93.73
Naskapi N-30	1469.00	532	Muscovite	44.53	0.66	32.75	0.03	2.90	0.00	0.63	0.06	0.97	9.39	91.92
Naskapi N-30	1469.00	533	Muscovite	44.27	0.72	32.04	0.00	3.14	0.00	0.69	0.01	0.48	9.63	90.98
Naskapi N-30	1469.89	526	Muscovite	45.75	0.44	31.97	0.05	2.65	0.04	1.13	0.03	0.33	9.48	91.87
Naskapi N-30	1469.89	527	Muscovite	45.16	0.64	33.50	0.03	2.78	0.15	0.78	0.01	0.36	9.71	93.12
Naskapi N-30	1469.89	589	Muscovite	46.02	0.22	32.20	0.01	2.43	0.01	1.46	0.00	0.13	10.76	93.24
Naskapi N-30	1469.89	590	Muscovite	45.82	0.40	36.29	0.03	0.81	0.00	0.64	0.00	0.98	9.81	94.78
Naskapi N-30	1469.89	591	Muscovite	45.54	0.42	36.37	0.04	0.92	0.00	0.55	0.01	1.01	9.70	94.56
Naskapi N-30	1469.89	592	Muscovite	44.86	0.59	34.90	0.01	1.35	0.00	0.50	0.01	0.17	10.15	92.54
Naskapi N-30	1469.89	593	Muscovite	45.23	0.67	35.43	0.05	1.03	0.00	0.51	0.02	0.27	10.34	93.55
Naskapi N-30	1469.89	594	Muscovite	45.65	0.41	36.37	0.03	1.50	0.00	0.40	0.03	0.66	9.98	95.03
Naskapi N-30	1470.50	515	Muscovite	44.53	0.84	32.16	0.05	3.73	0.00	1.05	0.00	0.41	10.74	93.51
Naskapi N-30	1470.50	516	Muscovite	45.04	0.58	33.84	0.02	3.30	0.00	0.79	0.00	0.75	9.99	94.31
Naskapi N-30	1471.75	595	Muscovite	45.03	0.64	35.00	0.02	1.81	0.00	0.53	0.00	1.06	10.15	94.24
Naskapi N-30	1471.75	596	Muscovite	46.57	0.08	36.66	0.02	0.58	0.00	0.53	0.00	0.88	9.72	95.04
Naskapi N-30	1471.75	597	Muscovite	45.25	0.86	33.44	0.01	3.84	0.01	0.76	0.00	0.52	10.29	94.98
Naskapi N-30	1472.25	588	Muscovite	46.42	0.28	36.34	0.01	0.70	0.05	0.43	0.01	1.05	8.62	93.91
Naskapi N-30	1472.36	576	Muscovite	46.79	0.42	37.54	0.00	0.46	0.00	0.46	0.00	1.02	9.21	95.90
Naskapi N-30	1472.36	577	Muscovite	46.81	0.41	35.43	0.00	1.66	0.00	0.62	0.00	0.80	9.10	94.83
Naskapi N-30	1472.36	578	Muscovite	47.38	0.10	32.55	0.01	3.32	0.00	1.13	0.01	0.21	10.06	94.77
Naskapi N-30	1472.36	579	Muscovite	46.19	0.15	35.17	0.00	1.28	0.00	0.44	0.05	0.34	9.49	93.11
Naskapi N-30	1472.36	580	Muscovite	46.11	0.77	35.21	0.01	1.76	0.03	0.67	0.01	0.63	10.14	95.34
Naskapi N-30	1472.36	581	Muscovite	46.72	0.55	31.45	0.03	2.97	0.04	1.26	0.00	0.31	9.66	92.99
Naskapi N-30	1472.36	582	Muscovite	46.77	0.46	36.43	0.00	0.81	0.00	0.65	0.02	0.53	10.05	95.72
Naskapi N-30	1472.36	583	Muscovite	46.54	0.53	37.09	0.02	0.78	0.00	0.38	0.00	1.17	9.29	95.80
Naskapi N-30	1473.51	584	Muscovite	45.20	0.57	35.98	0.00	0.86	0.00	0.39	0.00	0.96	9.45	93.41
Naskapi N-30	1473.51	585	Muscovite	46.13	1.03	35.58	0.00	1.26	0.00	0.66	0.00	0.56	10.29	95.51
Naskapi N-30	1473.51	586	Muscovite	45.99	0.02	34.80	0.00	1.46	0.00	0.71	0.00	0.41	10.52	93.91
Naskapi N-30	1473.51	587	Muscovite	45.68	0.00	35.13	0.00	1.41	0.00	0.79	0.01	0.51	10.02	93.55
Naskapi N-30	1473.51	598	Muscovite	45.25	0.06	34.76	0.00	2.07	0.00	0.43	0.00	1.14	7.92	91.63

Table 4: (continued)

Well	Depth	Analysis (Min22)	Mineral	SiO_2	TiO_2	Al_2O_3	Cr_2O_3	FeO_t	MnO	MgO	CaO	Na_2O	K_2O	Total
Naskapi N-30	1473.51	599	Muscovite	45.48	0.05	31.87	0.01	2.16	0.00	1.38	0.02	0.15	10.38	91.50
Naskapi N-30	1473.61	517	Muscovite	45.18	0.30	36.03	0.02	0.78	0.00	0.49	0.00	0.73	9.95	93.48
Naskapi N-30	1473.61	518	Muscovite	43.98	0.70	33.71	0.01	2.84	0.05	0.59	0.01	0.85	9.80	92.54
Naskapi N-30	1473.61	520	Muscovite	43.87	0.81	32.95	0.00	3.44	0.02	0.63	0.02	0.54	9.70	91.98
Naskapi N-30	1473.81	522	Muscovite	45.54	1.05	30.99	0.07	2.94	0.00	1.35	0.01	0.19	9.93	92.07
Naskapi N-30	1473.81	523	Muscovite	44.71	0.29	34.21	0.01	1.94	0.00	0.70	0.00	0.59	10.32	92.77
Naskapi N-30	1473.81	524	Muscovite	45.09	0.30	33.48	0.01	2.30	0.00	0.79	0.01	0.56	10.27	92.81
Naskapi N-30	1473.81	525	Muscovite	44.84	0.11	34.13	0.02	2.33	0.08	0.63	0.01	0.36	10.34	92.85
Naskapi N-30	1473.81	538	Muscovite	44.72	0.09	33.72	0.02	2.05	0.03	0.58	0.05	0.39	10.13	91.78
Naskapi N-30	1473.81	575	Muscovite	48.29	0.09	35.54	0.02	2.47	0.06	0.69	0.00	0.20	6.00	93.36
Naskapi N-30	1472.36	608	Plagioclase	58.58	0.12	26.95	0.00	0.00	0.01	0.00	8.82	6.67	0.05	101.20
Naskapi N-30	1467.96	611	Rutile	0.05	96.85	0.00	0.05	0.14	0.04	0.00	0.06	0.00	0.02	97.21
Naskapi N-30	1472.36	612	Rutile	0.00	97.05	0.02	0.22	0.18	0.04	0.00	0.06	0.00	0.06	97.63
Naskapi N-30	1472.36	613	Rutile	0.18	95.64	0.32	0.04	0.30	0.07	0.00	0.13	0.04	0.05	96.77
Naskapi N-30	1472.36	614	Rutile	0.40	96.07	0.10	0.05	0.26	0.10	0.00	0.29	0.01	0.06	97.34
Naskapi N-30	1472.36	615	Rutile	0.41	96.52	0.35	0.04	0.17	0.00	0.03	0.03	0.01	0.10	97.66
Naskapi N-30	1467.96	476	Tourmaline	35.73	1.02	29.07	0.06	8.56	0.03	6.68	1.71	1.69	0.02	84.57
Naskapi N-30	1467.96	477	Tourmaline	36.58	0.63	30.38	0.07	5.41	0.00	8.53	0.45	2.65	0.00	84.70
Naskapi N-30	1467.96	478	Tourmaline	35.58	0.95	29.85	0.12	9.04	0.00	6.57	1.32	1.92	0.00	85.35
Naskapi N-30	1467.96	482	Tourmaline	35.97	1.10	31.10	0.03	8.62	0.00	5.45	0.75	1.82	0.00	84.84
Naskapi N-30	1467.96	483	Tourmaline	36.73	0.10	33.69	0.02	7.21	0.05	5.45	0.16	2.31	0.02	85.74
Naskapi N-30	1468.65	479	Tourmaline	35.97	0.63	33.97	0.03	5.86	0.00	5.68	0.35	1.92	0.02	84.43
Naskapi N-30	1468.65	480	Tourmaline	36.34	0.58	32.22	0.03	6.39	0.04	6.48	0.05	2.43	0.02	84.58
Naskapi N-30	1469.00	484	Tourmaline	34.60	0.71	32.30	0.00	14.00	0.12	1.55	0.19	1.95	0.00	85.42
Naskapi N-30	1469.00	485	Tourmaline	35.46	0.70	32.48	0.01	9.06	0.06	4.91	0.24	2.30	0.00	85.22
Naskapi N-30	1469.89	495	Tourmaline	35.00	0.47	32.36	0.02	9.02	0.09	5.15	0.23	2.19	0.05	84.58
Naskapi N-30	1469.89	496	Tourmaline	35.70	0.79	31.01	0.04	7.95	0.00	6.10	0.82	1.94	0.05	84.40
Naskapi N-30	1469.89	570	Tourmaline	34.46	0.36	30.93	0.02	7.89	0.00	6.19	0.50	2.23	0.01	82.59
Naskapi N-30	1469.89	571	Tourmaline	36.11	0.29	34.71	0.01	5.93	0.03	5.50	0.43	1.75	0.02	84.78
Naskapi N-30	1469.89	572	Tourmaline	35.49	0.59	30.76	0.03	10.66	0.04	5.01	0.10	2.49	0.04	85.21

Table 4: (continued)

Well	Depth	Analysis (Min22)	Mineral	SiO_2	TiO_2	Al_2O_3	Cr_2O_3	FeO_t	MnO	MgO	CaO	Na_2O	K_2O	Total
Naskapi N-30	1469.89	573	Tourmaline	35.48	0.75	32.83	0.00	9.03	0.09	4.32	0.11	2.10	0.04	84.75
Naskapi N-30	1470.50	486	Tourmaline	34.49	0.64	32.68	0.05	8.23	0.00	5.40	0.80	1.87	0.04	84.20
Naskapi N-30	1470.50	487	Tourmaline	34.92	0.21	33.67	0.00	9.00	0.12	3.39	0.06	2.19	0.05	83.61
Naskapi N-30	1470.50	488	Tourmaline	35.44	0.66	29.54	0.09	7.58	0.02	6.75	0.86	2.14	0.02	83.10
Naskapi N-30	1470.50	489	Tourmaline	35.51	2.07	30.87	0.03	6.65	0.00	6.36	0.59	1.96	0.07	84.11
Naskapi N-30	1470.50	490	Tourmaline	35.65	0.88	32.95	0.04	5.79	0.00	6.42	0.52	1.97	0.00	84.22
Naskapi N-30	1471.75	574	Tourmaline	36.95	0.38	34.55	0.00	5.64	0.00	6.57	0.47	2.10	0.00	86.66
Naskapi N-30	1472.25	567	Tourmaline	36.33	0.28	31.48	0.04	8.25	0.00	5.96	0.37	2.02	0.00	84.73
Naskapi N-30	1472.25	568	Tourmaline	36.38	0.27	31.32	0.03	8.61	0.05	5.92	0.39	2.15	0.00	85.12
Naskapi N-30	1472.25	569	Tourmaline	35.62	0.14	31.56	0.01	10.69	0.01	4.18	0.04	1.92	0.00	84.17
Naskapi N-30	1473.61	491	Tourmaline	35.64	0.16	32.30	0.01	7.93	0.10	5.73	0.18	2.02	0.02	84.09
Naskapi N-30	1473.61	492	Tourmaline	34.73	0.64	32.66	0.01	8.18	0.02	4.77	0.10	2.23	0.02	83.36
Naskapi N-30	1473.81	493	Tourmaline	34.18	0.41	34.61	0.03	7.93	0.02	4.22	0.52	1.60	0.05	83.57
Naskapi N-30	1473.81	494	Tourmaline	33.82	2.84	30.33	0.03	9.24	0.02	4.95	0.61	1.97	0.05	83.86

* These analyses are from ilmenite grains altered to leucoxene.

Table 4: (continued)

Well	Depth	Analysis (Excel)	Mineral	SiO_2	TiO_2	Al_2O_3	Cr_2O_3	FeO_t	MnO	MgO	CaO	Na_2O	K_2O	NiO	P_2O_5	ZrO_2	Total
Naskapi N-30	1472.36	1	Apatite	0.41	0.00	0.01	0.00	0.04	0.36	0.03	55.16	0.06	0.00	0.00	41.33	0.11	97.51
Naskapi N-30	1469.89	2	Limonite	0.59	0.15	0.00	0.08	71.04	0.29	0.07	0.15	0.22	0.07	0.44	0.00	0.00	73.10
Naskapi N-30	1469.89	3	Limonite	0.72	0.18	0.04	0.11	68.48	0.34	0.10	0.17	0.24	0.06	0.47	0.00	0.00	70.91
Naskapi N-30	1469.89	12	Zircon	33.15	0.20	0.04	0.17	0.23	0.14	0.05	0.10	0.06	0.06	0.00	0.00	65.01	99.21
Naskapi N-30	1469.89	13	Zircon	33.25	0.20	0.02	0.13	0.25	0.20	0.07	0.10	0.06	0.06	0.00	0.00	65.35	99.69
Naskapi N-30	1469.89	14	Zircon	33.67	0.21	0.03	0.14	0.21	0.14	0.06	0.10	0.06	0.05	0.00	0.00	66.04	100.71
Naskapi N-30	1472.25	11	Zircon	33.98	0.25	0.06	0.15	0.28	0.26	0.07	0.08	0.08	0.04	0.00	0.00	62.84	98.09
Naskapi N-30	1472.36	4	Zircon	34.59	0.06	0.09	0.06	0.34	0.10	0.06	0.03	0.09	0.00	0.00	0.00	65.78	101.20
Naskapi N-30	1472.36	5	Zircon	34.36	0.26	0.27	0.17	0.23	0.24	0.05	0.09	0.06	0.05	0.00	0.00	65.43	101.21
Naskapi N-30	1472.36	6	Zircon	34.72	0.23	0.06	0.13	0.34	0.15	0.03	0.07	0.05	0.07	0.00	0.00	66.36	102.21
Naskapi N-30	1472.36	7	Zircon	33.72	0.28	0.06	0.18	0.16	0.15	0.04	0.11	0.05	0.08	0.00	0.00	66.82	101.65
Naskapi N-30	1473.51	8	Zircon	33.70	0.05	0.06	0.07	0.14	0.15	0.07	0.05	0.08	0.04	0.00	0.00	65.93	100.34
Naskapi N-30	1473.51	9	Zircon	33.18	0.07	0.06	0.09	0.12	0.05	0.07	0.06	0.07	0.02	0.00	0.00	65.25	99.04
Naskapi N-30	1473.51	10	Zircon	33.36	0.05	0.05	0.07	0.14	0.10	0.06	0.04	0.06	0.05	0.00	0.00	64.78	98.76

Table 5: Detrital and neomorphic mineral assemblages in conventional core from the Naskapi N-30 well (Missisauga Formation)

Depth (m)	**Detrital Minerals** (in addition to quartz)	**Neomorphic minerals**
1467.96	Tourmaline Muscovite Zircon Rutile Ilmenite + Rutile	Illite / Hydromuscovite Glauconite Pyrite Kaolinite Halloysite
1468.65	Tourmaline Muscovite Monazite Biotite Ilmenite Zircon	Halloysite Kaolinite Illite / Hydromuscovite Glauconite
1469.00	Tourmaline Muscovite Zircon Monazite Biotite Ilmenite	Halloysite Illite / Hydromuscovite Kaolinite Limonite Silica
1469.89	Tourmaline Muscovite Apatite Zircon Rutile Ilmenite	Hydromuscovite / Illite Kaolinite Glauconite Limonite Pyrite
1470.50	Tourmaline Muscovite Zircon Ilmenite	Illite / Hydromuscovite Glauconite Kaolinite Pyrite
1471.75	Ilmenite + Rutile Rutile Muscovite Zircon Tourmaline	Illite Pyrite
1472.25	Tourmaline Ilmenite Muscovite Zircon	Kaolinite Hydromuscovite Glauconite Pyrite Hematite
1472.36	Zircon Rutile Muscovite Ilmenite + Rutile Plagioclase (And/Labr) Apatite	Kaolinite / Halloysite Illite Pyrite

Table 5: (continued)

Depth (m)	**Detrital Minerals** (in addition to quartz)	**Neomorphic minerals**
1473.51	Rutile Zircon Muscovite Monazite Ilmenite	Illite / hydromuscovite Kaolinite / Halloysite Glauconite
1473.61	Muscovite Tourmaline Zircon Ilmenite + Rutile	Halloysite Illite / Hydromuscovite Pyrite
1473.81	Muscovite Tourmaline Ilmenite Zircon	Illite Kaolinite Pyrite Silica

Table 6: Representative whole rock chemical analysis of samples from the Naskapi N-30 and Sambro I-29 wells

Well	N-30	N-30	N-30	N-30	N-30	I-29
Depth (m)	1469.00	1469.89	1471.75	1472.25	1473.81	881
Major Elements (wt%)						
SiO_2	93.59	85.64	92.18	87.33	88.56	55.92
TiO_2	0.84	0.51	0.47	0.59	0.69	0.83
Al_2O_3	2.67	6.25	2.44	5.71	4.64	15.16
Fe_2O_{3t}	0.82	1.78	2.11	1.12	1.75	7.54
MnO	0.01	0.01	b.d.[1]	0.01	0.01	0.05
MgO	0.08	0.14	0.06	0.12	0.09	1.31
CaO	0.13	0.16	0.07	0.06	0.24	5.21
Na_2O	0.26	0.28	0.21	0.35	0.19	0.55
K_2O	0.21	0.65	0.20	0.58	0.39	1.86
P_2O_5	0.02	0.03	0.02	0.03	0.02	0.09
L.O.I	1.43	4.22	2.32	3.42	2.98	i.s.[2]
Total	100.06	99.67	100.09	99.31	99.56	88.52
Trace Elements (ppm)						
Ba	1960	5500	895	1600	1850	266
Rb	10	31	12	29	21	105
Sr	55	103	38	60	55	163
Y	12	14	10	16	15	30
Zr	154	169	186	228	183	204
Nb	10	9	6	8	8	13
Pb	15	37	14	14	22	27
Ga	4	9	4	9	7	22
Zn	38	103	40	45	31	72
Cu	18	29	15	15	15	17
Ni	7	30	17	16	34	53
V	24	38	23	39	29	121
Cr	86	77	60	64	78	124
La	18.3	20.3	13.3	23.5	17.7	39.4
Ce	40.0	42.0	28.2	48.9	37.4	83.2
Pr	4.67	4.67	3.11	5.84	4.29	9.68
Nd	16.8	16.4	11.1	19.4	15.4	35.8
Sm	3.2	3.1	2.0	3.7	3.0	6.9
Eu	0.55	0.54	0.39	0.73	0.56	1.49
Gd	2.5	2.7	1.7	3.2	2.7	5.5
Tb	0.4	0.4	0.3	0.5	0.4	1.0
Dy	2.1	2.4	1.6	2.7	2.4	5.6
Ho	0.4	0.5	0.3	0.5	0.5	1.1
Er	1.3	1.4	1.0	1.6	1.4	3.3
Tm	0.19	0.21	0.16	0.25	0.22	0.50
Yb	1.2	1.3	1	1.6	1.4	3.1
Lu	0.18	0.19	0.16	0.23	0.20	0.45
Co	2	19	6	8	20	14
Cs	b.d.	2.4	1.1	2.7	1.4	6.1
Hf	3.9	4.3	4.6	5.8	4.7	5.6
Sc	3	5	2	5	4	16
Ta	1.2	1.0	0.7	0.9	1.0	1.2
Th	3.5	5.5	3.6	5.5	4.8	10.6
U	1.6	1.7	1.2	1.8	1.9	2.3

[1] b.d. = below detection limit

[2] i.s. = insufficient sample to determine loss on ignition (L.O.I.)

Table 7: Heavy mineral separation of representative sandstone cuttings samples from Sambro I-29 well

SAMPLE (ft)	Depth (m)	Formation / Member	Wt of Bulk Sample (g)	Wt (g) >2mm	Wt (g) <2mm	Wt% >2mm
2600	790	LC	37.86	0.85	37.01	2.25%
2900	881	LC	24.93	4.66	20.11	18.69%
3080	936	LC	36.19	0.57	35.60	1.58%
3170	963	LC	37.95	19.67	18.19	51.83%
3350	1018	NS	15.68	7.53	8.14	48.02%
3470	1054	NS	17.77	1.84	15.95	10.35%
3700	1124	MS	46.22	7.91	38.26	17.11%
3740	1136	MS	55.51	6.34	49.18	11.42%
3880	1179	MS	33.16	7.51	25.65	22.65%
4000	1215	MS	39.55	8.10	31.40	20.48%
4080	1240	MS	47.08	8.17	38.90	17.35%
4100	1246	MS	58.33	18.18	40.14	31.17%
4160	1264	MS	21.24	6.26	14.96	29.47%
4200	1276	MS	66.10	24.14	42.09	36.52%

LC = Logan Canyon Formation; NS = Naskapi member (Logan Canyon); MS = Missisauga Formation

Sample (ft)	Depth(m)	Weight % of the < 2mm fraction	
		Sink	Float
2600	790	2.49	97.51
2900	881	3.46	96.54
3080	936	0.60	99.40
3170	963	4.75	95.25
3350	1018	6.01	93.99
3470	1054	2.01	97.99
3700	1124	0.57	99.43
3740	1136	0.38	99.62
3880	1179	0.26	99.74
4000	1215	0.76	99.24
4080	1240	2.29	97.71
4100	1246	4.85	95.15
4160	1264	5.69	94.31
4200	1276	0.69	99.31

Table 8: Petrographic description of selected cuttings of fraction >2mm from Sambro I-29 well

Sample (ft)	Depth (m)	Formation	Preliminary Identification	Figure in Appendix 3	Petrographic Description	Detrital Minerals	Diagenetic Minerals
3170A	963	Logan Canyon	5 lithic grains	Fig. 6 (grain 1)	meta-quartz arenite clast (looks like Goldenville lithology)	qtz+ms+chl+ttn+ep (metamorphic assemblage)	
				Fig. 7 (grain 2)	phosphate - carbonate - cemented mudstone	qtz+K-feld+chl	fran+cal+py
				Fig. 8 (grain 3)	phosphate - carbonate - cemented mudstone	qtz+rt	fran+cal+ chl+gln+py
					Two more grains looking like grains 2 and 3		
3170B	963	Logan Canyon	5 lithic grains	Fig. 1 (grain 1)	fine-grained calcite-cemented glauconitic quartz arenite	qtz+K-feld+ms	cal+gln+sd
				Fig. 2 (grain 2)	siderite-cemented sandstone	qtz+K-feld	sd+gln
				Fig. 3 (grain 3)	fine to medium-grained calcite-cemented glauconitic quartz arenite	qtz+K-feld	cal+gln+sd
				Fig. 4 (grain 4)	poorly sorted fossiliferous muddy sandstone	qtz+K-feld+pl+ilm	cal+fran+gln
				Fig. 5 (grain 5)	porous, very fine-grained, slightly glauconitic quartz arenite with late stage euhedral sideritic cement	qtz+K-feld	gln+sd
3880	1179	Missisauga	3 lithic grains	Fig. 13 (grain 2)	pyrite nodules developed in silty mudstone	qtz	py+clays
				Fig. 14 (grain 3)	meta-quartz arenite (biotite grade)	qtz+ms+bt+chl+ep+ilm (metamorphic assemblage)	rt
					One quartz granule	without inclusions	
4000	1215	Missisauga	1 rhyolite grain	Fig. 15	siderite cemented mudstone	qtz+K-feld+ilm+chl	sd+hem
			4 quartz grains	Fig. 16	one quartz granule	with ms inclusions	
					one quartz granule	with sd inclusions	
					one quartz granule	without inclusions	
					one quartz granule	without inclusions	

Table 8: (continued)

Sample (ft)	Depth (m)	Formation	Preliminary Identification	Figure in Appendix 2	Petrographic Description	Detrital Minerals	Diagenetic Minerals
4080	1240	Missisauga	4 lithic grains	Fig. 17 (grain 1)	silty limestone cut by calcite vein	qtz+K-feld+ms	cal+gln+sd+py
				Fig18 (grain 2)	very fine-grained calcite-cemented quartz arenite Two siderite-cemented mudstones	qtz+ms+K-feld+ilm+bt	cal+rt+gln+py
4100	1246	Missisauga	7 lithic grains		six siderite-cemented mudstones one pyrite-cemented quartz arenite		
4200	1276	Missisauga	3 lithic grains	Fig. 19 (grain 5)	very fine-grained calcite-cemented siltstone	qtz+K-feld+ms+ilm	cal+sd+rt
			2 quartz grains	Fig. 20 (grain 4)	very fine-grained carbonate-cemented quartz arenite-siltstone to subarkose	qtz+K-feld+ms+chl	cal+sd (zoned) +py+chl
				Fig. 21 (grain 1)	coarse-grained pyrite-cemented quartz arenite Two quartz granules with euhedral pyrite along fractures	qtz+ms+ilm	py

Notes on Table 8

One additional polished thin section of five lithic grains was studied using only petrographic microscope, from depth 2600 ft.
These grains were identified as follows:

3 grains: meta-quartz arenites to siltstone similar to the grain in Fig. 6 (3170A), Appendix 3; but with less chl+ep

1 grain is very fine-grained carbonate-cemented glauconitic quartz arenite similar to grain in Fig. 1 (3170B), Appendix 3

1 grain is a concentric siderite concretion with predominantly siderite grains and few very fine quartz and muscovite grains

Mineral abbreviations (mostly after Kretz 1983): bi = biotite; cal = calcite; chl = chlorite; ep = epidote; gln = glauconite; fran = francolite; hem = hematite; ilm = ilmenite; K-fld = K-feldspar; ms = muscovite; pl = plagioclase; py = pyrite; qtz = quartz; rt = rutile; sid = siderite; ttn = titanite;

Table 9: Summary of lithological character of cuttings samples > 2 mm in Sambro I-29

top depth (ft)	2600	2900	3080	3170	3350	3470	3700	3740	3880	4000	4080	4100	4160	4200
top depth (m)	789.9	881	935.7	963	1018	1054	1124	1136	1179	1215	1240	1246	1264	1276
total number of grains	33	223	35	609	240	55	304	196	312	313	325	685	173	1174
Sandstone, vf.-fine	10	77	3	51	78	18	19	5			7	20	10	5
Sandstone, medium	2											6		
(includes fine-medium)														
Sandstone, coarse-v.crs							1	1	1					2
(includes medium-coarse)														
Calcareous sandstones		114	3		7		20							
Conglomerate														
Shell fragments	8	21	6	39	72	3	1				1	1		
Coal and shaly coal	1		3		1		2			143	10	31	22	2
Silty shale							6							
Shale/mudstone										5				
Slate/schist									1					
White calcareous mudstone/chalk							44			4	6	8	2	
Calcareous shales														
Limestone														
Granules-white quartz	6	5		343	50	21	123	153	285	132	146	297	88	693
Granules-pink quartz	2								2			1		
Granules-yellow quartz				9		2	3	6	17	5		15	18	7
Granules-dark quartz	3	4	8	148	19		84	29	3	23	151	293	31	463
Granules-lithic clasts					12						2	1		2
Granules-feldspar				7			1	1				3		
Basalt/gabbro								1	1					
Rhyolite				3						1	2	6		
Quartzites/cherts		2		4					1					
Pyritized fossil/pyrite				3					1			2		
Pyroclastic														
Calcite	1				1									
"Common Unknown"			12	2		11						1	2	

Table 10: Petrographic description of selected cuttings from the < 2 mm fraction from Sambro I-29 well

Depth (ft)	Depth (m)	Petrographic description of representative grains	Minerals identified
3740	1136	1. siderite-cemented quartz arenite 2. quartz arenite with kaolinite and siderite cement 3. crystals: the majority of the crystals identified are pyrite either isolated or in association with quartz. Also isolated quartz, limonite, goethite, and siderite crystals have been identified.	qtz+ilm+K-feld; sd[x] qtz+K-feld+rt; sd+kln
3888	1181	1. siderite nodule developed in sands (Fig. 9)* 2. very fine-grained siderite-cemented subarkose (Fig. 10)* 3. siderite -cemented mudstone (Fig. 11)* 4.staurolite porphyroblasts with quartz and pyrite inclusions (Fig. 12)*	bt+K-feld+qtz; sd qtz+K-feld+ilm; sd+py+chl ms; sd+py+cal+chl

* these figures are in Appendix 3

[x] mineral name abbreviations as in Table 8

Table 11: Summary of dominant cuttings examined in Sambro I-29

Top (ft)	Top (m)	Predominant (in order if >1) or other interpreted as in place	Interpretation	Possible contamination
2600	790	qtz granules	v. crs sandstone, poorly indurated	might be contamination
		glauconitic fine sandstone		might be contamination
2900	881	fine grey sandstone		qtz granules
		fine calcareous sandstone		
3080	936			
3170	963	qtz qranules	v. crs sandstone, poorly indurated	
		fine glauconitic sandstone		
3316	*1007*	*top of Naskapi*		
3350	1018	fine glauconitic sandstone		qtz granules
3470	1054	fine glauconitic sandstone		qtz granules
3620	*1100*	*top of Missisauga*		
3700	1124	calcareous mudstone		
		qtz granules		
3740	1136	qtz granules		
3880	1179	qtz granules		
4000	1215	calcareous mudstone		(?) qtz granules
		coal-bearing sediment		
4080	1240	qtz granules		
		calcareous mudstone		
4100	1246	qtz granules		
		calcareous mudstone		
4160	1264	yellow fine sandstone, coaly		(?) qtz granules
4200	1276	qtz granules		

Table 12: Chemical analyses by electron microprobe of minerals in representative samples from Sambro I-29

Well	Analysis (min26)	FM[x]	Sample	Depth (m)	Mineral	SiO_2	TiO_2	Al_2O_3	Cr_2O_3	FeO_t	MnO	MgO	CaO	Na_2O	K_2O	Total
Sambro	25	MS	3880	1179	Biotite (H)[+]	36.00	3.85	17.74	0.00	20.32	0.29	4.85	0.09	0.16	8.68	91.98
Sambro	79	MS	3880	1179	Biotite	34.95	2.50	17.18	0.00	21.48	0.32	7.99	0.05	0.03	9.94	94.44
Sambro	80	MS	3880	1179	Biotite	34.60	2.62	17.46	0.00	21.95	0.33	8.19	0.04	0.04	10.22	95.45
Sambro	24	MS	4080	1240	Biotite	37.07	1.75	18.86	0.00	17.66	0.10	8.16	0.36	0.09	7.96	92.01
Sambro	56	LC	3170A	963	Chlorite	23.24	0.02	21.03	0.00	26.56	0.58	12.38	0.02	0.01	0.00	83.84
Sambro	57	LC	3170A	963	Chlorite	23.76	0.03	20.64	0.00	26.14	0.06	12.67	0.02	0.02	0.00	83.34
Sambro	54	MS	3880	1179	Chlorite (H)	32.29	0.02	11.25	0.00	30.52	0.21	9.45	0.48	0.34	0.40	84.96
Sambro	55	MS	3880	1179	Chlorite (H)	28.96	0.12	12.63	0.00	34.02	0.22	6.83	0.50	0.43	0.00	83.71
Sambro	82	MS	3880	1179	Chlorite	24.53	0.25	21.05	0.00	27.49	0.59	13.21	0.03	0.00	0.03	87.18
Sambro	83	MS	3880	1179	Chlorite	24.61	0.18	21.32	0.00	27.49	0.60	13.02	0.03	0.00	0.09	87.34
Sambro	50	MS	4000	1215	Chlorite	30.29	0.07	11.77	0.05	35.70	0.22	6.59	0.54	0.38	0.00	85.61
Sambro	51	MS	4000	1215	Chlorite	25.59	0.00	21.58	0.00	27.99	0.05	13.38	0.03	0.05	0.00	88.67
Sambro	52	MS	4000	1215	Chlorite	25.74	0.00	22.48	0.00	29.62	0.07	8.65	0.08	0.07	0.00	86.71
Sambro	53	MS	4000	1215	Chlorite	32.67	0.00	13.93	0.11	30.59	0.05	3.51	1.06	0.61	0.37	82.90
Sambro	58	LC	3170A	963	Epidote	37.21	0.14	25.28	0.00	7.70	0.11	0.05	23.08	0.01	0.00	93.58
Sambro	78	MS	3880	1179	Epidote	37.49	0.15	25.23	0.00	9.40	0.19	0.04	23.87	0.00	0.01	96.38
Sambro	48	LC	3170A	963	Glauconite	46.97	0.03	8.73	0.00	21.20	0.04	3.60	0.17	0.46	7.29	88.49
Sambro	49	LC	3170A	963	Glauconite	45.41	0.02	9.04	0.00	17.84	0.05	3.39	0.54	0.21	6.28	82.78
Sambro	26	LC	3170B	963	Glauconite	43.96	0.08	8.81	0.02	20.15	0.01	3.39	0.23	0.05	6.66	83.36
Sambro	27	LC	3170B	963	Glauconite	43.40	0.36	12.40	0.03	19.50	0.06	3.82	0.49	0.17	6.82	87.05
Sambro	28	LC	3170B	963	Glauconite	42.72	0.09	7.55	0.02	25.92	0.06	3.93	0.53	0.19	7.12	88.13
Sambro	29	LC	3170B	963	Glauconite	41.66	0.08	11.12	0.02	19.68	0.04	2.92	0.39	0.13	5.94	81.98

Table 12: (continued)

Well	Analysis (min26)	FM[x]	Sample	Depth (m)	Mineral	SiO_2	TiO_2	Al_2O_3	Cr_2O_3	FeO_t	MnO	MgO	CaO	Na_2O	K_2O	Total
Sambro	30	LC	3170B	963	Glauconite	49.02	0.14	12.18	0.03	15.80	0.03	2.96	0.33	0.22	4.99	85.70
Sambro	31	LC	3170B	963	Glauconite	43.50	0.13	12.82	0.02	13.59	0.02	3.36	0.53	0.18	6.07	80.22
Sambro	32	LC	3170B	963	Glauconite	45.63	0.13	9.32	0.01	20.63	0.06	3.85	0.47	0.07	7.03	87.20
Sambro	33	LC	3170B	963	Glauconite	41.56	0.09	13.66	0.03	19.56	0.06	3.02	0.90	0.30	5.32	84.50
Sambro	34	LC	3170B	963	Glauconite	43.90	0.17	9.11	0.00	20.94	0.02	3.63	0.22	0.06	6.79	84.84
Sambro	35	LC	3170B	963	Glauconite	36.27	0.10	11.32	0.06	30.19	0.13	5.57	0.74	0.20	3.27	87.85
Sambro	36	LC	3170B	963	Glauconite	43.80	0.05	10.76	0.01	20.74	0.00	2.52	0.30	0.36	6.05	84.59
Sambro	37	LC	3170B	963	Glauconite	48.27	0.07	12.92	0.00	19.56	0.00	2.36	0.22	0.26	5.97	89.43
Sambro	38	LC	3170B	963	Glauconite	41.82	0.05	8.42	0.00	22.53	0.00	2.49	0.52	0.44	6.23	82.50
Sambro	39	LC	3170B	963	Glauconite	46.34	0.00	7.50	0.00	22.94	0.03	3.38	0.33	0.09	8.12	88.73
Sambro	40	LC	3170B	963	Glauconite	45.57	0.00	6.40	0.02	24.17	0.03	3.43	0.39	0.23	7.73	87.97
Sambro	41	LC	3170B	963	Glauconite	47.31	0.04	6.83	0.03	22.48	0.03	3.54	0.22	0.07	8.41	88.96
Sambro	42	LC	3170B	963	Glauconite	45.35	0.09	7.37	0.04	23.73	0.06	3.49	0.25	0.20	8.22	88.80
Sambro	43	LC	3170B	963	Glauconite	45.93	0.05	7.09	0.05	23.23	0.06	3.42	0.39	0.14	8.53	88.89
Sambro	44	LC	3170B	963	Glauconite	42.98	0.09	8.54	0.03	20.97	0.02	3.21	0.67	0.14	6.43	83.08
Sambro	45	LC	3170B	963	Glauconite	46.30	0.03	9.80	0.03	20.12	0.03	3.10	0.43	0.11	7.46	87.41
Sambro	46	MS	4080	1240	Glauconite	43.45	0.03	8.31	0.00	20.36	0.02	2.44	0.79	0.78	5.75	81.93
Sambro	47	MS	4080	1240	Glauconite	47.82	0.08	10.75	0.00	19.68	0.02	2.89	1.00	0.52	5.62	88.38
Sambro	75	MS	3740	1136	Goethite (H)	0.00	0.11	0.08	0.04	80.03	0.28	0.00	0.07	0.02	0.00	80.63
Sambro	74	MS	3740	1136	Goethite (H)	0.00	0.10	0.12	0.06	80.79	0.37	0.00	0.07	0.01	0.00	81.52
Sambro	73	MS	4000	1215	Hematite	0.32	0.71	0.24	0.01	87.13	0.04	0.09	0.26	0.01	0.00	88.81
Sambro	67	MS	3740	1136	Ilmenite	0.00	50.26	0.11	0.07	43.51	1.81	0.60	0.16	0.00	0.00	96.52
Sambro	63	MS	3740	1136	Ilmenite* (H)	0.13	66.76	0.21	0.13	24.28	2.13	0.08	0.20	0.03	0.00	93.95
Sambro	64	MS	3740	1136	Ilmenite* (H)	0.25	68.17	0.26	0.19	22.95	2.84	0.05	0.22	0.05	0.00	94.98
Sambro	65	MS	3740	1136	Ilmenite* (H)	0.20	68.81	0.18	0.14	24.62	1.29	0.05	0.23	0.04	0.00	95.56
Sambro	66	MS	3740	1136	Ilmenite* (H)	0.21	68.31	0.29	0.14	22.28	2.96	0.05	0.24	0.07	0.00	94.55
Sambro	68	MS	3880	1179	Ilmenite (H)	0.03	52.47	0.18	0.00	42.51	0.79	4.74	0.13	0.03	0.00	100.88
Sambro	88	MS	3880	1179	Ilmenite	0.00	53.12	0.00	0.00	41.89	4.83	0.04	0.11	0.00	0.00	99.99
Sambro	62	MS	4000	1215	Ilmenite	0.03	52.33	0.08	0.00	42.26	0.55	2.05	3.62	0.04	0.00	100.96
Sambro	69	MS	4200	1276	Ilmenite*	0.38	73.25	0.70	0.00	15.05	0.74	0.14	0.14	0.20	0.00	90.60
Sambro	70	MS	4200	1276	Ilmenite*	0.07	66.68	0.30	0.00	20.33	2.13	0.13	0.07	0.06	0.00	89.77

Table 12: (continued)

Well	Analysis (min26)	FM[x]	Sample	Depth (m)	Mineral	SiO_2	TiO_2	Al_2O_3	Cr_2O_3	FeO_t	MnO	MgO	CaO	Na_2O	K_2O	Total
Sambro	14	LC	3170A	963	K-Feldspar	61.92	0.03	18.56	0.00	0.04	0.00	0.01	0.09	1.22	15.89	97.46
Sambro	1	LC	3170B	963	K-Feldspar	63.65	0.03	18.28	0.00	0.09	0.00	0.00	0.04	0.91	16.79	99.79
Sambro	2	LC	3170B	963	K-Feldspar	63.86	0.00	18.14	0.00	0.06	0.00	0.01	0.01	0.72	17.52	100.32
Sambro	3	LC	3170B	963	K-Feldspar	64.14	0.00	17.87	0.00	1.31	0.00	0.02	0.00	0.35	17.31	101.00
Sambro	4	LC	3170B	963	K-Feldspar	63.54	0.04	18.38	0.00	0.30	0.00	0.00	0.02	0.86	16.61	99.75
Sambro	5	LC	3170B	963	K-Feldspar	63.60	0.01	13.14	0.00	0.35	0.00	0.00	0.00	0.28	17.27	94.65
Sambro	8	MS	3740	1136	K-Feldspar (H)	63.00	0.00	17.79	0.00	1.54	0.00	0.00	0.02	0.73	16.99	100.07
Sambro	6	MS	4000	1215	K-Feldspar	64.41	0.00	18.38	0.01	0.94	0.00	0.01	0.02	0.12	17.96	101.85
Sambro	7	MS	4000	1215	K-Feldspar	64.51	0.00	18.28	0.00	0.72	0.00	0.01	0.00	1.52	14.75	99.79
Sambro	9	MS	4080	1240	K-Feldspar	62.97	0.00	18.36	0.00	0.09	0.00	0.01	0.13	0.36	18.20	100.12
Sambro	10	MS	4080	1240	K-Feldspar	64.05	0.00	18.61	0.00	0.08	0.00	0.01	0.34	0.33	18.04	101.46
Sambro	11	MS	4080	1240	K-Feldspar	62.20	0.00	18.29	0.00	0.07	0.00	0.01	0.40	0.58	16.85	98.40
Sambro	12	MS	4080	1240	K-Feldspar	63.68	0.00	19.07	0.00	0.00	0.00	0.02	0.04	1.32	16.32	100.45
Sambro	13	MS	4080	1240	K-Feldspar	63.63	0.00	18.31	0.00	0.03	0.00	0.02	0.07	0.33	17.82	100.21
Sambro	15	MS	4200	1276	K-Feldspar	62.55	0.00	18.34	0.00	0.01	0.00	0.00	0.03	0.52	17.77	99.22
Sambro	71	MS	3170B	963	Plagioclase	63.05	0.00	22.00	0.00	0.15	0.00	0.04	3.67	10.08	0.11	99.10
Sambro	72	MS	3740	1136	Limonite	0.00	0.10	0.28	0.09	73.14	0.35	0.00	0.15	0.00	0.00	74.11
Sambro	16	LC	3170B	963	Muscovite	46.31	0.58	35.63	0.01	0.91	0.00	0.53	0.09	1.52	9.65	95.23
Sambro	17	LC	3170B	963	Muscovite	45.42	0.42	33.80	0.00	1.45	0.00	0.66	0.25	0.33	10.70	93.03
Sambro	18	LC	3170B	963	Muscovite	45.15	0.56	34.49	0.00	2.25	0.00	0.50	0.00	1.06	9.47	93.48
Sambro	20	MS	3880	1179	Muscovite (H)	45.68	0.28	33.55	0.00	3.66	0.00	0.92	0.04	0.40	7.45	92.28
Sambro	84	MS	3880	1179	Muscovite	45.65	1.00	33.72	0.00	1.74	0.02	1.12	0.01	0.28	9.66	93.20
Sambro	85	MS	3880	1179	Muscovite	46.00	0.26	30.11	0.00	4.01	0.02	1.77	0.00	0.18	8.80	91.15
Sambro	81	MS	3880	1179	Muscovite	47.00	1.22	30.45	0.00	2.55	0.03	1.83	0.02	0.16	9.01	92.27
Sambro	19	MS	4080	1240	Muscovite	44.70	0.43	35.90	0.00	0.94	0.00	0.55	0.12	1.19	9.12	92.95
Sambro	21	MS	4200	1276	Muscovite	44.17	0.33	29.42	0.00	5.58	0.06	2.50	0.00	0.19	9.62	91.87
Sambro	22	MS	4080	1240	Hydromuscovite	46.62	0.03	30.23	0.00	5.66	0.00	1.15	0.32	0.45	7.31	91.77
Sambro	23	MS	4200	1276	Hydromuscovite	44.17	0.39	33.95	0.00	1.93	0.00	0.47	0.07	1.00	8.08	90.06
Sambro	60	MS	3740	1136	Rutile	0.07	97.92	0.13	0.07	2.61	0.05	0.00	0.19	0.00	0.00	101.04
Sambro	86	MS	3880	1179	Rutile	0.00	100.00	0.36	0.00	0.38	0.07	0.01	0.36	0.00	0.00	101.18
Sambro	59	MS	4000	1215	Rutile	0.27	92.98	0.99	0.00	2.29	0.00	0.06	0.62	0.16	0.00	97.37
Sambro	87	MS	4080	1240	Rutile	0.13	98.74	0.41	0.00	0.63	0.00	0.03	0.96	0.00	0.00	100.90
Sambro	61	MS	4200	1276	Rutile	0.00	100.85	0.00	0.00	0.34	0.05	0.00	0.79	0.00	0.00	102.03
Sambro	76	MS	3880	1179	Staurolite (H)	26.33	0.32	53.17	0.00	13.98	0.36	1.49	0.00	0.04	0.00	95.69
Sambro	77	LC	3170A	963	Titanite	29.74	32.45	4.44	0.00	0.29	0.00	0.02	28.22	0.01	0.00	95.17

Table 12: (continued)

Well	Analysis (excel)	FM[x]	Sample	Depth (m)	Mineral	SiO_2	TiO_2	Al_2O_3	Cr_2O_3	FeO_t	MnO	MgO	CaO	Na_2O	K_2O	P_2O_5	NiO	BaO	ZrO_2	Total
Sambro	1	LC	3170B	963	Calcite	0.00	0.00	0.00	0.00	0.26	0.01	1.37	57.30	2.04	0.06	0.05	0.01	0.05	0.00	61.15
Sambro	2	LC	3170B	963	Calcite	0.00	0.00	0.00	0.00	0.26	0.00	0.46	59.25	0.14	0.01	0.03	0.00	0.00	0.00	60.15
Sambro	3	LC	3170B	963	Calcite	0.00	0.00	0.00	0.00	0.18	0.02	0.15	60.60	0.23	0.01	0.05	0.03	0.00	0.00	61.27
Sambro	4	LC	3170B	963	Calcite	0.00	0.00	0.00	0.00	0.13	0.29	1.05	52.70	0.08	0.00	0.06	0.00	0.00	0.00	54.31
Sambro	5	LC	3170B	963	Calcite	0.00	0.00	0.00	0.00	3.25	0.43	0.28	60.04	0.00	0.00	0.01	0.00	0.00	0.00	64.01
Sambro	6	LC	3170B	963	Calcite	0.00	0.00	0.00	0.00	0.15	0.51	0.77	60.32	0.10	0.00	0.04	0.00	0.00	0.00	61.89
Sambro	7	LC	3170B	963	Calcite	0.00	0.00	0.00	0.00	0.26	0.12	1.00	59.14	0.17	0.00	0.02	0.00	0.00	0.00	60.71
Sambro	8	LC	3170B	963	Calcite	0.00	0.00	0.00	0.01	4.76	0.43	0.43	60.20	0.04	0.00	0.07	0.00	0.01	0.00	65.95
Sambro	9	LC	3170B	963	Calcite	0.00	0.00	0.05	0.01	2.87	0.30	0.42	60.85	0.04	0.00	0.09	0.00	0.11	0.00	64.74
Sambro	16	MS	3880	1179	Calcite (H)	0.16	0.00	0.04	0.00	2.84	0.40	1.35	49.09	0.07	0.00	0.14	0.00	0.00	0.00	54.09
Sambro	10	MS	4080	1240	Calcite	0.00	0.00	0.00	0.00	3.69	0.25	0.65	58.41	0.00	0.00	0.03	0.00	0.00	0.00	63.03
Sambro	11	MS	4080	1240	Calcite	0.00	0.00	0.00	0.00	0.08	0.00	0.34	59.79	0.15	0.00	0.04	0.00	0.00	0.00	60.40
Sambro	12	MS	4080	1240	Calcite	0.00	0.00	0.00	0.00	0.76	0.03	0.06	63.19	0.00	0.00	0.01	0.00	0.00	0.00	64.05
Sambro	13	MS	4080	1240	Calcite	0.00	0.00	0.12	0.00	1.04	0.09	0.18	48.15	0.33	0.00	0.05	0.00	0.00	0.00	49.96
Sambro	14	MS	4080	1240	Calcite	0.00	0.00	0.00	0.00	3.25	0.19	0.47	60.97	0.00	0.00	0.05	0.00	0.00	0.00	64.93
Sambro	15	MS	4080	1240	Calcite	0.00	0.00	0.00	0.00	1.75	0.95	0.19	57.94	0.02	0.00	0.03	0.00	0.00	0.00	60.88
Sambro	50	MS	4080	1240	Calcite	0.00	0.00	0.40	0.00	2.16	0.14	0.41	57.40	0.02	0.06	0.04	0.10	0.00	0.00	60.73
Sambro	17	MS	4200	1276	Calcite	0.00	0.00	0.00	0.00	2.45	0.42	0.54	60.20	0.00	0.00	0.01	0.00	0.00	0.00	63.62
Sambro	49	MS	4200	1276	Calcite	0.66	0.00	0.26	0.00	1.31	0.45	0.17	60.54	0.00	0.00	0.00	0.00	0.00	0.00	63.39
Sambro	18	LC	3170B	963	Siderite	0.00	0.04	0.00	0.01	40.85	0.63	9.31	6.44	0.00	0.03	0.05	0.06	0.03	0.00	57.45
Sambro	19	LC	3170B	963	Siderite	0.99	0.18	0.54	0.00	44.27	0.79	5.83	5.62	0.08	0.00	0.25	0.00	0.01	0.00	58.56
Sambro	20	LC	3170B	963	Siderite	0.16	0.00	0.11	0.00	43.38	1.19	7.09	5.91	0.06	0.00	0.13	0.00	0.00	0.00	58.03
Sambro	21	LC	3170B	963	Siderite	0.00	0.01	0.00	0.03	44.10	0.42	6.02	6.89	0.03	0.00	0.08	0.00	0.04	0.00	57.62
Sambro	22	LC	3170B	963	Siderite	0.00	0.09	0.10	0.04	44.23	1.92	3.39	7.26	0.08	0.00	0.25	0.04	0.24	0.00	57.64
Sambro	23	LC	3170B	963	Siderite	0.00	0.04	0.26	0.04	44.48	1.64	3.58	7.31	0.09	0.00	0.26	0.03	0.19	0.00	57.92

Table 12: (continued)

Well	Analysis (excel)	FM[x]	Sample	Depth (m)	Mineral	SiO_2	TiO_2	Al_2O_3	Cr_2O_3	FeO_t	MnO	MgO	CaO	Na_2O	K_2O	P_2O_5	NiO	BaO	ZrO_2	Total
Sambro	24	LC	3170B	963	Siderite	5.04	0.01	3.60	0.02	38.78	0.69	4.58	7.17	0.07	0.07	0.21	0.09	0.09	0.00	60.42
Sambro	29	MS	3740	1136	Siderite	0.00	0.06	0.00	0.02	56.00	1.02	0.00	0.30	0.00	0.00	0.41	0.07	0.06	0.00	57.94
Sambro	30	MS	3740	1136	Siderite	0.00	0.06	0.00	0.02	54.88	0.15	1.01	1.66	0.00	0.00	0.12	0.06	0.09	0.00	58.05
Sambro	31	MS	3740	1136	Siderite	0.00	0.06	0.00	0.01	41.98	0.35	8.85	5.32	0.00	0.00	0.02	0.07	0.01	0.00	56.67
Sambro	32	MS	3740	1136	Siderite	1.06	0.10	0.54	0.01	47.11	0.51	7.42	2.57	0.04	0.01	0.03	0.04	0.04	0.00	59.48
Sambro	33	MS	3740	1136	Siderite	0.00	0.05	0.00	0.02	45.44	0.60	6.28	4.86	0.07	0.00	0.21	0.05	0.06	0.00	57.64
Sambro	34	MS	3740	1136	Siderite	0.00	0.10	0.10	0.07	76.60	0.29	0.00	0.08	0.00	0.00	0.50	0.16	0.16	0.00	78.06
Sambro	40	MS	3880	1179	Siderite (H)	0.59	0.00	0.54	0.00	42.32	0.37	7.20	5.61	0.13	0.00	0.29	0.00	0.00	0.00	57.05
Sambro	41	MS	3880	1179	Siderite (H)	0.21	0.06	0.21	0.00	42.35	0.33	8.24	5.88	0.04	0.00	0.02	0.00	0.00	0.00	57.34
Sambro	42	MS	3880	1179	Siderite (H)	0.90	0.03	0.53	0.00	40.24	0.35	5.69	7.46	0.16	0.00	0.54	0.00	0.00	0.00	55.90
Sambro	25	MS	4000	1215	Siderite	2.37	0.14	0.59	0.03	42.58	0.39	5.82	8.20	0.25	0.14	0.32	0.04	0.09	0.00	60.96
Sambro	26	MS	4000	1215	Siderite	5.94	0.00	2.43	0.00	45.36	0.38	3.92	8.10	0.53	0.00	0.95	0.00	0.00	0.00	67.61
Sambro	27	MS	4000	1215	Siderite	1.24	0.00	0.17	0.00	44.07	0.32	5.29	8.89	0.27	0.00	0.35	0.00	0.00	0.00	60.60
Sambro	28	MS	4000	1215	Siderite	1.61	0.00	0.02	0.00	43.45	0.30	5.75	8.20	0.29	0.00	0.24	0.00	0.00	0.00	59.86
Sambro	47	MS	4000	1215	Siderite	4.48	0.09	0.04	0.04	51.44	0.55	4.01	5.88	0.66	0.00	0.38	0.07	0.11	0.00	67.75
Sambro	35	MS	4080	1240	Siderite	0.00	0.04	0.11	0.00	45.41	0.37	5.56	5.59	0.04	0.00	0.14	0.00	0.10	0.00	57.36
Sambro	36	MS	4080	1240	Siderite	2.36	0.04	0.34	0.00	36.50	0.66	4.79	6.13	0.21	0.00	0.12	0.00	0.02	0.00	51.17
Sambro	37	MS	4080	1240	Siderite	0.00	0.01	0.10	0.00	39.04	0.37	6.25	6.00	0.06	0.00	0.12	0.00	0.00	0.00	51.95
Sambro	38	MS	4080	1240	Siderite	0.00	0.01	0.02	0.00	40.96	0.53	8.41	6.71	0.10	0.00	0.11	0.00	0.03	0.00	56.88
Sambro	39	MS	4080	1240	Siderite	0.22	0.02	0.09	0.00	42.56	0.79	8.10	5.53	0.15	0.00	0.04	0.00	0.03	0.00	57.53
Sambro	43	MS	4200	1276	Siderite	0.00	0.01	0.00	0.00	40.09	0.49	8.26	7.06	0.03	0.00	0.05	0.00	0.02	0.00	56.01
Sambro	44 c	MS	4200	1276	Siderite	0.00	0.07	0.00	0.00	49.72	1.95	1.52	3.06	0.01	0.00	0.12	0.00	0.07	0.00	56.52
Sambro	46 r	MS	4200	1276	Siderite	0.76	0.06	0.53	0.00	40.22	1.06	6.37	7.68	0.04	0.00	0.07	0.00	0.08	0.00	56.87
Sambro	45	MS	4200	1276	Siderite	0.44	0.05	0.27	0.00	41.19	0.45	6.91	6.53	0.03	0.00	0.07	0.00	0.08	0.00	56.02
Sambro	48	LC	3170A	963	Apatite	0.00	0.00	0.00	0.00	0.21	0.01	0.03	53.82	0.44	0.00	36.15	0.00	0.00	0.00	90.66

[+] (H) = Analyses indicated with (H) are from heavy mineral seperates. All others are from the fraction >2mm

* = These ilmenite chemical analyses have low totals, probably because of alteration

[x] = symbols as in Table 7

Table 13: Representative electron microprobe chemical analyses of calcium phosphate minerals

Sample	Sambro 3170A (963 m)			
Analysis	9	10	11	12
SiO_2	0.00	0.00	0.00	0.00
Al_2O_3	1.72	4.36	2.80	2.19
FeO_t	1.34	2.78	2.43	2.07
CaO	44.02	38.32	43.52	45.84
Na_2O	1.13	1.00	1.06	1.01
K_2O	0.00	0.00	0.00	0.00
BaO	0.00	0.00	0.00	0.00
SrO	0.40	0.30	0.32	0.30
P_2O_5	28.67	25.46	28.46	29.81
As_2O_5	0.00	0.00	0.00	0.00
Ce_2O_3	0.28	0.46	0.45	0.41
La_2O_3	0.68	0.66	0.72	0.73
SO_3	1.52	1.87	2.07	1.97
H_2O	13.68	14.72	13.59	10.38
F	3.27	3.00	3.38	3.38
Cl	0.13	0.09	0.10	0.09
Total	96.84	93.02	98.89	98.18

Table 14: Summary of the detrital and neomorphic mineral assemblages with depth in Sambro I-29 well

Sample (feet)	Depth (m)	Detrital minerals (in addition to quartz)	Neomorphic minerals
3170A (LC)*	963	K-feldspar Chlorite Titanite Epidote Rutile	Francolite Calcite Pyrite Chlorite Galena Glauconite
3170B (LC)	963	K-feldspar Muscovite Ilmenite Plagioclase	Calcite Galena Siderite Francolite Glauconite
3740 (MS)*	1136	K-feldspar Ilmenite Rutile	Siderite Kaolinite Goethite
3880 (MS)	1179	K-feldspar Biotite Ilmenite Muscovite Chlorite Epidote Staurolite	Siderite Pyrite Chlorite Calcite Clays Rutile
4000 (MS)	1215	K-feldspar Ilmenite Chlorite Muscovite	Siderite Hematite
4080 (MS)	1240	K-feldspar Muscovite Ilmenite Biotite	Calcite Galena Siderite Pyrite Rutile Glauconite
4100 (MS)	1246		Siderite Pyrite
4200 (MS)	1276	K-feldspar Muscovite Ilmenite Chlorite	Calcite Siderite Pyrite Chlorite Rutile

* LC = Logan Canyon; MS = Missisauga

APPENDIX 1

List of studied samples

Naskapi N-30

Sample	Depth (m)	Formation	Activities
D4-1-1	1467.96	Missisauga	ps
D4-1-2P	1467.96	Missisauga	palynology
D4-1-3	1468.65	Missisauga	ps
D4-1-4	1469.00	Missisauga	ps, gs, ca
D4-1-5P	1469.05	Missisauga	palynology
D4-1-6	1469.89	Missisauga	gs, ca
D4-1-7	1470.50	Missisauga	ps
D4-1-8	1471.75	Missisauga	ps, gs, ca
D4-1-9	1472.25	Missisauga	ps, gs, ca
D4-1-10	1472.36	Missisauga	ps
D4-1-11	1473.51	Missisauga	ps
D4-1-12	1473.61	Missisauga	ps
D4-1-13	1473.81	Missisauga	ps, gs, ca
D4-1-14P	1474.00	Missisauga	palynology

Sambro I-29

Sample (ft)	Depth (m)	Formation	Activities
2600	790	Logan Canyon	pi, h, ps (g)
2900	881	Logan Canyon	pi, h
3080	936	Logan Canyon	pi, h
3170	963	Logan Canyon	pi, h, ps (gA), ps (gB)
3350	1018	Naskapi	pi, h
3470	1054	Naskapi	pi, h
3700	1124	Missisauga	pi, h
3740	1136	Missisauga	pi, h, ps (h)
3880	1179	Missisauga	pi, h ps (h), ps (g)
4000	1215	Missisauga	pi, h, ps (g)
4080	1240	Missisauga	pi, h, ps (g)
4100	1246	Missisauga	pi, h, ps (g)
4160	1264	Missisauga	pi, h
4200	1276	Missisauga	pi, h, ps (g)

Abbreviations under activities:
h = heavy mineral separation; gs = grain size analysis; ps = probe thin section; ps (h) = polished thin section of heavy fraction; ps (g) polished thin section of grains from the light fraction (>2mm); ca = whole rock chemical analysis; pi = petrographic identification of all grains >2mm

APPENDIX 2

PHOTOGRAPHS OF CONVENTIONAL CORE FROM NASKAPI N-30

(a) Photographs of conventional core as received from Operator.

(b) Detailed photographs of split core face. Photographs located in Figure 2B.

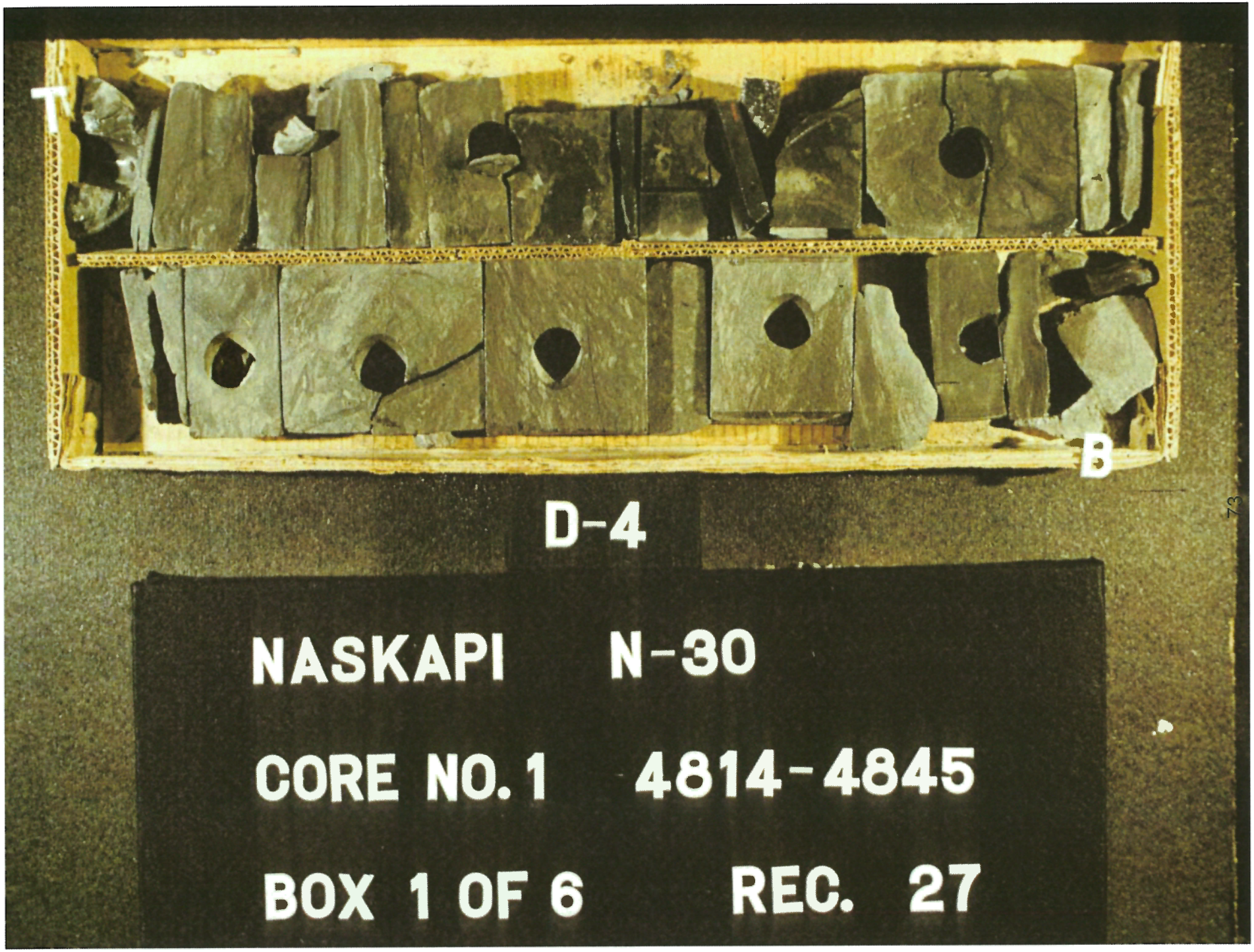
T
B
D-4
NASKAPI N-30
CORE NO. 1 4814-4845
BOX 1 OF 6 REC. 27

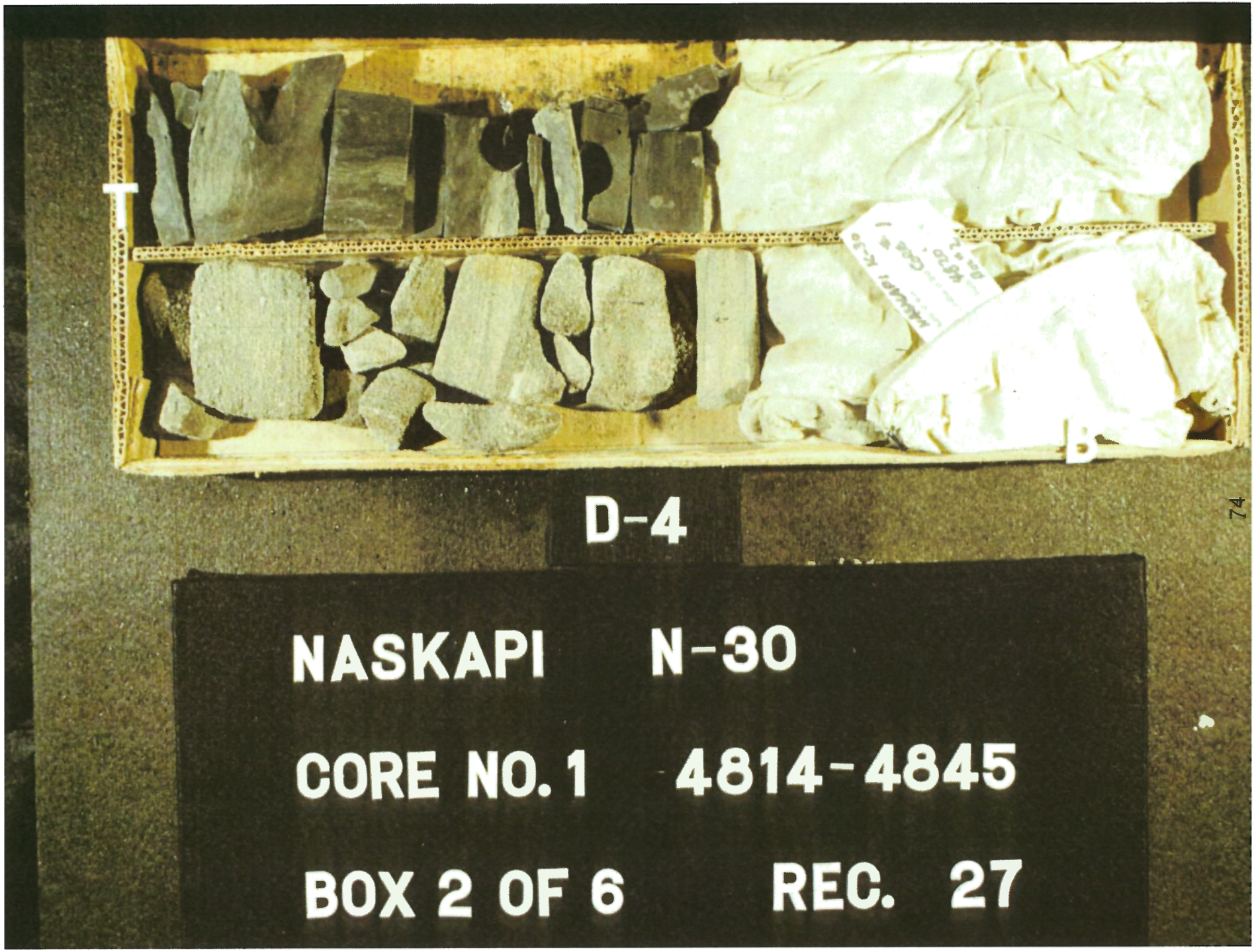
D-4
NASKAPI N-30
CORE NO. 1 4814-4845
BOX 2 OF 6 REC. 27

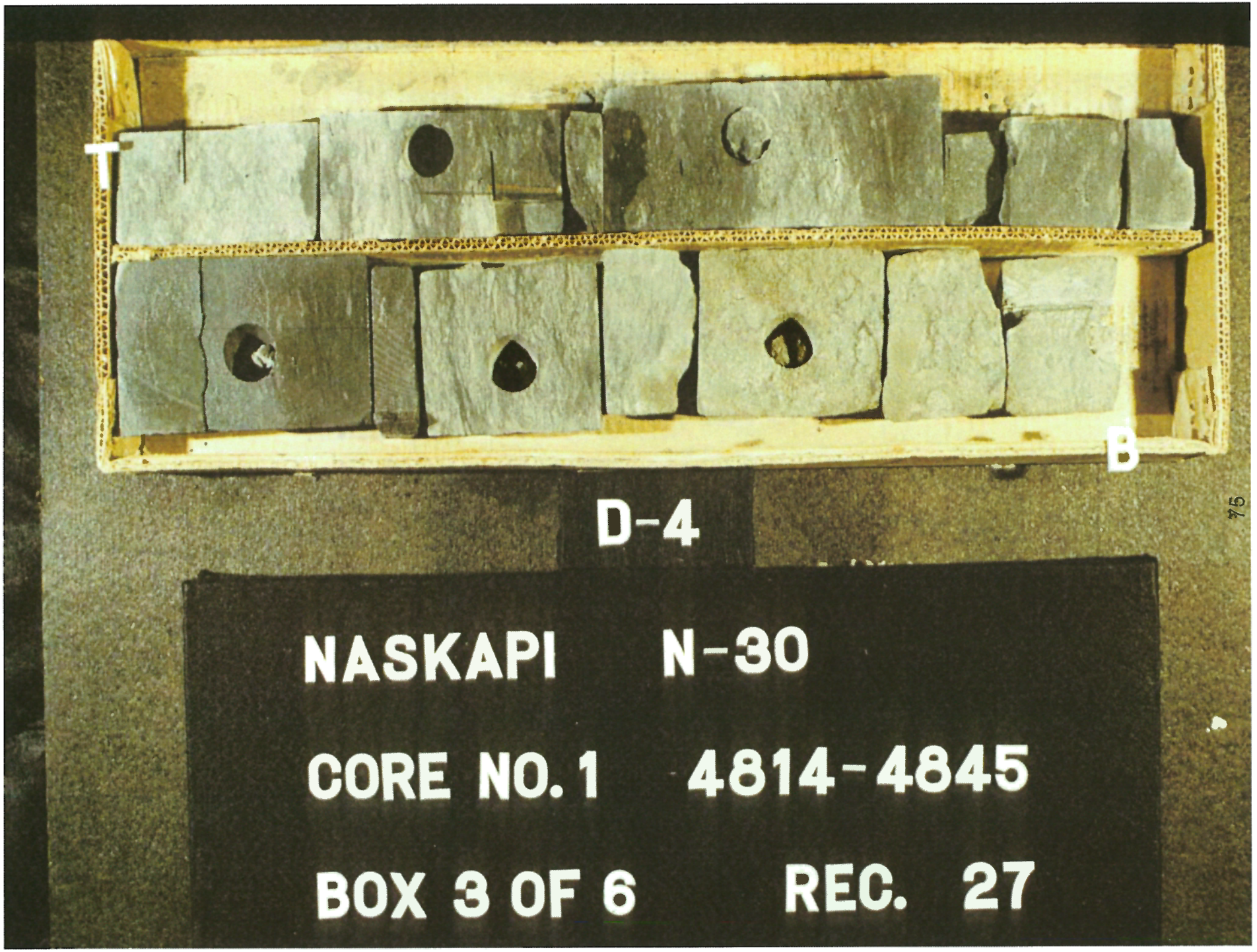
T
B
D-4
NASKAPI N-30
CORE NO. 1 4814-4845
BOX 3 OF 6 REC. 27
15

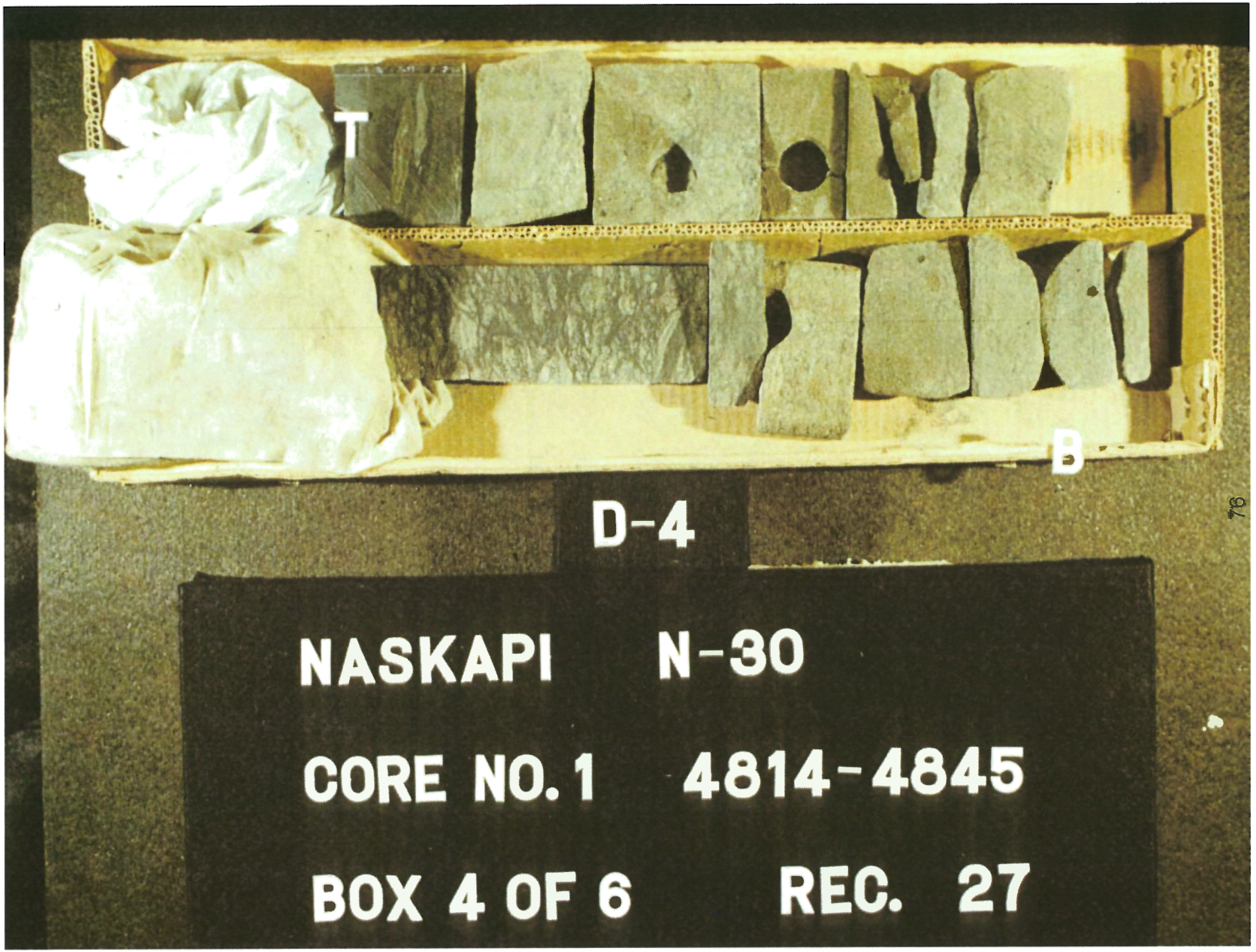
T
B
D-4
NASKAPI N-30
CORE NO. 1 4814-4845
BOX 4 OF 6 REC. 27

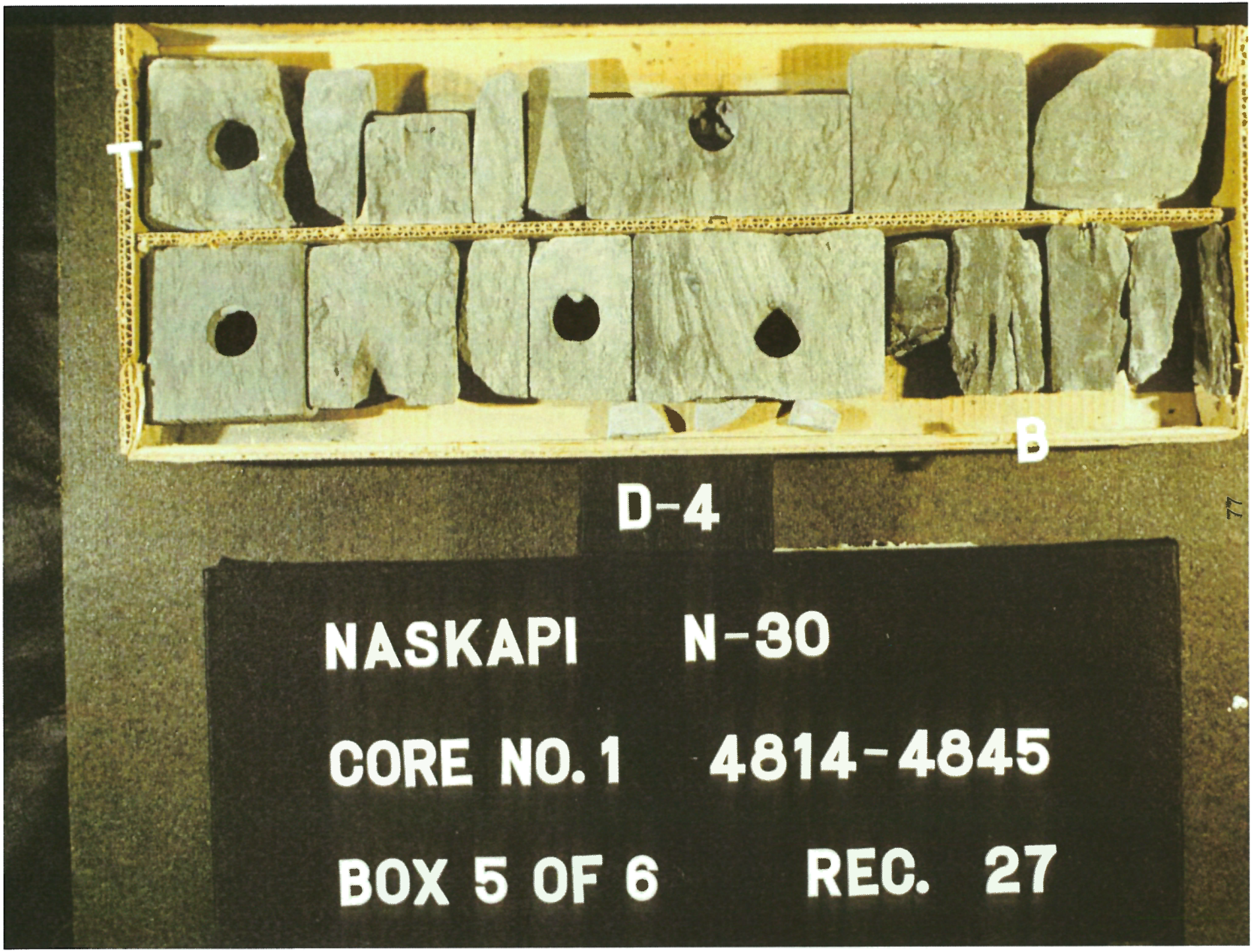
T
B
D-4
NASKAPI N-30
CORE NO. 1 4814-4845
BOX 5 OF 6 REC. 27

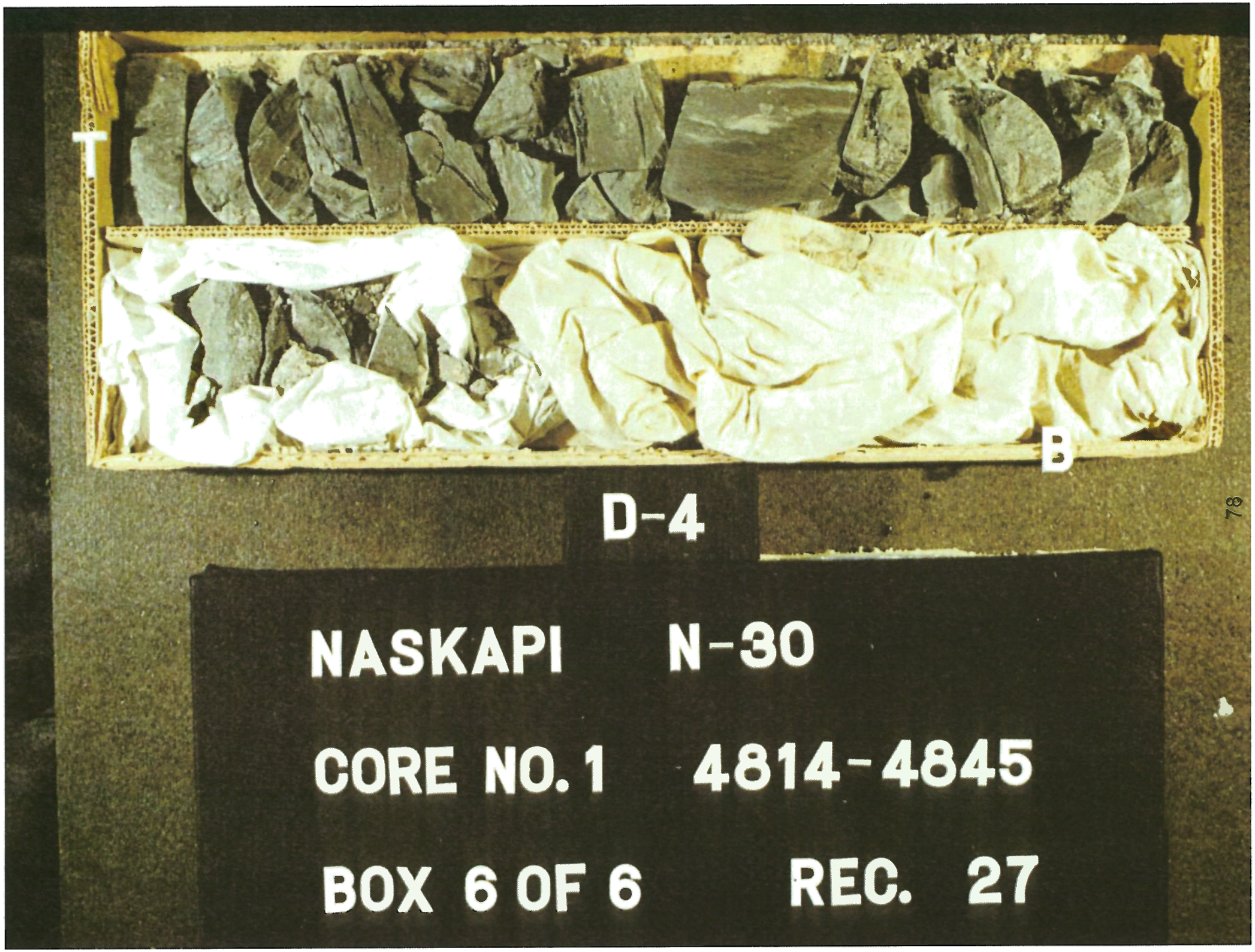
T
B
D-4
NASKAPI N-30
CORE NO. 1 4814-4845
BOX 6 OF 6 REC. 27
78

Photo 1: Completely bioturbated silty mudstone, some remnants of sorted fine-grained sandstone, some 5 mm phytodetritus. Unit 1.

Photo 2: Completely bioturbated fine-grained sandstone with phytodetritus. Locally, more mudstone. Unit 2.

Photo 3: Completely bioturbated fine-grained sandstone with phytodetritus. Interbedded mudstone bed. Unit 2.

Photo 4: Bioturbated fine-grained sandstone, subsequently deformed into s-fold. Unit 2.

Photo 5: Deformed, fine-grained sandstone with lamina of phytodetritus at top, over dark silty mudstone. Unit 2.

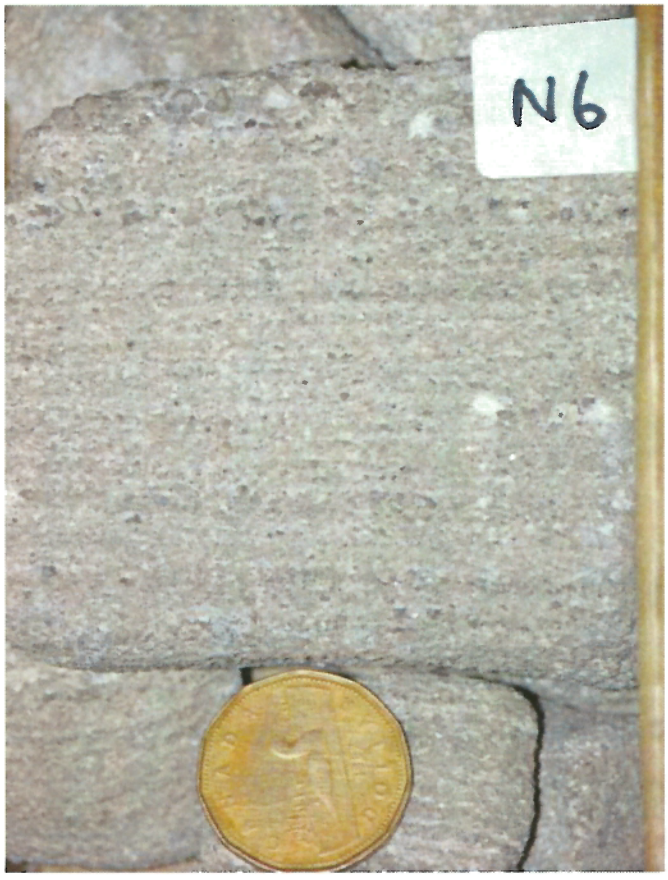

Photo 6: Parallel laminated, very coarse-grained sandstone, no bioturbation. Unit 3.

Photo 7: Parallel laminated, fine-grained sandstone, no bioturbation. Unit 3.

Photo 8: Parallel laminated, fine-grained sandstone and mudstone with siltstone laminae. Sparse or no bioturbation. Unit 3.

Photo 9: Completely bioturbated fine-grained sandstone, some phytodetritus, minor mudstone. Unit 4.

Photo 10: Completely bioturbated fine-grained sandstone and mudstone, with phytodetritus. Unit 4.

Photo 11: Completely bioturbated fine sandstone and mudstone, with phytodetritus. Unit 4.

Photo 12: Completely bioturbated fine sandstone and mudstone, with phytodetritus. Unit 4.

Photo 13: Fine-grained sandstone with thin mud drapes and minor bioturbation. Top of Unit 5.

Photo 14: Completely bioturbated mudstone and fine- grained sandstone with phytodetritus. Top of Unit 7.

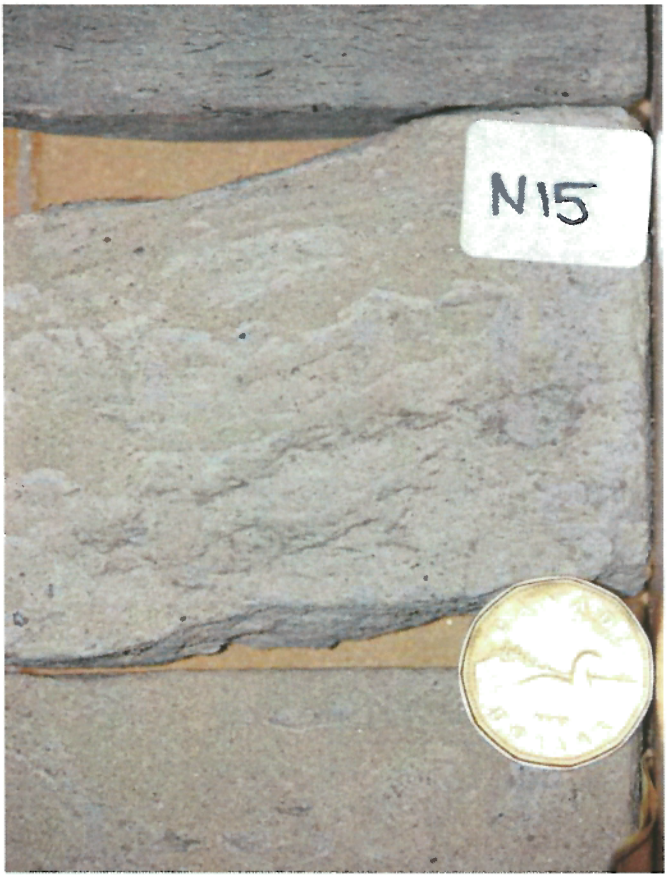

Photo 15: Fine-grained sandstone with mud drapes and mud-lined burrows. Below photo, overlies medium-grained sandstone. Unit 7.

Photo 16: Completely bioturbated fine-grained sandstone and lesser mudstone. Unit 8.

Photo 17: Fine-grained sandstone with mud drapes and mud-lined burrows. Unit 9.

Photo 18: Moderately bioturbated, fine-grained sandstone with mud drapes and mud-lined burrows. Unit 10.

Photo 19: Cross-laminated sandstone, overlain by poorly sorted muddy sandstone with scattered granules. Base of Unit 10.

Photo 20: Fine-grained sandstone with large pieces of phytodetritus visible on bedding planes. Unit 11.

Photo 21: Silty mudstone with large pieces of phytodetritus. Unit 11.

Photo 22: Fine-grained sandstone abruptly overlying coarse-grained sandstone, overlying medium-grained sandstone with large phytodetritus. Unit 12.

Photo 23: Fine-grained sandstone abruptly overlying very coarse-grained sandstone. Unit 12.

APPENDIX 3

BACKSCATTERED ELECTRON IMAGES AND POSITION OF ELECTRON MICROPROBE ANALYSES FROM CUTTINGS FROM SAMBRO I-29

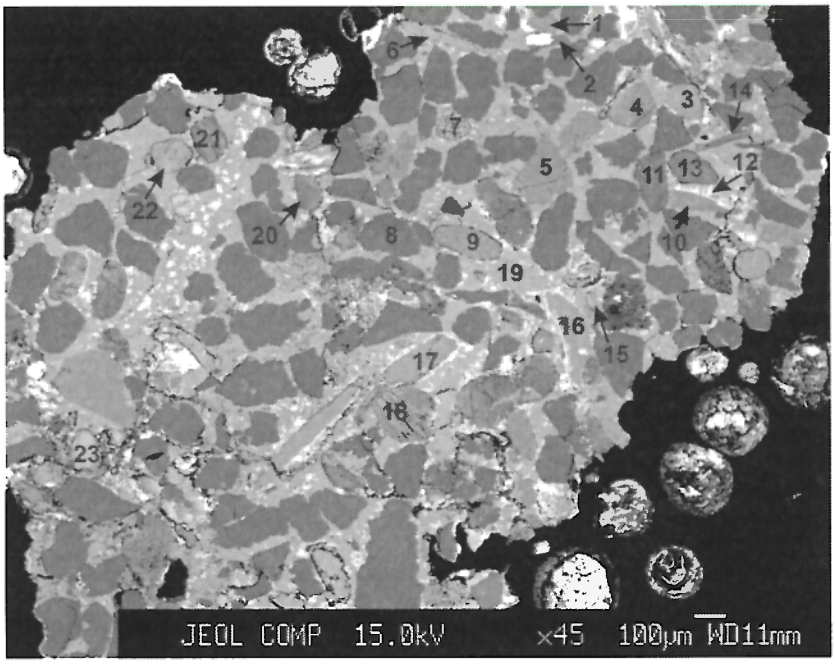

1. K-feldspar
2. muscovite
3. glauconite
4. glauconite
5. K-feldspar
6. calcite
7. glauconite
8. quartz
9. glauconite
10. calcite
11. glauconite
12. siderite
13. glauconite
14. muscovite
15. glauconite
16. calcite
17. calcite
18. glauconite
19. calcite
20. glauconite
21. glauconite
22. glauconite
23. glauconite

Figure 1 **3170B :** >2mm, fine-grained calcite-cemented glauconitic quartz arenite (grain 1).

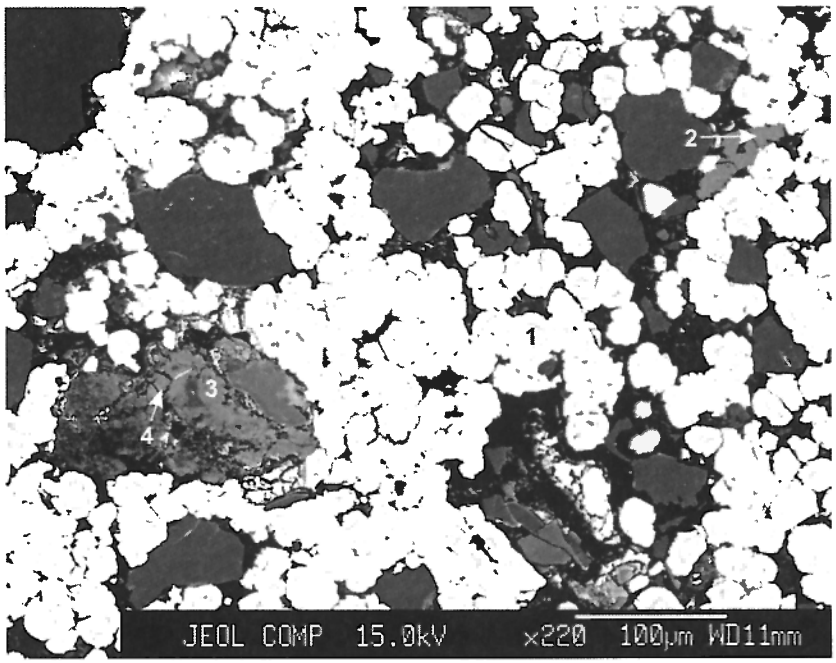

1. siderite
2. K-feldspar
3. glauconite
4. glauconite

Figure 2 **3170B :** >2mm, siderite-cemented sandstone (grain 2).

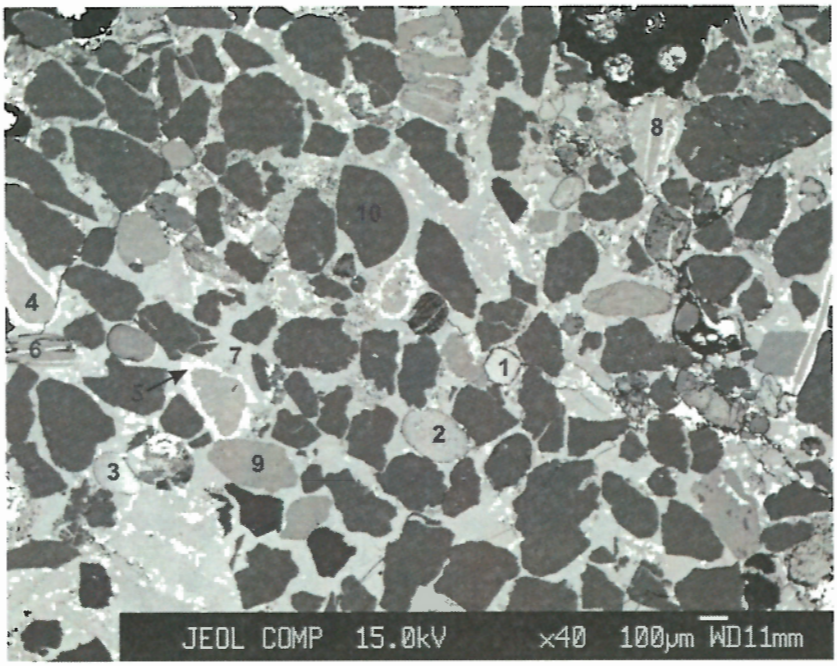

1. glauconite
2. glauconite
3. glauconite
4. calcite
5. siderite
6. glauconite
7. calcite
8. calcite
9. K-feldspar
10. quartz

Figure 3 **3170B :** >2mm, fine to medium-grained calcite-cemented glauconitic quartz arenite (grain 3).

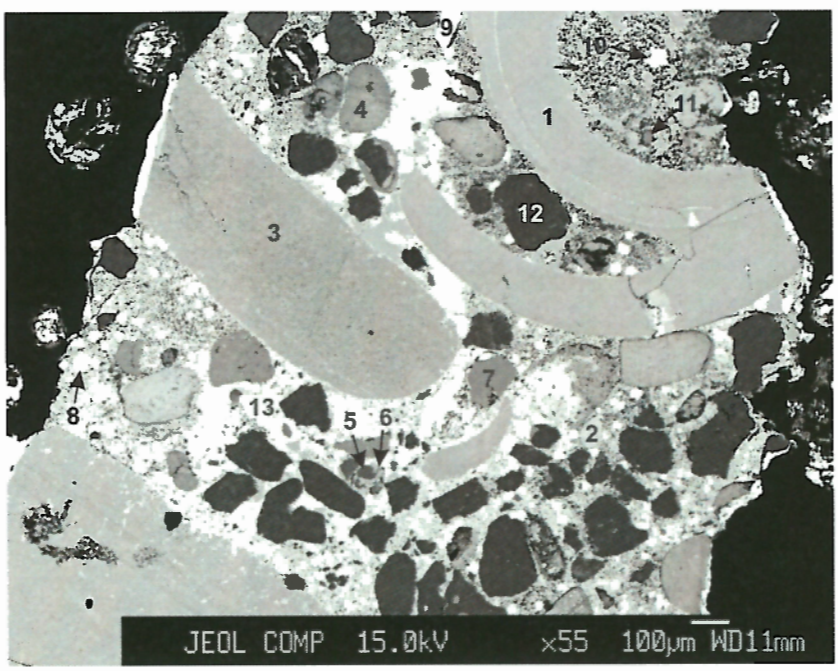

1. calcite
2. glauconite
3. calcite
4. glauconite
5. plagioclase
6. calcite
7. K-feldspar
8. siderite
9. ilmenite
10. siderite
11. glauconite
12. quartz
13. francolite

Figure 4 **3170B :** >2mm, poorly sorted fossiliferous muddy sandstone (grain 4).

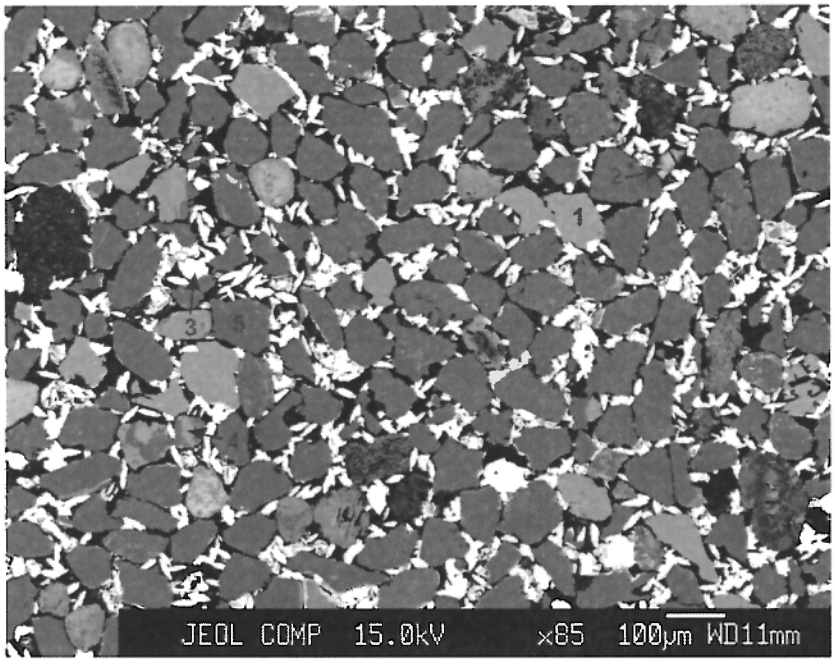

1. K-feldspar
2. glauconite
3. siderite
4. K-feldspar
5. quartz

Figure 5 **3170B :** >2mm, porous, very fine-grained, slightly glauconitic quartz arenite with late stage euhedral sideritic cement (grain 5).

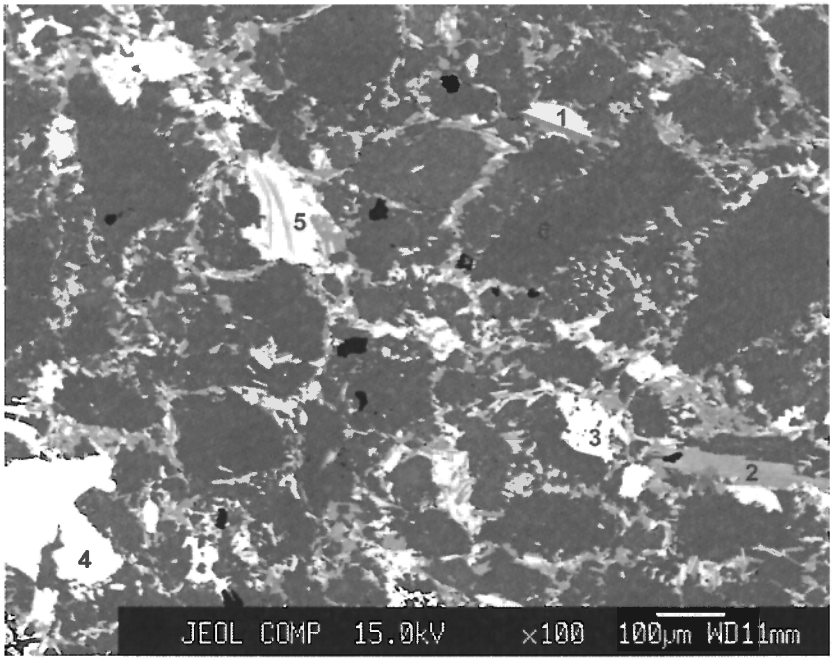

1. chlorite
2. muscovite
3. titanite
4. epidote
5. chlorite
6. quartz

Figure 6 **3170A :** >2mm, meta-quartz arenite clast (grain 1).

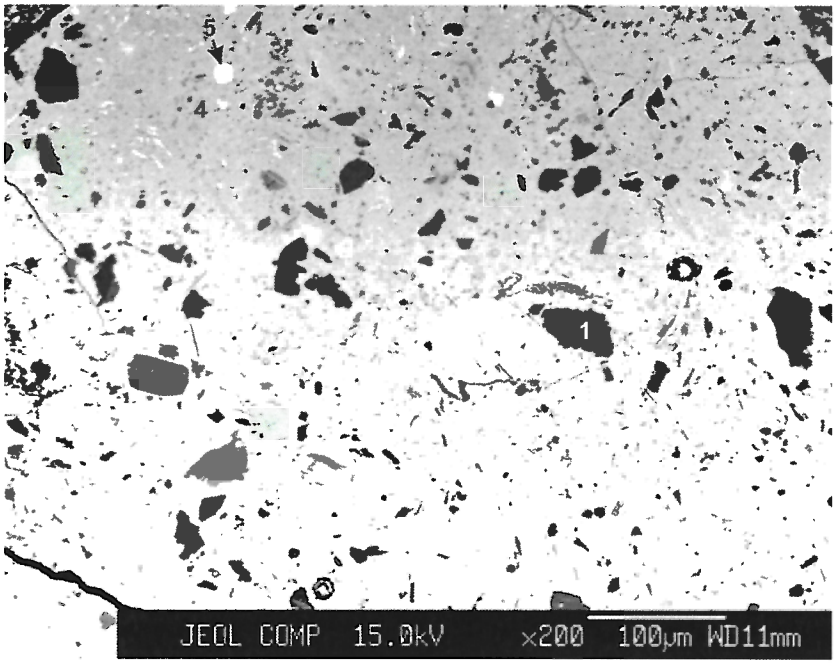

1. quartz
2. K-feldspar
3. chlorite
4. francolite
5. pyrite

Figure 7 **3170A :** >2mm, phosphate-carbonate-cemented mudstone (grain 2).

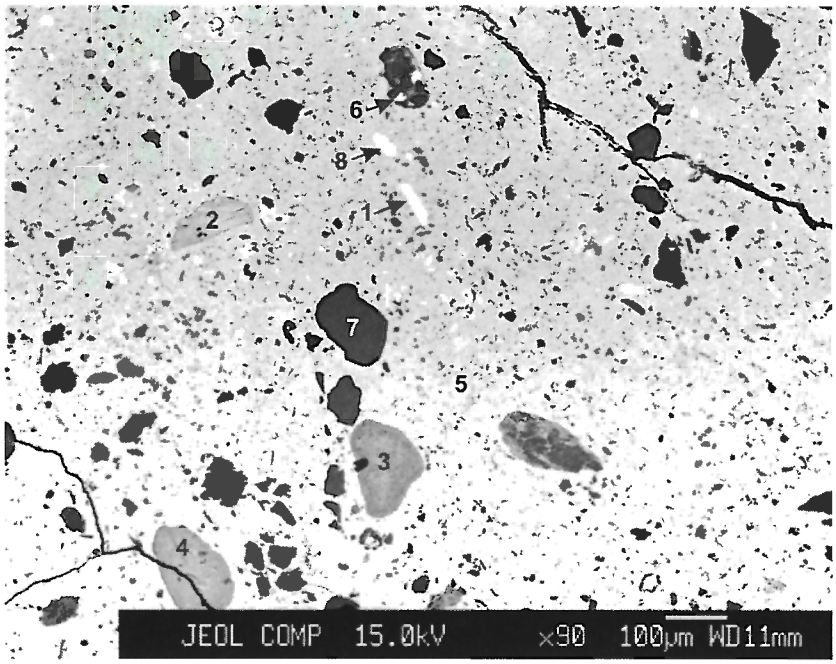

1. francolite
2. chlorite
3. glauconite
4. glauconite
5. francolite
6. rutile
7. quartz
8. pyrite

Figure 8 **3170A :** >2mm, phosphate-carbonate-cemented mudstone (grain 3).

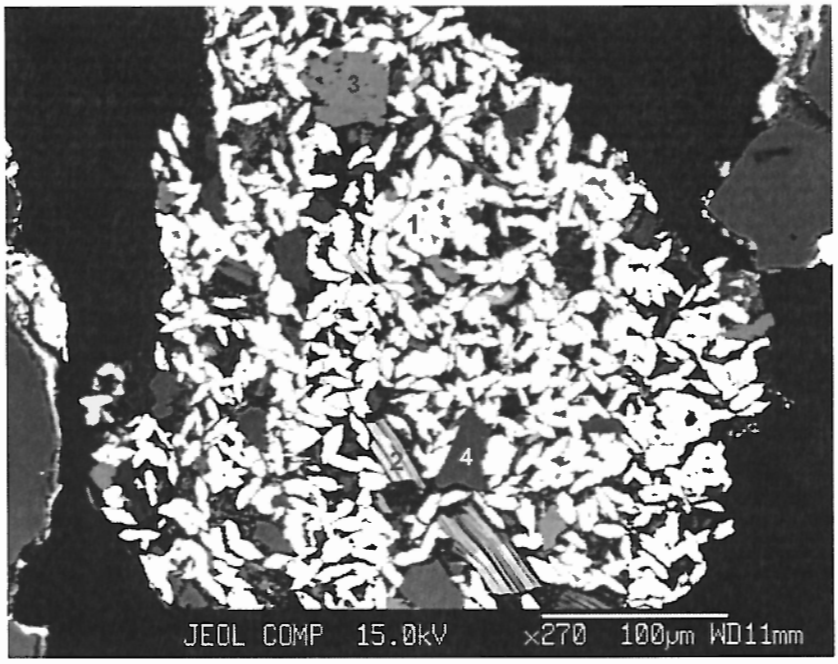

1. siderite
2. biotite
3. K-feldspar
4. quartz

Figure 9 **3880 :** <2mm (heavy fraction), siderite nodule developed in sands.

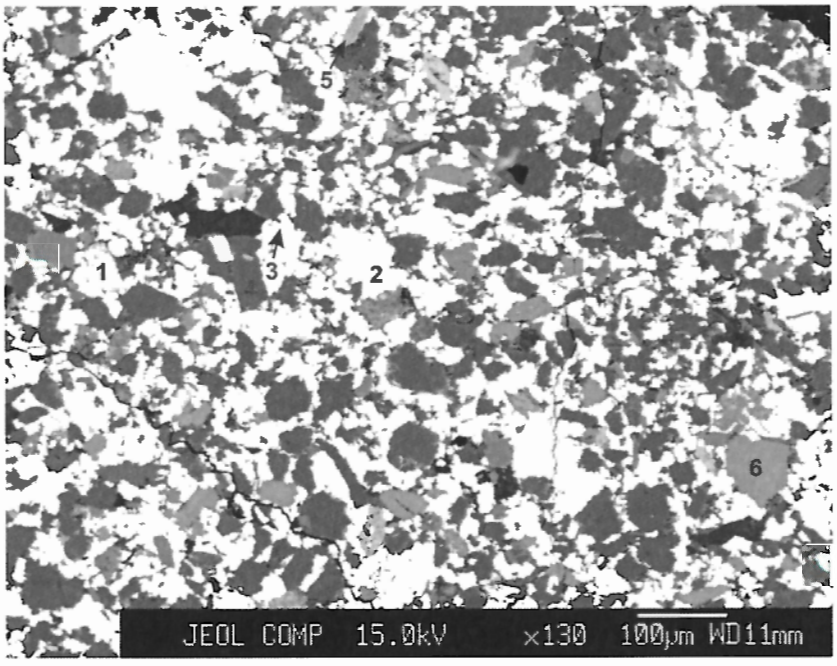

1. chlorite
2. siderite
3. ilmenite
4. quartz
5. chlorite
6. K-feldspar

Figure 10 **3880 :** <2mm (heavy fraction), very fine-grained siderite-cemented subarkose.

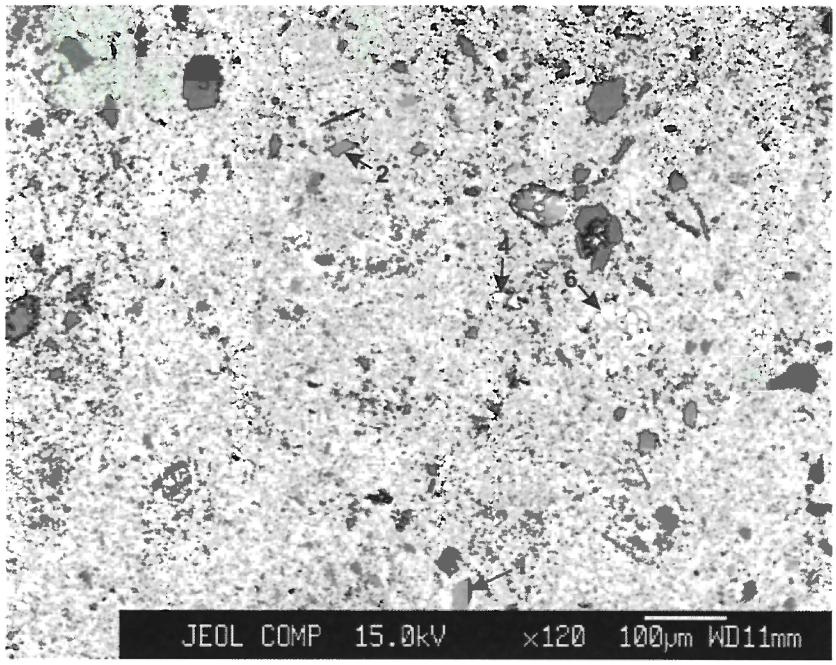

1. calcite
2. muscovite
3. siderite
4. chlorite
5. quartz
6. pyrite

Figure 11 **3880 :** <2mm (heavy fraction), siderite-cemented mudstone.

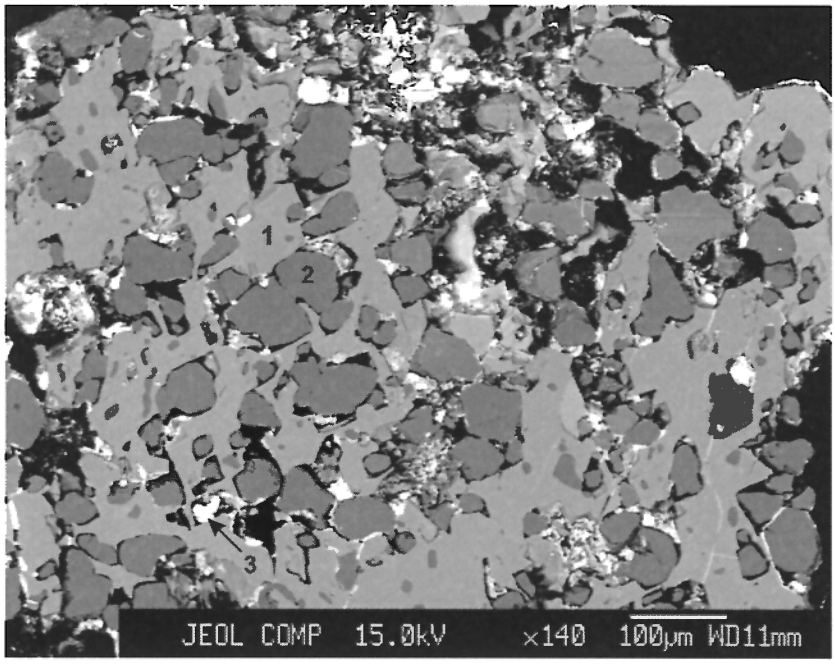

1. staurolite
2. quartz
3. pyrite

Figure 12 **3880 :** <2mm (heavy fraction), staurolite porphyroblast with inclusions.

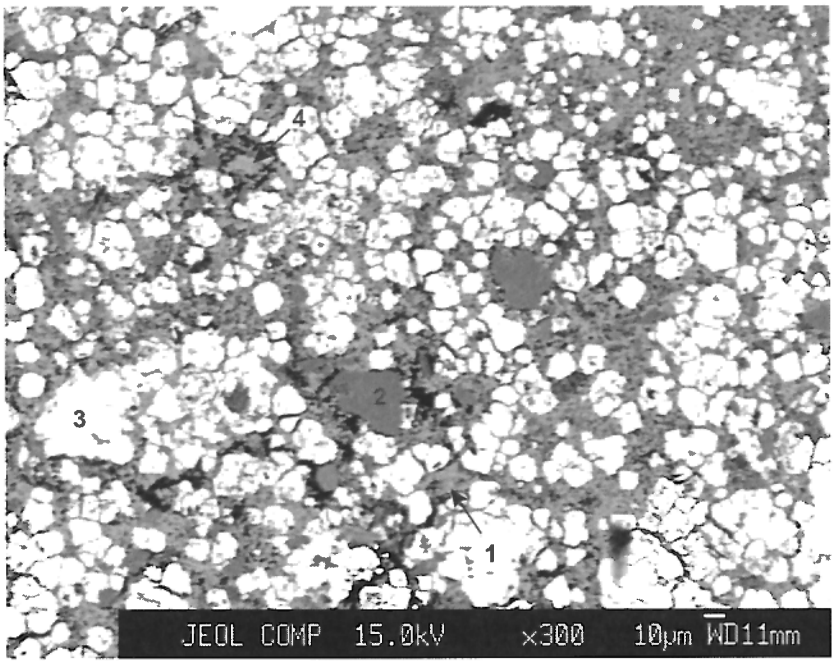

1. ?clays
2. quartz
3. pyrite
4. ?clays

Figure 13 **3880 :** >2mm, pyrite nodules developed in silty mudstone (grain 2).

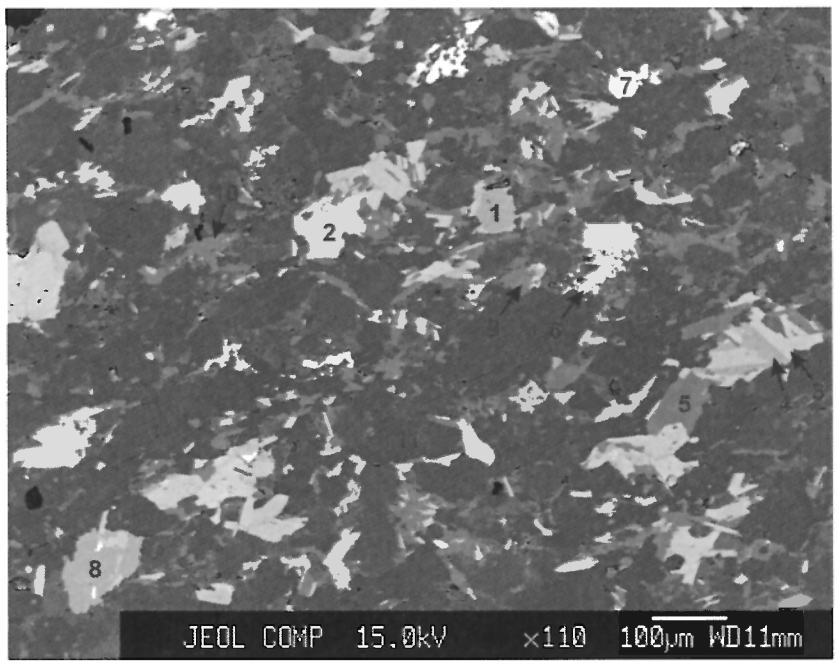

1. epidote
2. biotite
3. biotite
4. chlorite
5. muscovite
6. rutile
7. ilmenite
8. chlorite
9. biotite
10. muscovite
11. quartz

Figure 14 **3880 :** >2mm, meta-quartz arenite clast (grain 3).

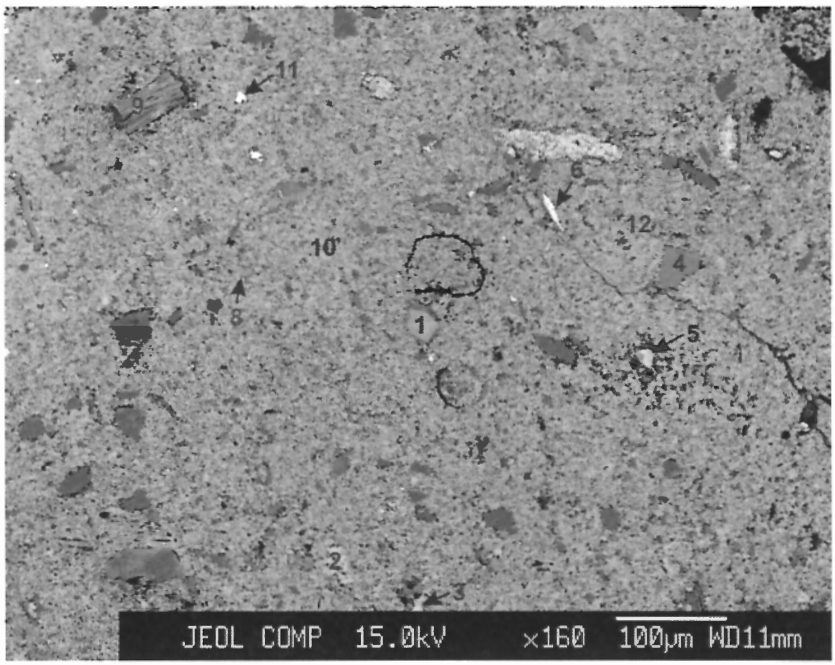

1. chlorite
2. siderite
3. siderite
4. K-feldspar
5. ilmenite
6. hematite
7. quartz
8. chlorite
9. chlorite
10. siderite
11. ilmenite
12. siderite

Figure 15 **4000 :** >2mm, siderite-cemented mudstone.

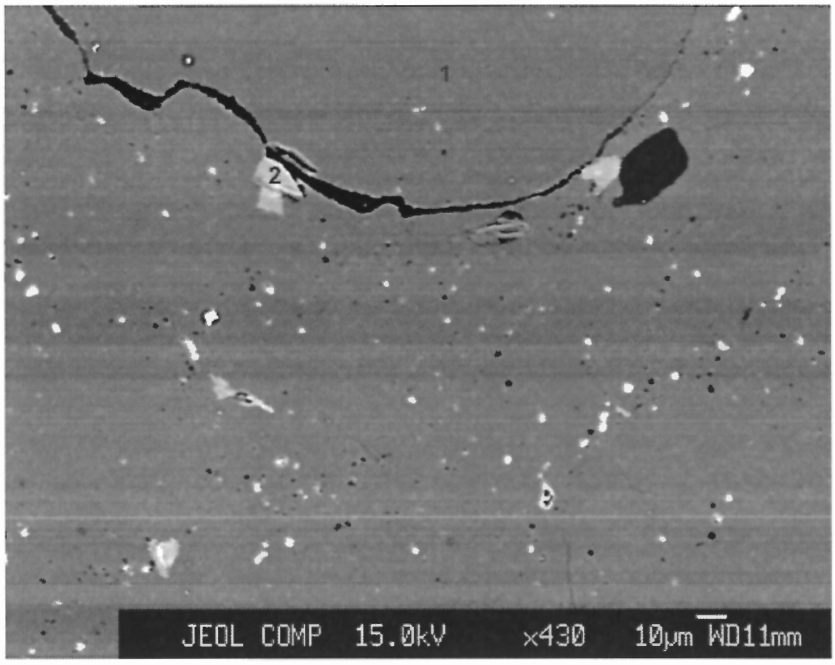

1. quartz
2. muscovite

Figure 16 **4000 :** >2mm, quartz granule clast with muscovite inclusions.

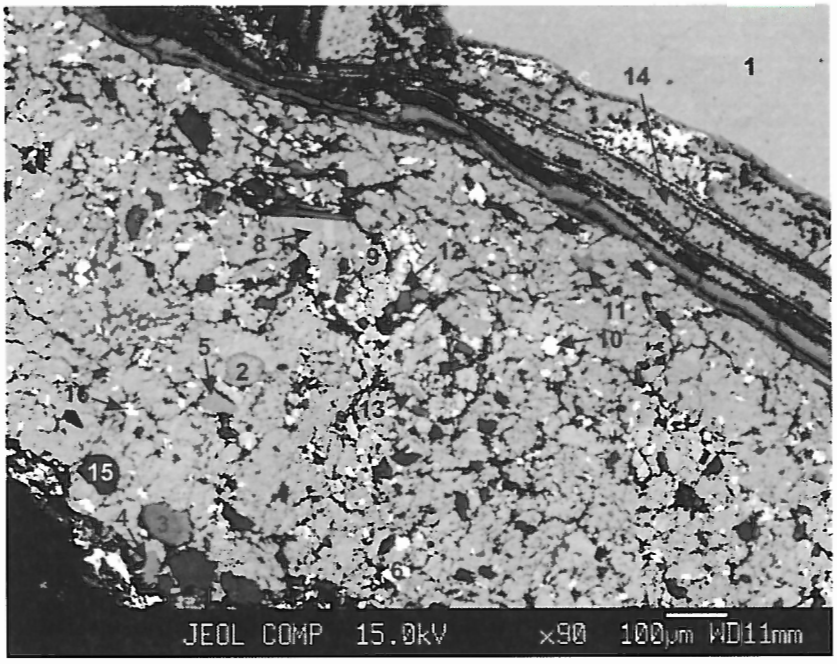

1. calcite
2. glauconite
3. glauconite
4. K-feldspar
5. calcite
6. siderite
7. hydromuscovite
8. calcite
9. siderite
10. siderite
11. K-feldspar
12. calcite
13. K-feldspar
14. calcite
15. quartz
16. pyrite

Figure 17 **4080 :** >2mm, silty limestone or carbonate concretion cut by calcite vein (grain 1).

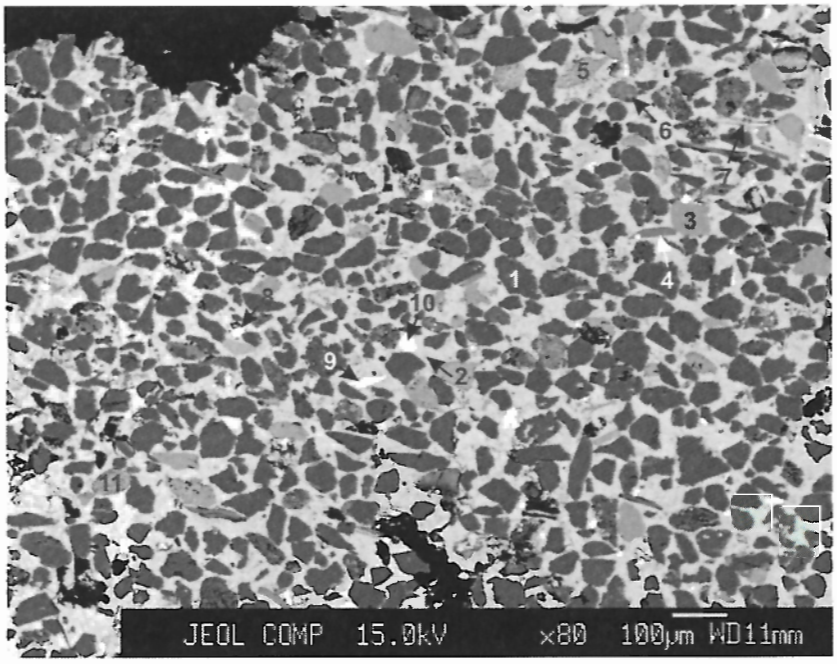

1. quartz
2. calcite
3. K-feldspar
4. muscovite
5. K-feldspar
6. muscovite
7. biotite
8. rutile
9. rutile
10. pyrite
11. glauconite

Figure 18 **4080 :** >2mm, very fine-grained calcite-cemented quartz arenite (grain 2).

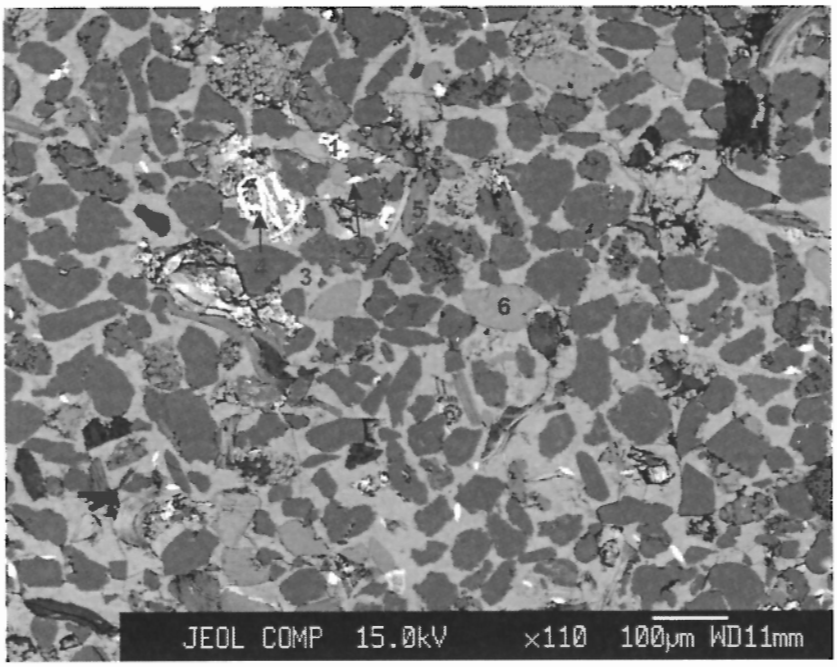

1. rutile
2. siderite
3. calcite
4. rutile
5. hydromuscovite
6. K-feldspar
7. quartz

Figure 19 **4200 : >**2mm, very fine-grained calcite-cemented siltstone (grain 5).

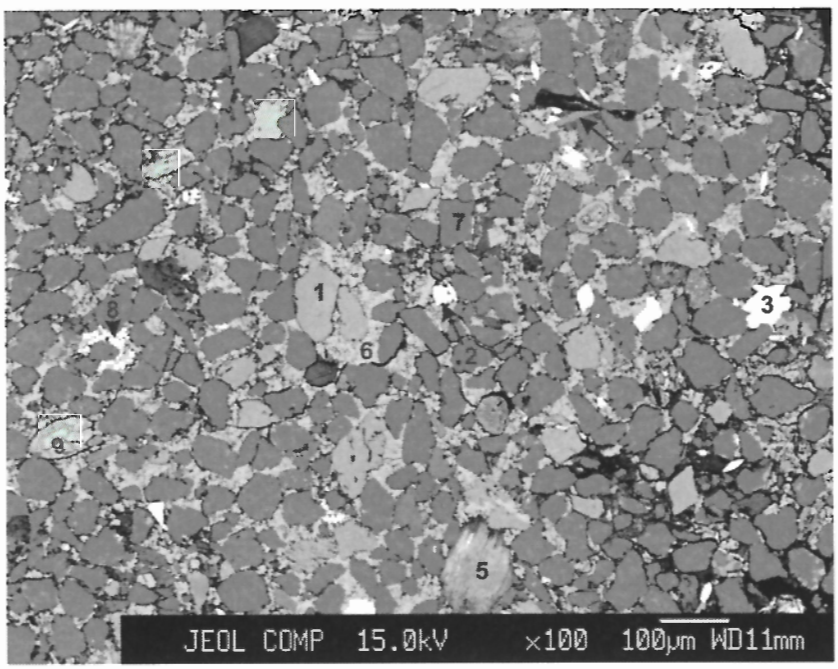

1. K-feldspar
2. siderite
3. siderite
4. hydromuscovite
5. ?chlorite
6. calcite
7. quartz
8. pyrite
9. ?chlorite

Figure 20 **4200 : >**2mm, very fine-grained carbonate-cemented quartz arenite (to subarkose) siltstone (grain 4).

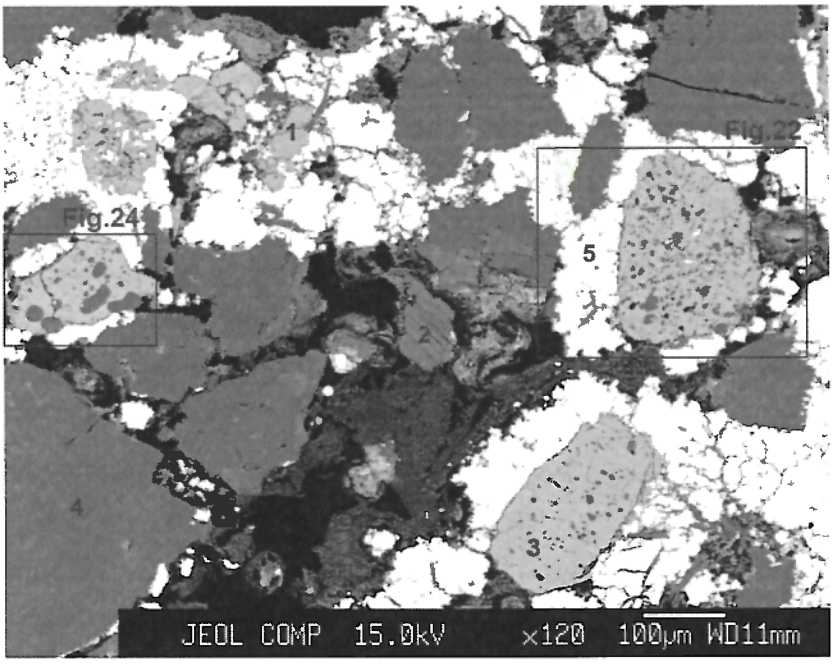

1. ilmenite
2. muscovite
3. ilmenite
4. quartz
5. pyrite

Figure 21 **4200 :** >2mm, coarse-grained pyrite-cemented quartz arenite (grain 1).

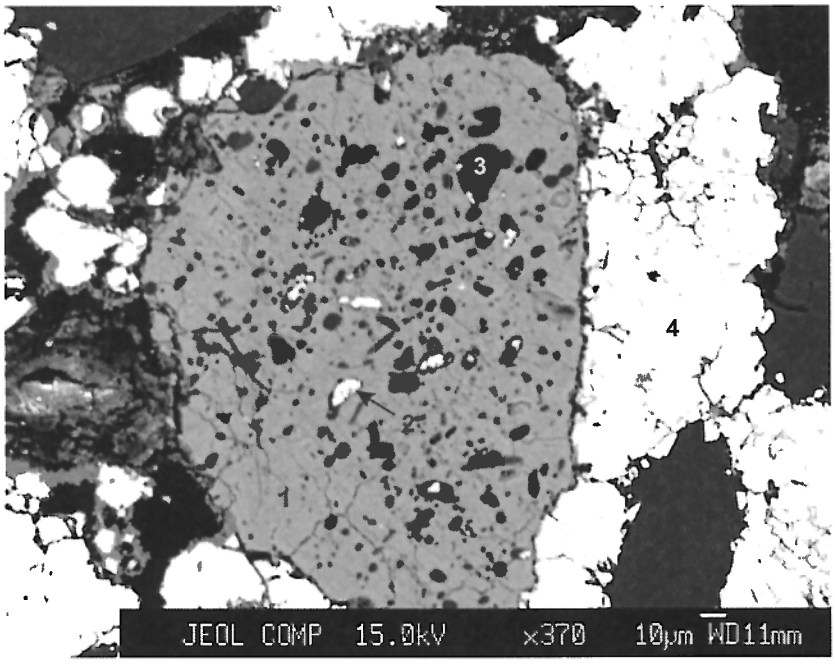

1. ilmenite
2. pyrite
3. quartz
4. pyrite

Figure 22 **4200 :** >2mm, ilmenite crystal with inclusions (ref: Fig.21).

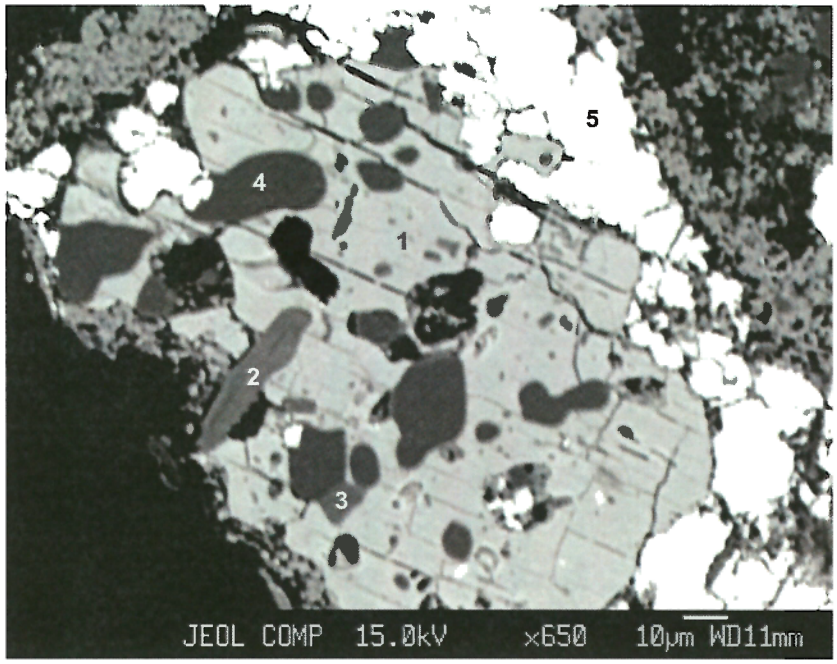

1. ilmenite
2. muscovite
3. muscovite
4. quartz
5. pyrite

Figure 23 **4200 :** >2mm, ilmenite crystal with inclusions in coarse-grained pyrite-cemented quartz arenite shown in Fig.21.

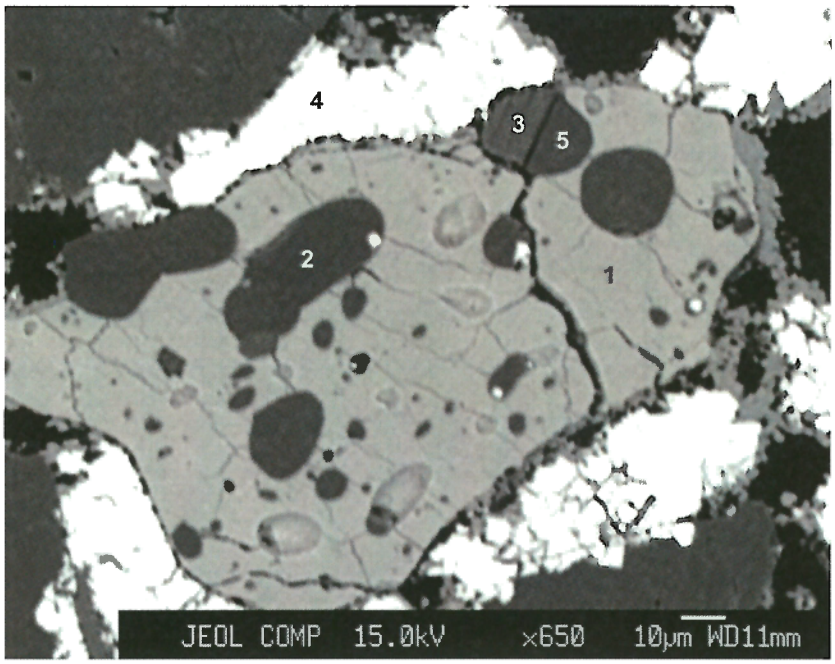

1. ilmenite
2. quartz
3. muscovite
4. pyrite
5. quartz

Figure 24 **4200 :** >2mm, ilmenite crystal with inclusions (ref: Fig.21).

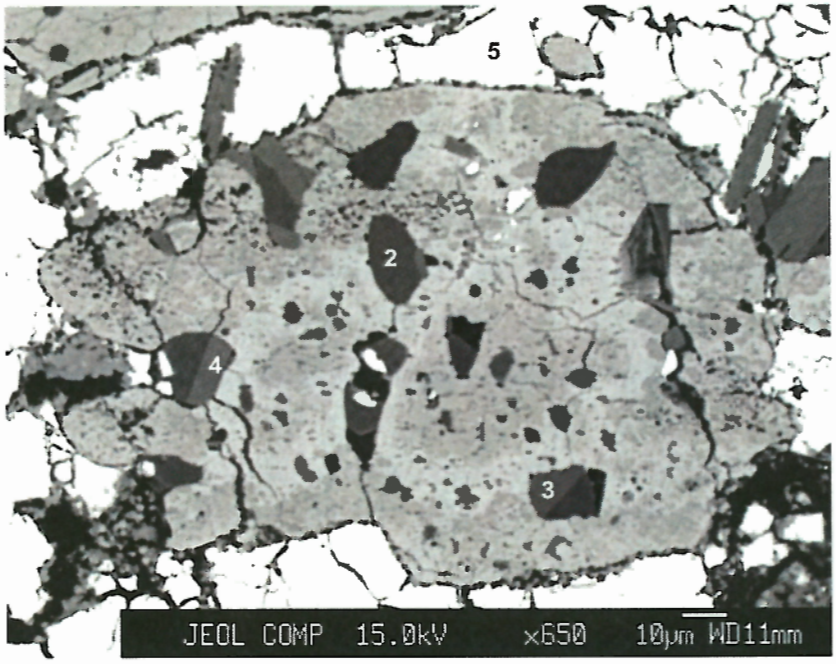

1. ilmenite
2. quartz
3. muscovite
4. muscovite
5. pyrite

Figure 25 **4200 :** >2mm, ilmenite crystal with inclusions in coarse-grained pyrite-cemented quartz arenite shown in Fig.21.

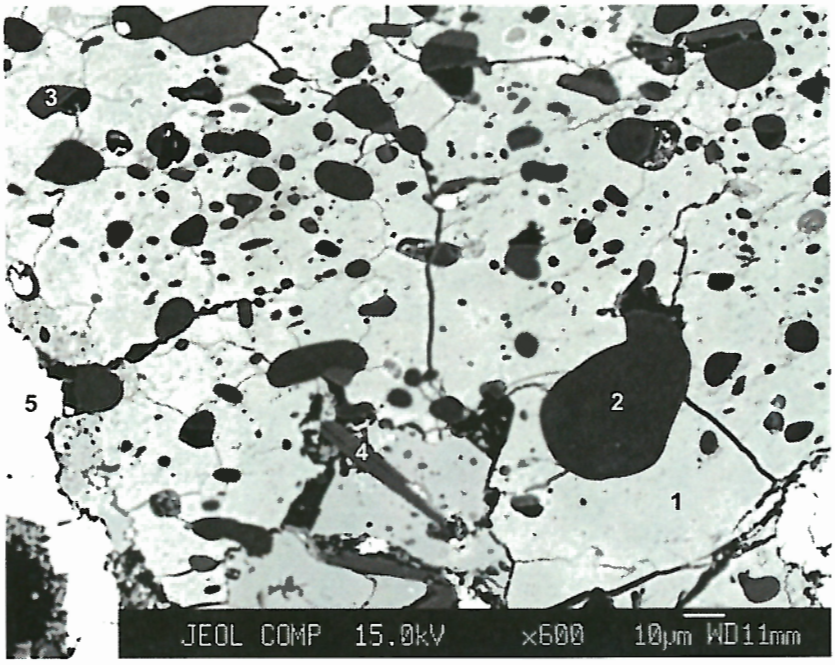

1. ilmenite
2. quartz
3. muscovite
4. muscovite
5. pyrite

Figure 26 **4200 :** >2mm, ilmenite crystal with inclusions in coarse-grained pyrite-cemented quartz arenite shown in Fig.21.